Glut3 Addiction Is a Druggable Vulnerability for a Molecularly Defined Subpopulation of Glioblastoma

Erika Cosset, Sten Ilmjärv, Valérie Dutoit, Kathryn Elliott, Tami von Schalscha, Maria F Camargo, Alexander Reiss, Toshiro Moroishi, Laetitia Seguin, German Gomez, et al.

Glut3 addiction is a druggable vulnerability for a molecularly defined subpopulation of glioblastoma

Érika Cosset[1*], Sten Ilmjärv[2], Valérie Dutoit[3], Kathryn Elliott[1], Tami von Schalscha[1], Maria F. Camargo[1], Alexander Reiss[1], Toshiro Moroishi[4], Laetitia Seguin[1], German Gomez[1], Jung-Soon Moo[4], Olivier Preynat-Seauve[5], Karl-Heinz Krause[2], Hervé Chneiweiss[6], Jann N. Sarkaria[7], Kun-Liang Guan[4], Pierre-Yves Dietrich[3], Sara M. Weis[1], Paul S. Mischel[8], David A. Cheresh[1*]

[1]Department of Pathology, Moores Cancer Center, Sanford Consortium for Regenerative Medicine & UC San Diego School of Medicine, La Jolla, USA.
[2]Department of Pathology and Immunology, Medical School, University of Geneva, Geneva, Switzerland
[3]Laboratory of Tumor Immunology, Centre of Oncology, Geneva University Hospitals, University of Geneva, Switzerland.
[4]Department of Pharmacology, Moores Cancer Center, Sanford Consortium for Regenerative Medicine & UC San Diego School of Medicine, La Jolla, USA
[5]Division of Hematology, Department of Internal Medicine, Faculty of Medicine, University of Geneva, Switzerland; Department of Human Protein Sciences, Faculty of Medicine, University of Geneva, Switzerland.
[6]INSERM, Sorbonne Universities, UPMC, CNRS, IBPS, NPS, Paris, France
[7] Department of Radiation Oncology, Mayo Clinic, Rochester, MN 55905, USA
[8]Ludwig Institute for Cancer Research, University of California San Diego, La Jolla, CA 92093, USA; Department of Pathology, UCSD School of Medicine, La Jolla, CA 92093, USA; Moores Cancer Center, UCSD School of Medicine, La Jolla, CA 92093, USA
Department of Radiation Oncology, Mayo Clinic, Rochester, MN 55905, USA

*Address correspondence to:

David Cheresh (dcheresh@ucsd.edu): Sanford Consortium for Regenerative Medicine, 2880 Torrey Pines Scenic Drive, #0695, La Jolla, California, 92037, USA. Phone: 858.822.2232

Érika Cosset (ecosset@ucsd.edu): Sanford Consortium for Regenerative Medicine, 2880 Torrey Pines Scenic Drive, #0695, La Jolla, California, 92037, USA. Phone: 858.846.0681 (Present affiliation: University of Geneva, Geneva, Switzerland; erika.cosset@unige.ch)

SUMMARY: While molecular subtypes of glioblastoma (GBM) are defined using gene expression and mutation profiles, we identify a unique subpopulation based on addiction to the high affinity glucose transporter, Glut3. Although Glut3 is a known driver of a cancer stem cell phenotype, direct targeting is complicated by its expression in neurons. Using established GBM lines and patient-derived stem cells, we identify a subset of tumors within the “Proneural” and “Classical” subtypes that are addicted to aberrant signaling from integrin αvβ3 that activates a PAK4-YAP/TAZ signaling axis to enhance Glut3 expression. This defined subpopulation of GBM is highly sensitive to agents that disrupt this pathway, including the integrin antagonist cilengitide, providing a targeted therapeutic strategy for this unique subset of GBM tumors.

KEY WORDS: Glioblastoma, cancer stem cells, integrin, glucose metabolism, Glut3

SIGNIFICANCE: While GBM tumors are highly aggressive and therapy-resistant, individual tumors achieve this state via distinct molecular pathways. Here, we define a unique biological subpopulation addicted to an integrin αvβ3-mediated pathway that enhances glucose uptake, making tumors highly sensitive to a variety of agents that disrupt this advantage. Interestingly, αvβ3 expression alone is not sufficient to define this population, as only a subset of αvβ3-expressing GBM tumors are addicted to this pathway. Our findings may explain why the integrin antagonist cilengitide in clinical trial had a benefit in some patients, but not others. By revealing a direct link between aberrant integrin expression and altered glucose metabolism, this work identifies a context-dependent druggable vulnerability that can be exploited for GBM therapy.

INTRODUCTION

Glioblastoma multiforme (GBM) represents high grade gliomas and remains the most frequent and deadliest primary brain tumor in adults. Despite major research efforts and some clinical progress, GBM ultimately become resistant to all current forms of treatment helping to explain why the overall survival rate has not dramatically changed over the past 20 years (Stupp et al., 2005). By identifying distinct gene expression profiles, GBM have been stratified by various gene signatures profiles into four molecular subtypes (Classical, Neural, Proneural, and Mesenchymal) with specific driver mutations, prognoses, and response to therapy (Brennan et al., 2013; Freije et al., 2004; Noushmehr et al., 2010; Nutt et al., 2003; Phillips et al., 2006; Verhaak et al., 2010). However, this advance in knowledge has yet to reveal new druggable targets and development of new therapeutic strategies to impact disease progression and/or outcome.

GBM typically contain cancer stem cells (CSCs) that are associated with both tumor progression and resistance to therapeutic intervention (Lathia et al., 2015). GBM CSCs not only possess self-renewing and tumor-initiating properties, but they are able to survive in a nutrient deficient microenvironment, giving them a particular advantage in the brain. In fact, Flavahan and colleagues revealed that CSCs thrive in part by upregulating the high affinity glucose transporter Glut3, enabling these cells to survive glucose deprivation (Flavahan et al., 2013). Understanding how Glut3 expression is regulated or how to target it therapeutically would therefore provide an opportunity to attack the most aggressive and drug resistant cells within the tumor.

Integrins are αβ heterodimers composed of an extracellular domain, transmembrane domain, and a short cytoplasmic tail. Noncovalent association between αβ subunits

defines their specificity for particular components of the extracellular matrix, such as vitronectin, fibronectin, or laminin (Desgrosellier and Cheresh, 2010; Weis and Cheresh, 2011). By modulating cell-matrix adhesion, integrins impact diverse aspects of cancer cell behavior, including invasion, proliferation, survival, and the promotion of angiogenesis (Desgrosellier and Cheresh, 2010). In GBM, expression of αvβ3 and its ligand vitronectin are both linked to tumor progression and invasive behavior at the tumor margin in the brain of patients with GBM (Gladson and Cheresh, 1991). This prompted development of cilengitide, a cyclic peptide antagonist capable of targeting the ligand binding site of a αvβ3. Despite encouraging phase I/II results showing a durable response to cilengitide for some patients (Nabors et al., 2007; Reardon et al., 2008), phase III CENTRIC and phase II CORE trials failed to meet overall survival endpoints (Stupp et al., 2014). In a follow-up study, immunohistological analysis of tissues obtained during the CORE trial revealed that higher αvβ3 levels were associated with improved survival in patients treated with cilengitide (Weller et al., 2016). Because this was not the case for the CENTRIC trial, it is still not clear how to identify patients who may benefit from this drug.

By analyzing clinical GBM samples and patient-derived glioblastoma-initiating cells, we identified a subpopulation of GBM tumors for which αvβ3 integrin controls Glut3 expression to regulate glucose metabolism, thus allowing cells to avoid senescence. Here, we propose a strategy to identify those GBM that are particularly sensitive to αvβ3 antagonists, including cilengitide.

RESULTS

Integrin β3 mRNA expression correlates with poor survival and expression of genes involved in glucose metabolism

To investigate the clinical relevance of integrin expression in gliomas, we analyzed the correlation between integrin expression and glioma patient survival for the “Freije” dataset (Freije, Cancer Res, 2004). Expression of the integrin β subunit is a rate-limiting determinant of integrin heterodimer formation (Cheresh, 1987), and our analysis of TCGA dataset reveals *ITGB3* (β3) as the only β subunit whose mRNA expression correlates with poor survival in gliomas (P-value = 0.03) (**figure 1A**) and for the Freije dataset (**figure 1B**). Because β3 pairs exclusively with the αv subunit in GBM cells, this finding is consistent with our previous report of integrin αvβ3 protein expression in GBM, but not in low grade astroglial-derived tumors (Gladson and Cheresh, 1991). We also generated Kaplan-Meier curves from additional datasets, which confirm *ITGB3* as a strong prognostic factor associated with poor survival (**supplementary table 1**). By generating a hierarchical cluster and stratifying patients into two groups according to median survival, we identify a $\beta3^{high}$ subset of TCGA samples within the shorter-survival group (**figure 1A**). We reasoned that understanding how integrin β3 contributes to the aggressive phenotype for this subpopulation would enable the design of a targeted therapy approach to exploit the vulnerabilities of this subset.

To consider how high integrin β3 expression may lead to poor survival in GBM, we compared gene expression profiles between $\beta3^{high}$ versus $\beta3^{low}$ samples in GBM patients from the Freije dataset. We find genes involved in glucose metabolism (*ALDOC*, *PFKM* and *GLUT3*) as one of the main family of genes correlated with β3 expression (**figure 1C, supplementary table 2A-2B** and **table 1**). As for integrin β3, Kaplan-Meier analysis indicates that poor survival correlates with expression of *GLUT3* (P-value = 0.0021),

ALDOC (P-value = 0.0065) and *PFKM* (P-value = 0.00032) in glioma patients (**figure 1D**). To further validate the clinical relevance of this profile, we generated Kaplan-Meier curves from the “Lee” and “TCGA” datasets. Whereas *ALDOC* and *PFKM* do not consistently correlate with patient outcome, we find that *GLUT3* expression tracks with poor survival for all datasets (**supplementary table 3**). Moreover, analysis of multiple datasets using MEM reveals *ITGB3* and *GLUT3* as co-expressed genes not only in GBM (**figure 1E**), but also in other cancer types (**supplementary figure 1A**).

Targeting β3 strongly inhibits Glut3 expression to decrease cell survival and anchorage-independence

We next considered whether the ability of integrin αvβ3 to promote an aggressive GBM phenotype might be linked to Glut3-mediated cell survival and glucose uptake. For three established GBM cell lines, shRNA-mediated knockdown of integrin β3 strongly inhibits Glut3 expression (**figure 2A-2B**), glucose uptake (**figure 2C**), and lactate production (**figure 2D**). In fact, the effect of β3 knockdown on cell survival is accentuated under low glucose conditions (**supplementary figure 2A**). Moreover, we observed that knockdown of either β3 or Glut3 decreases anchorage independence (**figure 2E**) and tumorsphere formation (**figure 2F**), properties associated with cancer stem cells.

To determine whether highly efficient glucose uptake provides a competitive advantage for $\beta3^+$ cells, we co-cultured $\beta3^+$ (GFP^-) and $\beta3^-$ (GFP^+) cells under standard (4.5g/L) or low (0.4g/L) glucose conditions and monitored their ratio using flow cytometry. Indeed, there are significantly more viable $\beta3^+$ cells present after 1 week of glucose restriction compared with cells for which either β3 or Glut3 had been knocked down (**figure 2G**).

More importantly, knockdown of either β3 or Glut3 significantly delays the orthotopic growth of GBM tumors in mice (**figure 2H** and **supplementary figure 2B**). Collectively, these results indicate that β3 and Glut3 promote the survival of GBM cells and their tumorigenic capacity in the brain.

We previously reported that knockdown of β3 induced a senescent phenotype in GBM cells (Franovic et al., 2015). Here we show that Glut3 knockdown also induces multiple markers of senescence *in vitro*, including β-galactosidase (SA-β-gal) activity, G0/G1 cell cycle arrest and pH2A.X expression (**figure 2I-2J** and **supplementary figure 2C-2D-2E**). *In vivo*, cells with knockdown of either β3 or Glut3 show increased SA-β-galactosidase activity within subcutaneous xenografts (**figure 2K**). In contrast, knockdown of the Glut1 or Glut6 glucose transporters does not induce a senescent phenotype (**supplementary figure 2F**). We therefore asked whether ectopic expression of Glut3 is sufficient to drive GBM growth in the absence of β3. Indeed, ectopic Glut3 “rescues” the effects of β3 knockdown on 2D and 3D growth and prevents the senescent phenotype *in vitro* and within tumors *in vivo* (**figure 2K-2L-2M-2N-2O** and **supplementary figure 2G-2H**), suggesting that the regulation of Glut3 expression may largely account for the impact of integrin αvβ3 on GBM progression.

Integrin αvβ3 modulates Glut3 expression through PAK4-YAP/TAZ axis

To understand how integrin αvβ3 regulates Glut3 expression in GBM cells, we considered transcriptional regulators that correlate with β3 expression. We identified “cell signaling” as an important family of genes associated with β3 expression (**table 1**), and found the transcriptional co-activator *WWTR1* (WW domain-containing transcription regulator 1,

also known as TAZ) as the top transcription factor in our list of genes (**table 1**). Along with its paralog Yes-associated protein (YAP), YAP/TAZ impacts a wide variety of cellular functions, including epithelial-mesenchymal transition, cell growth, organ development, metabolism, and stress responses (Moroishi et al., 2015). Of note, the Kaplan-Meier curves generated from the Freije (**figure 3A**) dataset reveals that *WWTR1* (TAZ) expression correlates with poor survival (P-value = 0.02). Moreover, we find that β3 knockdown leads to a marked decrease of YAP/TAZ expression (**figure 3B-3C**). Consistent with previous reports of Glut3 as a YAP-regulated gene (Wang et al., 2015), we find that YAP/TAZ knockdown decreases Glut3 expression (**figure 3D-3E** and **supplementary figure 3A**), and this also induces senescence as evidenced by SA-β-galactosidase activity (**figure 3F**). Furthermore, ectopic expression of YAP can rescue colony forming ability in β3-knockdown cells (**figure 3G** and **supplementary figure 3B**). Since we recently implicated PAK4 as a mediator of β3 function (Franovic et al., 2015), we considered whether this kinase may also be required for β3-mediated regulation of YAP/TAZ expression. Indeed, inhibition of PAK4 activity using the PAK4 kinase inhibitor PF-03758309 or knockdown of PAK4 expression using shRNA led to a decrease of YAP/TAZ (and Glut3) expression (**supplementary figure 3C-3D-3E-3F** and **figure 3H**). Moreover, knockdown of PAK4 (like YAP/TAZ) induced markers of senescence, including SA-β-gal and G0/G1 cell cycle arrest (**figure 3I-3J**). Whereas a critical role for Glut3 in GBM has recently been reported (Flavahan et al., 2013), there have so far been no therapeutic agents capable of targeting its function. By understanding how Glut3 expression is regulated in GBM cells, our findings highlight multiple strategies to therapeutically target this signaling axis in cells that are addicted to Glut3 for survival.

Integrin αvβ3 is required for Glut3 expression in patient-derived gliomaspheres

To further examine the link between β3 and Glut3 in models that reflect the genetic heterogeneity of human glioblastoma, we derived glioblastoma stem cells (GSCs) from twelve GBM patients and confirmed tumorigenicity, multipotency capacity, and expression of stem cell markers (**supplementary figure 4A-4B-4C**). For this panel, a third of the GSCs models show high integrin β3 expression (**figure 4A**), and this correlates with positive expression of Glut3 (**figure 4A**). Similarly, histological analysis of a GBM tissue array confirms that a subset of GBM specimens show high expression of both β3 and Glut3 (**supplementary figure 4D-4E**). For the β3-positive GSC models (Ge479, Ge518 and Ge269), knockdown of β3 decreases Glut3 expression (**figure 4B** and **supplementary figure 4F4G**), whereas ectopic expression of β3 in the β3-negative GBM6 model induces both Glut3 and YAP expression (**supplementary figure 4H**). While only a subset of the GSC panel shows this phenotype, all of the established GBM cell lines examined contain high levels of both αvβ3 and Glut3 (**figure 2A** and **supplementary figure 4I**), highlighting the inability of cultured cell lines to accurately reflect the heterogeneity of GBM in this context.

Patient-derived gliomaspheres show heterogeneity in Glut3 "addiction"

In contrast to the established GBM cell lines that are uniformly addicted to both αvβ3 and Glut3, we find that not all of the $\alpha v\beta 3^{+}$/$Glut3^{+}$ patient-derived GSC models are dependent on glucose and/or Glut3 expression for survival. While the patient-derived cells Ge479 and GBM39 are highly sensitive to glucose deprivation, others (Ge269 and Ge518) show

less sensitivity or appear glucose indifferent (Ge738 and GBM6), as demonstrated by their equivalent viability under low or high glucose conditions (**figure 4C**). Importantly, Glut3 knockdown decreases the survival of the glucose-addicted GSC model, Ge479 and GBM39 while Ge269 and Ge518 are only moderately dependent on glucose and not dependent on Glut3 (**figure 4D** and **supplementary figure 4G**). For the glucose-addicted model, Ge479, β3 and Glut3 knockdown induces the same pattern of gene expression (increased *ALDOC* and a trend toward increased *HK3*), which is in line with the differential gene expression analysis (**figure 4E**). The apparent dichotomy in αvβ3/Glut3 expression vs. addiction prompted us to consider how the two groups of GSC models may differ in terms of molecular subtype. Indeed, the Glut3-addicted GSC models Ge479 and GBM39 express genes consistent with a "Proneural-Classical" GBM subtype (*EGFR*, *GLI1*, *NES*, *DLL3*, *OLIG2*), while the Glut3-independent GSC models Ge269 and Ge518 express markers indicating the Mesenchymal GBM subtype (*CHI3L1* (YKL40), *LOX*, *CD44*, and *RELB*) (**supplementary figure 4J**). Altogether, our results indicate that within the population of GSCs defined by dual high expression of both αvβ3 and Glut3, only a subset of these tumors (i.e. those with Proneural-Classical markers) depend on Glut3 for survival.

The Mesenchymal subtype of GBM is enriched for glycolytic genes, but is insensitive to antagonists of the αvβ3/PAK4/YAP/TAZ pathway

GBM cells avidly take up glucose and are highly metabolically active. This particularity has been exploited clinically by Positron Emission Tomography (PET) combined with an intravenous injection of 18F-fluorodeoxy-glucose (18FDG), a glucose analog. However,

not all GBM subtypes avidly take up FDG, suggesting metabolic heterogeneity which is not clearly understood. To investigate how αvβ3 might impact the metabolic landscape of GBM, we performed an enrichment analysis of GBM patients with high versus low expression of genes involved in the glycolytic/gluconeogenesis pathway. As previously reported (Bhat et al., 2011; Mao et al., 2013), we found the Mesenchymal subtype to be significantly enriched for several genes involved in the glycolytic pathway, including *HK3*, *LDHA*, *PFKL*, *PGK1*, *GLUT3*, *GLUT5*, and *GLUT10*, with a trend toward enrichment for *HK2*, *ENO1*, *PFKM*, *GAPDH*, and *ALDOA*, and significantly low expression of *ALDOC*, *PFKP*, and *LDHB* (**figure 5A** and **supplementary figure 5A**). Kaplan-Meier analysis confirms the clinical relevance for several of these genes (**figure 5B** and **supplementary figure 5B-5C-5D-5E**). Despite the highly glycolytic expression signature of the Mesenchymal subtype in the Freije dataset and the enrichment of β3, Glut3, YAP, and TAZ (**figure 5C**), we find that the Glut3 non-addicted models show Mesenchymal-like signature (**supplementary figure 4J**). It is possible that the abundance of glycolytic genes can compensate for the role of Glut3, thus explaining its non-essential role in tumors of this subtype. Alternatively, the Mesenchymal subtype may depend on metabolic pathways, other than the glycolytic pathway, for survival. Together, these findings suggest that agents targeting the αvβ3/PAK4/YAP/TAZ/Glut3 signaling axis would be most effective for αvβ3/Glut3^{high} tumors that show markers defining a Proneural/Classical, but not Mesenchymal, subtype.

We then considered how the Glut3 addiction status of a given tumor might be predicted using molecular profiling. To do this, we identified samples from the Freije dataset with high expression of Glut3 by comparing gene expression profiles between Glut3^{high} versus

Glut3^{low} samples in GBM patients. For the Glut3^{high} subset, we asked which genes tracked with Glut3 in terms of patient survival. This generated a list of Glut3/survival-associated genes predicted to identify the Glut3 addicted phenotype (**supplementary table 6)**. As a validation, we asked if this profile could differentiate between the Proneural/Classical Glut3-addicted GSC models (GBM39 and Ge479) and the Mesenchymal Glut3-non-addicted GSC models (Ge269 and Ge518). Out of a 96-gene panel, a 19-gene subset (**figure 5D and supplementary table 6**) allowed us to distinguish between Mesenchymal (*LOX*, *THBS1, and DCN*) and Proneural/Classical subtypes (*DLL3*, *OLIG2*, *CDK17*, and *MAP2*). Therefore, assessing GBM molecular subtype or using this gene expression panel could provide a means to identify which αvβ3/Glut3^{high} tumors are addicted to Glut3.

We hypothesized that αvβ3/Glut3^{high}, Glut3-addicted GSCs (GBM39 and Ge479) would be highly sensitive to agents that disrupt the β3-PAK4-YAP/TAZ axis. To test this, we evaluated GSC survival in the presence of the αv integrin antagonists cilengitide (a cyclic peptide that inhibits αv integrins) or LM609 (a function blocking monoclonal antibody specific for human but not rodent integrin αvβ3) (**figure 6A**). Indeed, we found that sensitivity to integrin blockade does not exclusively depend on αvβ3/Glut3 expression or mutation status, but rather on Glut3 addiction status (**supplementary table 7**), which appears to be linked to a Proneural/Classical-like subtype. In contrast, GSC with low β3/Glut3 expression (Ge738, GBM6, Ge904, Ge970.2, Ge835 and Ge885) consistently show either a moderate or a significant enhancement of viability when treated with cilengitide or LM609 (**figure 6A**). Similar to blockade of αvβ3 directly, inhibitors of YAP or

PAK4 reduce *in vitro* viability of the Glut3-addicted Proneural-like Ge479 GSC, but not the Glut3-non-addicted Mesenchymal-like Ge518 model (**figure 6B**).

To validate our hypothesis and test the ability of our signature to predict sensitivity to αvβ3 antagonists, we analyzed the available gene expression data for 41 models from the Mayo Clinic Brain Tumor Patient-Derived Xenograft National Resource. Based on their expression of genes associated with the Glut3 addicted versus non-addicted signature we generated, we predicted that 8 of the models (~20%) should be sensitive based on their high expression of β3/Glut3 and the Glut3 addicted signature. We therefore obtained 3 models predicted to be addicted, 2 non-addicted, and 2 with β3/Glut3-low to directly test sensitivity to the αvβ3 antagonists cilengitide and LM609 (**figure 6C** and **supplementary table 8** and **supplementary figure 5G**). Similar to Ge479 and GBM39, we find sensitivity to integrin blockade for GBM14, 85 and 64, which we predicted to be Glut3 addicted (**figure 6C-6D**). Consistently, GBM150 and GBM59 with Glut3 non-addicted signatures are not affected by the integrin antagonists. Like the other GSC with low β3/Glut3 expression, GBM26 and GBM12 show no effect or a moderate enhancement of viability upon cilengitide or LM609 treatment (**figure 6C-6D**). Based on gene expression alone, we were able to predict whether a given GBM PDX model would be sensitive or insensitive to αvβ3 blockade for this collection of samples. Our success with a modest sample size suggests promise for expanding this strategy to clinical testing.

Notably, we also find that ectopic expression of β3 in a GCS in a model with low β3/Glut3 (GBM6) it is not sufficient to sensitize the tumor cells to integrin blockade, while β3

knockdown in the Glut3 addicted Ge479 model abolishes their sensitivity (**figure 6E-6F**). More importantly, systemic treatment with the integrin antagonist cilengitide dramatically prolongs the survival of mice bearing Ge479, but not Ge518, orthotopic tumors (**figure 6G** and **supplementary figure 5H**), further linking Glut3 addiction to a differential selectivity to αvβ3 blockade *in vivo*. Altogether, our results identify a molecularly defined subset of GBM tumors that are highly sensitive to inhibition of the β3-PAK4-YAP/TAZ axis by virtue of their Glut3 addiction (**figure 6H**).

DISCUSSION

Previous studies have linked αvβ3 expression to GBM progression (Gladson and Cheresh, 1991). Here, we reveal that integrin αvβ3-mediated activation of PAK4 is required for Glut3 expression in GBM cells, which in some patients leads to Glut3 addiction and sensitivity to αvβ3 antagonists. Although all established GBM cell lines we examined express αvβ3 as a biomarker predicting both Glut3 addiction and sensitivity to inhibitors of αvβ3 integrin, PAK4 or YAP/TAZ, we find this holds true for only a subset of patient-derived gliomasphere models that may more accurately represent the genetic heterogeneity of GBM. Indeed, dual expression of αvβ3/Glut3 drives addiction to this pathway only for GBM tumors with expression of Proneural-Classical subtype markers. In contrast, elements of this pathway are not critical for the growth and viability of patient-derived gliomaspheres that show a gene signature consistent with the Mesenchymal GBM subtype. Thus, our findings provide a possible explanation for the failure of cilengitide to meet its primary survival endpoint in phase II/III trials, and we predict that

patients with αvβ3-positive Proneural-Classical subtype tumors might be the best candidates for this drug.

Integrin αvβ3 as a target for GBM therapy

While a number of integrins contribute to the growth and progression of a wide array of cancers (Desgrosellier and Cheresh, 2010; Desgrosellier et al., 2014; Seguin et al., 2014), we find that αvβ3 expression is significantly linked to glioblastoma progression. This is consistent with our previous studies showing αvβ3 protein expression on the most advanced form of this disease, and most highly expressed on those cells at the tumor margin (Gladson and Cheresh, 1991). However, despite promising activity in phase I (Nabors et al., 2007) and II (Reardon et al., 2008) trials, the αv integrin antagonist cilengitide failed to produce a significant overall survival benefit in the phase III CENTRIC trial (Stupp et al., 2014), and further clinical development of cilengitide for GBM has been halted (Mason, 2015).

A number of factors may have contributed to the clinical failure of cilengitide, including the stability and pharmacokinetic properties of the drug, its combination with alkylating agents, and use in highly aggressive, drug-resistant cancer (Paolillo et al., 2016). However, in this era of precision medicine, it may be important to select a more focused GBM patient population. While higher levels of αvβ3 were associated with a modest survival benefit in the phase II CORE trial, αvβ3 expression did not correlate with outcome for the phase III CENTRIC trial (Weller et al., 2016). These findings, along with our new data, suggest that profiling αvβ3 expression alone is not sufficient to predict sensitivity to this drug. Instead, we have linked cilengitide sensitivity with the ability of αvβ3 to drive

Glut3 addiction since orthotopic GBM tumors with this depence show a significant survival benefit compared to tumors not addicted to Glut3.

Understanding why certain tumors are addicted to αvβ3, glucose, and Glut3

Using loss/gain-of-function approaches, we have determined that integrin αvβ3 is required for expression of the high affinity glucose transporter, Glut3, in a PAK4 and YAP/TAZ-dependent manner. In turn, Glut3 appears to be a critical mediator of αvβ3 addiction in GBM, as ectopic Glut3 expression can completely rescue the orthotopic tumor growth capacity of β3-knockdown cells by allowing them to avoid senescence. While normal astrocytes do not express Glut3, its expression level correlates to astrocytoma grade (Boado et al., 1994). Previous studies have reported a correlation between glucose level/uptake and poor survival (Patronas et al., 1985), and Flavahan and colleagues reported that brain tumor initiating cells express Glut3, allowing them to outcompete non-tumor cells for glucose within the glucose-limited tumor environment (Flavahan et al., 2013). Recently, Birsoy and collaborators reported that certain glucose-sensitive cell lines do not increase oxygen consumption upon glucose limitation, and gene expression analysis revealed that these lines have low Glut3 and Glut1 expression (Birsoy et al., 2014). A recent single cell RNA-seq study highlighted the strong heterogeneity in GBM specimens that was not previously well appreciated (Patel et al., 2014). Indeed, among all five tumors analyzed, the authors have shown individual cells corresponding to different GBM subtypes. Together, these studies suggest a complicated heterogeneity and metabolic landscape among individual GBM tumors that may not only explain clinical trial failures but also highlight the need to better understand GBM heterogeneity in order to design appropriate therapeutic regimens.

Despite the functional advantages offered by Glut3 expression, we find that only a subpopulation of our patient-derived GSC models actually depend on glucose/Glut3 for their survival. In contrast, all long term established GBM cultured cell lines express high level of Glut3 and are addicted to this transporter for survival. As such, these well-established GBM cell lines may somehow enrich for this phenotype, providing a poor reflection of its frequency within patient tumors. The fact that only ~15% of our patient-derived GSC models appear to be αvβ3/Glut3 addicted suggests a similar portion of patients might thus be sensitive to αvβ3 antagonists. In this respect, our study reinforces the need to carefully consider whether biomarkers and drug sensitivity established using cell-based models will relate to the heterogeneity of GBM.

Identification of glucose/Glut3 addicted tumors

While we are able to determine glucose/Glut3 addiction status using cell viability assays, we can also identify these cells based on a genetic signature. Indeed, we find that αvβ3-positive glucose/Glut3 addicted vs. non-addicted tumors can be differentiated in terms of a molecular GBM subtype. Specifically, the glucose/Glut3 addicted tumors represent a subpopulation within the Proneural and Classical subgroups and can be further delineated based on their stem cell behavior. In contrast, a subpopulation of tumors in the Mesenchymal group tend to be positive for αvβ3/Glut3, yet surprisingly are not addicted to Glut3 and remain insensitive to αvβ3 antagonists. Thus, we estimate that 10-15% of GBM patients may show very significant responses to agents targeting αvβ3/Glut3. Indeed, a number of individual patients showed very significant, durable, yet unexplained responses to cilengitide (Nabors et al., 2007; Reardon et al., 2008) . In the Mesenchymal subtype, we found an abundance of glycolytic genes and we found that all Mesenchymal

patient-derived cells non-addicted to Glut3. Thus, the role of Glut3 may be negligible when other glycolytic genes are highly-expressed. Or, this subtype might be addicted to another glycolytic gene product, as suggested by Mao and co-workers (Mao P., 2013). At present, it is unclear why certain GBM tumors are, and/or become, addicted to Glut3, while others can circumvent this dependence.

Broader implications for GBM therapeutics

We report that among αvβ3/Glut3-expressing tumors, only a subpopulation is “addicted” to glucose/Glut3. Not only does this phenotype render them particularly sensitive to αvβ3 integrin inhibitors (including αv integrin-targeting cyclic peptide cilengitide or the monoclonal αvβ3 antibody LM609), but we show that such tumors are also sensitive to inhibitors of PAK4 or YAP/TAZ, that suppress αvβ3-mediated Glut3 expression in GBM cells. While the importance of YAP/TAZ in GBM aggressiveness has been reported, our new findings provide some insights into its regulation, signaling, and function within a molecularly defined GBM subpopulation.

Aside from cilengitide, there are a number of αvβ3-targeted strategies in development for GBM, including GLPG0187, a small molecule antagonist of multiple integrins including αvβ3, αvβ5, αvβ6, and α5β1 (Cirkel et al., 2016), as well as approaches that use RGD peptides for αvβ3-targeted delivery of radionuclides (Jin et al., 2017), siRNA (He et al., 2017), and chemotherapy-loaded nanoparticles or nanogels (Chen et al., 2017; Fang et al., 2017). Considering that Glut3 addiction is also a feature of GBM cancer stem cells (Flavahan et al., 2013), targeting this phenotype with an αvβ3 antagonist has the potential to eradicate the most aggressive and drug resistant subpopulation within the tumor.

AUTHOR CONTRIBUTIONS

E.C. designed and supervised the study, carried out experiments, analyzed and interpreted data, and wrote the paper. S.I wrote the code to analyze differential gene expression and gene enrichment for Freije dataset. K.E, T.V.S, F.C and J.S carried out experiments and contributed to discussions. S.I, K.E and T.V.S provided critical feedback on the manuscript. V.D, P-Y.D and P.M provided the patient-derived stem cells. K-L.G, T.M and J.S provided critical feedback and technical assistance. P.M, S.M.W, O.P.S, H.S, V.D, P-Y.D and D.A.C gave conceptual advice, contributed to discussions, and S.M.W. and D.A.C wrote the paper. All co-authors proofread the manuscript.

ACKNOWLEDGEMENTS

We thank B Walsh and M. Hall for technical support. We also thank M. Yebra, M. Gozo, B. Walsh, J. Desgrosellier, T. Rakhshandehroo, J. Wawrzyniak and H. Wettersten and members of Sarkaria and Chneiweiss lab for helpful discussions and collaboration. E.C. was supported by The Fonds National Suisse, D.A.C. was supported by NCI-CA45726. The authors also thank the Mayo SPORE in Brain Cancer (CA108961) for financial support.

REFERENCES

Adler, P., Kolde, R., Kull, M., Tkachenko, A., Peterson, H., Reimand, J., and Vilo, J. (2009). Mining for coexpression across hundreds of datasets using novel rank aggregation and visualization methods. Genome Biol *10*, R139.

Aguirre-Gamboa, R., Gomez-Rueda, H., Martinez-Ledesma, E., Martinez-Torteya, A., Chacolla-Huaringa, R., Rodriguez-Barrientos, A., Tamez-Pena, J. G., and Trevino, V. (2013). SurvExpress: an online biomarker validation tool and database for cancer gene expression data using survival analysis. PLoS ONE *8*, e74250.

Bhat, K. P., Salazar, K. L., Balasubramaniyan, V., Wani, K., Heathcock, L., Hollingsworth, F., James, J. D., Gumin, J., Diefes, K. L., Kim, S. H.*, et al.* (2011). The transcriptional coactivator TAZ regulates mesenchymal differentiation in malignant glioma. Genes Dev *25*, 2594-2609.

Birsoy, K., Possemato, R., Lorbeer, F. K., Bayraktar, E. C., Thiru, P., Yucel, B., Wang, T., Chen, W. W., Clish, C. B., and Sabatini, D. M. (2014). Metabolic determinants of cancer cell sensitivity to glucose limitation and biguanides. Nature *508*, 108-112.

Boado, R. J., Black, K. L., and Pardridge, W. M. (1994). Gene expression of GLUT3 and GLUT1 glucose transporters in human brain tumors. Brain Res Mol Brain Res *27*, 51-57.

Brennan, C. W., Verhaak, R. G., McKenna, A., Campos, B., Noushmehr, H., Salama, S. R., Zheng, S., Chakravarty, D., Sanborn, J. Z., Berman, S. H.*, et al.* (2013). The somatic genomic landscape of glioblastoma. Cell *155*, 462-477.

Chen, W., Zou, Y., Zhong, Z., and Haag, R. (2017). Cyclo(RGD)-Decorated Reduction-Responsive Nanogels Mediate Targeted Chemotherapy of Integrin Overexpressing Human Glioblastoma In Vivo. Small (Weinheim an der Bergstrasse, Germany) *13*.

Cheresh, D. A. (1987). Human endothelial cells synthesize and express an Arg-Gly-Asp-directed adhesion receptor involved in attachment to fibrinogen and von Willebrand factor. Proc Natl Acad Sci U S A *84*, 6471-6475.

Cirkel, G. A., Kerklaan, B. M., Vanhoutte, F., Van der Aa, A., Lorenzon, G., Namour, F., Pujuguet, P., Darquenne, S., de Vos, F. Y., Snijders, T. J.*, et al.* (2016). A dose escalating phase I study of GLPG0187, a broad spectrum integrin receptor antagonist, in adult patients with progressive high-grade glioma and other advanced solid malignancies. Investigational new drugs *34*, 184-192.

Cosset, E., Petty, T., Dutoit, V., Tirefort, D., Otten-Hernandez, P., Farinelli, L., Dietrich, P. Y., and Preynat-Seauve, O. (2016). Human tissue engineering allows the identification of active miRNA regulators of glioblastoma aggressiveness. Biomaterials *107*, 74-87.

Desgrosellier, J. S., and Cheresh, D. A. (2010). Integrins in cancer: biological implications and therapeutic opportunities. Nat Rev Cancer *10*, 9-22.

Desgrosellier, J. S., Lesperance, J., Seguin, L., Gozo, M., Kato, S., Franovic, A., Yebra, M., Shattil, S. J., and Cheresh, D. A. (2014). Integrin alphavbeta3 drives slug activation and stemness in the pregnant and neoplastic mammary gland. Dev Cell *30*, 295-308.

Fang, Y., Jiang, Y., Zou, Y., Meng, F., Zhang, J., Deng, C., Sun, H., and Zhong, Z. (2017). Targeted glioma chemotherapy by cyclic RGD peptide-functionalized reversibly core-

crosslinked multifunctional poly(ethylene glycol)-b-poly(epsilon-caprolactone) micelles. Acta biomaterialia *50*, 396-406.

Flavahan, W. A., Wu, Q., Hitomi, M., Rahim, N., Kim, Y., Sloan, A. E., Weil, R. J., Nakano, I., Sarkaria, J. N., Stringer, B. W.*, et al.* (2013). Brain tumor initiating cells adapt to restricted nutrition through preferential glucose uptake. Nat Neurosci *16*, 1373-1382.

Franovic, A., Elliott, K. C., Seguin, L., Camargo, M. F., Weis, S. M., and Cheresh, D. A. (2015). Glioblastomas require integrin alphavbeta3/PAK4 signaling to escape senescence. Cancer Res *75*, 4466-4473.

Freije, W. A., Castro-Vargas, F. E., Fang, Z., Horvath, S., Cloughesy, T., Liau, L. M., Mischel, P. S., and Nelson, S. F. (2004). Gene expression profiling of gliomas strongly predicts survival. Cancer Res *64*, 6503-6510.

Gladson, C. L., and Cheresh, D. A. (1991). Glioblastoma expression of vitronectin and the alpha v beta 3 integrin. Adhesion mechanism for transformed glial cells. J Clin Invest *88*, 1924-1932.

He, S., Cen, B., Liao, L., Wang, Z., Qin, Y., Wu, Z., Liao, W., Zhang, Z., and Ji, A. (2017). A tumor-targeting cRGD-EGFR siRNA conjugate and its anti-tumor effect on glioblastoma in vitro and in vivo. Drug delivery *24*, 471-481.

Jin, Z. H., Furukawa, T., Ohya, T., Degardin, M., Sugyo, A., Tsuji, A. B., Fujibayashi, Y., Zhang, M. R., Higashi, T., Boturyn, D.*, et al.* (2017). 67Cu-Radiolabeling of a multimeric RGD peptide for alphaVbeta3 integrin-targeted radionuclide therapy: stability, therapeutic efficacy, and safety studies in mice. Nuclear medicine communications *38*, 347-355.

Lathia, J. D., Mack, S. C., Mulkearns-Hubert, E. E., Valentim, C. L., and Rich, J. N. (2015). Cancer stem cells in glioblastoma. Genes Dev *29*, 1203-1217.

Mao, P., Joshi, K., Li, J., Kim, S. H., Li, P., Santana-Santos, L., Luthra, S., Chandran, U. R., Benos, P. V., Smith, L.*, et al.* (2013). Mesenchymal glioma stem cells are maintained by activated glycolytic metabolism involving aldehyde dehydrogenase 1A3. Proc Natl Acad Sci U S A *110*, 8644-8649.

Mason, W. P. (2015). End of the road: confounding results of the CORE trial terminate the arduous journey of cilengitide for glioblastoma. Neuro-oncology *17*, 634-635.

Mi, H., Poudel, S., Muruganujan, A., Casagrande, J. T., and Thomas, P. D. (2016). PANTHER version 10: expanded protein families and functions, and analysis tools. Nucleic Acids Research *44*, D336-D342.

Moroishi, T., Hansen, C. G., and Guan, K.-L. (2015). The emerging roles of YAP and TAZ in cancer. Nat Rev Cancer *15*, 73-79.

Nabors, L. B., Mikkelsen, T., Rosenfeld, S. S., Hochberg, F., Akella, N. S., Fisher, J. D., Cloud, G. A., Zhang, Y., Carson, K., Wittemer, S. M.*, et al.* (2007). Phase I and correlative biology study of cilengitide in patients with recurrent malignant glioma. J Clin Oncol *25*, 1651-1657.

Noushmehr, H., Weisenberger, D. J., Diefes, K., Phillips, H. S., Pujara, K., Berman, B. P., Pan, F., Pelloski, C. E., Sulman, E. P., Bhat, K. P.*, et al.* (2010). Identification of a CpG island methylator phenotype that defines a distinct subgroup of glioma. Cancer Cell *17*, 510-522.

Nutt, C. L., Mani, D. R., Betensky, R. A., Tamayo, P., Cairncross, J. G., Ladd, C., Pohl, U., Hartmann, C., McLaughlin, M. E., Batchelor, T. T.*, et al.* (2003). Gene expression-based classification of malignant gliomas correlates better with survival than histological classification. Cancer Res *63*, 1602-1607.

Paolillo, M., Serra, M., and Schinelli, S. (2016). Integrins in glioblastoma: Still an attractive target? Pharmacol Res *113*, 55-61.

Parsons, D. W., Jones, S., Zhang, X., Lin, J. C., Leary, R. J., Angenendt, P., Mankoo, P., Carter, H., Siu, I. M., Gallia, G. L.*, et al.* (2008). An integrated genomic analysis of human glioblastoma multiforme. Science *321*, 1807-1812.

Patel, A. P., Tirosh, I., Trombetta, J. J., Shalek, A. K., Gillespie, S. M., Wakimoto, H., Cahill, D. P., Nahed, B. V., Curry, W. T., Martuza, R. L.*, et al.* (2014). Single-cell RNA-seq highlights intratumoral heterogeneity in primary glioblastoma. Science *344*, 1396-1401.

Patronas, N. J., Di Chiro, G., Kufta, C., Bairamian, D., Kornblith, P. L., Simon, R., and Larson, S. M. (1985). Prediction of survival in glioma patients by means of positron emission tomography. J Neurosurg *62*, 816-822.

Phillips, H. S., Kharbanda, S., Chen, R., Forrest, W. F., Soriano, R. H., Wu, T. D., Misra, A., Nigro, J. M., Colman, H., Soroceanu, L.*, et al.* (2006). Molecular subclasses of high-grade glioma predict prognosis, delineate a pattern of disease progression, and resemble stages in neurogenesis. Cancer Cell *9*, 157-173.

Reardon, D. A., Fink, K. L., Mikkelsen, T., Cloughesy, T. F., O'Neill, A., Plotkin, S., Glantz, M., Ravin, P., Raizer, J. J., Rich, K. M.*, et al.* (2008). Randomized phase II study of cilengitide, an integrin-targeting arginine-glycine-aspartic acid peptide, in recurrent glioblastoma multiforme. J Clin Oncol *26*, 5610-5617.

Seguin, L., Kato, S., Franovic, A., Camargo, M. F., Lesperance, J., Elliott, K. C., Yebra, M., Mielgo, A., Lowy, A. M., Husain, H.*, et al.* (2014). An integrin beta(3)-KRAS-RalB complex drives tumour stemness and resistance to EGFR inhibition. Nat Cell Biol *16*, 457-468.

Stupp, R., Hegi, M. E., Gorlia, T., Erridge, S. C., Perry, J., Hong, Y. K., Aldape, K. D., Lhermitte, B., Pietsch, T., Grujicic, D.*, et al.* (2014). Cilengitide combined with standard treatment for patients with newly diagnosed glioblastoma with methylated MGMT promoter (CENTRIC EORTC 26071-22072 study): a multicentre, randomised, open-label, phase 3 trial. The lancet oncology *15*, 1100-1108.

Stupp, R., Mason , W. P., van den Bent , M. J., Weller , M., Fisher , B., Taphoorn , M. J. B., Belanger , K., Brandes , A. A., Marosi , C., Bogdahn , U.*, et al.* (2005). Radiotherapy plus Concomitant and Adjuvant Temozolomide for Glioblastoma. New England Journal of Medicine *352*, 987-996.

Verhaak, R. G., Hoadley, K. A., Purdom, E., Wang, V., Qi, Y., Wilkerson, M. D., Miller, C. R., Ding, L., Golub, T., Mesirov, J. P.*, et al.* (2010). Integrated genomic analysis identifies clinically relevant subtypes of glioblastoma characterized by abnormalities in PDGFRA, IDH1, EGFR, and NF1. Cancer Cell *17*, 98-110.

Wang, W., Xiao, Z.-D., Li, X., Aziz, K. E., Gan, B., Johnson, R. L., and Chen, J. (2015). AMPK modulates Hippo pathway activity to regulate energy homeostasis. Nat Cell Biol *17*, 490-499.

Weis, S. M., and Cheresh, D. A. (2011). Tumor angiogenesis: molecular pathways and therapeutic targets. Nature Medicine *17*, 1359-1370.

Weller, M., Nabors, L. B., Gorlia, T., Leske, H., Rushing, E., Bady, P., Hicking, C., Perry, J., Hong, Y. K., Roth, P.*, et al.* (2016). Cilengitide in newly diagnosed glioblastoma: biomarker expression and outcome. Oncotarget *advance online*.

Yan, H., Parsons, D. W., Jin, G., McLendon, R., Rasheed, B. A., Yuan, W., Kos, I., Batinic-Haberle, I., Jones, S., Riggins, G. J.*, et al.* (2009). IDH1 and IDH2 mutations in gliomas. N Engl J Med *360*, 765-773.

FIGURE LEGENDS

Figure 1. β3 levels correlate with poor survival in GBM and expression of genes involved in glucose metabolism

(A) Hierarchical clustering of integrin β subunit expression correlated to a risk score predicting the patient survival.

(B) Kaplan-Meier analysis of Freije dataset for ITGB3 (β3) expression (n = 42 β3 low, n = 43 β3 high; P-value (p) = 0.03). Low = low risk group; High: high risk group.

(C) Functional annotation clustering (series GSE4412, Freije dataset) of gene set enrichment analysis based on $\beta3^{high}$ versus $\beta3^{low}$ expression. Graph shows the percent enrichment for each family of genes.

(D) Kaplan-Meier analysis of Freije dataset for SLC2A3 (Glut3), ALDOC and PFKM expression. SLC2A3 (P-value=0.002); ALDOC (P-value=0.0065); PFKM (P-value=0.0003). See also figure S1, tableS1, S2 and S3.

(E) β3 and Glut3 expression are significantly correlated across a range of GBM datasets according to the MEM output.

Figure 2. The impact of integrin αvβ3 on GBM is attributed to its regulation of Glut3 expression

(A) Immunoblots show expression of indicated proteins for U87MG, LN229 and LN18 GBM cells infected by shRNA Control (Ctrl) or shβ3. Graph shows the fold change of protein expression determined by densitometry analysis.

(B) mRNA expression was determined by qPCR in U87MG, LN229 and LN18 infected with shRNA Control (shCtrl) or shβ3.

(C) Relative glucose uptake in U87MG, LN229 and LN18 cells with β3 knockdown compared to control (shCtrl).

(D) Bars represent the relative lactate production in U87MG and LN229 cells with β3 knockdown compared to control (shCtrl).

(E) Effect of β3 and Glut3 knockdown on anchorage-independent growth of U87MG under high (4.5 g/l) or low (0.4 or 0.8 g/L) glucose conditions.

(F) Effect of β3 and Glut3 knockdown on tumorsphere formation of U87MG under low glucose conditions (0.4 g/L).

(G) Flow cytometry was used to quantify $\beta3^+$ versus $\beta3^-$ as well as $Glut3^+$ versus $Glut3^-$ in a growth competition assay under low glucose conditions (0.4 g/L).

(H) Effect of β3 and Glut3 knockdown on tumor growth *in vivo*: U87MG shCtrl and U87MG β3 and Glut3 shRNA. (n=15 mice per group).

(I) Graph represents the fold change of β-galactosidase positive cells versus the total cell number. Inverted microscopy images of acidic senescence-associated β-galactosidase staining in U87MG shCtrl and U87MG β3 and Glut3 shRNA (n=5 fields counted per group).

(J) Cell-cycle analysis showing the percentage of cells in G0/G1, S, and G2/M in U87MG cells with β3 and Glut3 knockdown.

(K) Images show acidic senescence-associated β-galactosidase staining, a marker of senescence, in mice implanted with U87MG shCtrl, shβ3, shGlut3, or shβ3 with ectopic expression of Glut3. Scale bar, 100μM (top left). Scale bar, 25μM (top right).

(L) Flow cytometry was used to quantify U87MG shCtrl (GFP-) versus U87MG shβ3-Glut3+ (GFP+) in a growth competition assay.

(M) Effect of ectopic expression of Glut3 on U87MG β3 shRNA on anchorage-independence growth.

(N) Graph represents the fold change of β-galactosidase positive cells versus the total cell number. Inverted microscopy images of acidic senescence-associated β-galactosidase staining in U87MG β3 shRNA overexpressing Glut3 compared to U87MG shCtrl (n=5 fields counted per group).

(O) Effect of ectopic expression of Glut3 on tumor growth *in vivo*: U87MG shCtrl and U87MG β3 and Glut3 shRNA. (n=15 mice per group). This experiment was performed at the same time as the *in vivo* experiment shown in figure 2H.

Data are represented as mean (n=3-5) ± SEM (*p<0.05, **p<0.01 and ***p<0.001). See also figure S2.

Figure 3. β3 modulates Glut3 expression through PAK4-YAP/TAZ axis

(A) Kaplan-Meier analysis of Freije dataset for TAZ expression (n=42 for β3 low and n=43 for β3 high; P-value = 0.02). Low = low risk group; High: high risk group.

(B) Immunoblots show the effect of β3 knockdown on protein expression of YAP and β3. Bars represent the fold change of protein expression determined by densitometry analysis. Data are represented as mean (n=3-5) ± SEM (*p<0.05, **p<0.01 and ***p<0.001).

(C) Graph shows the effect of β3 knockdown on mRNA expression of YAP and TAZ determined by qRT-PCR, displayed as fold change for gene expression normalized to sh-control in U87MG (n=3), LN229 (n=3) and U251 (n=2).

(D) Immunoblots show the effect of YAP/TAZ knockdown on Glut3 protein expression, and the graph shows the fold increase determined by densitometry analysis. U87MG (n=3), LN229 (n=3) and U251 (n=2).

(E) Graph shows the effect of YAP/TAZ knockdown on mRNA expression for Glut3, YAP and TAZ determined by qRT-PCR, displayed as fold change of gene expression normalized to sh-control in U87MG (n=3) and LN229 (n=2).

(F) Acidic senescence-associated β-galactosidase staining in U87MG shCtrl versus YAP/TAZ shRNA (n=3). Scale bar, 50μM.

(G) Effect of ectopic expression of YAP on U87MG β3 shRNA on anchorage-independent growth in U87MG (n=3).

(H) Graph shows the fold change of protein expression in U87MG (n=2) and LN229 (n=2) determined by densitometry analysis.

(I) Acidic senescence-associated β-galactosidase staining in U87MG shCtrl and PAK4 siRNA (n=3).

(J) Cell-cycle analysis showing the percentage of cells in G0/G1, S, and G2/M in U87MG cells with PAK4 siRNA (n=3).

Data are represented as mean (n=2-5) ± SEM (*$p<0.05$, **$p<0.01$ and ***$p<0.001$). See also figure S2.

Figure 4. Integrin αvβ3 is required for Glut3 expression in patient-derived gliomaspheres that show heterogeneity in Glut3 “addiction”

(A) Representative immunoblots show expression of β3, Glut3, and TAZ in GSCs with a schematic representing the decision tree for selecting GSCs based on β3/Glut3 expression (n=2).

(B) Immunoblots show effect of β3 knockdown on expression of indicated proteins in Ge479 (n=3). Graph represents the fold change of protein expression relative to sh-control determined by densitometry analysis.

(C) Effect of glucose concentration on cell viability measured by CellTiter-Glo in GSCs (n=3-5).

(D) Effect of Glut3 knockdown on cell viability measured by CellTiter-Glo in GSCs (n=2-4).

(E) Expression of glycolytic, pentose phosphate and mitochondrial oxidative phosphorylation (OXPHOS) related genes were determined by qRT-PCR after β3 or Glut3 knockdown in Ge479 (n=3). Bars show the fold change of gene expression normalized to sh-control.

Data are represented as mean (n=2-5) ± SEM (*p<0.05, **p<0.01 and ***p<0.001). See also figure S4.

Figure 5. The Mesenchymal subtype of GBM is enriched for genes involved in glycolytic pathway and correspond to a Glut3 non-addicted genetic signature

(A) Enrichment analysis of glycolytic genes for the Freije dataset. Compared to other subtypes (Other sub), the Mesenchymal subtype showed high expression of Glut3, HK3,

PFKP, PGK1, LDHA, Glut5 and Glut10, and no or low expression of LDHB, PFKP and ALDOC.

(B) Kaplan-Meier analysis of Freije dataset for PGK1 expression (n=42 for β3 low and n=43 for β3 high; P=0.00000007).

(C) Enrichment analysis for β3, Glut3 (also found in figure 5A), YAP and TAZ.

(D) Glut3 addicted vs Glut3 non-addicted samples are identified using 96 signature genes. mRNA was determined by qRT-PCR (n=2) and Biorad software has been used for analysis. Only the most significant genes are shown. See also Table S5.

Figure 6. The Proneural/Classical subtype of GBM is sensitive to antagonists of αvβ3, YAP and PAK4

(A) Effect of LM609 (αvβ3 function blocking antibody) and cilengitide (cyclic peptide antagonist of αv integrins including αvβ3 and αvβ5) on cell viability measured by CellTiter-Glo in GSCs (n=3-5).

(B) Effect of YAP inhibitor (Verteporfin) or PAK4 inhibitor (PF-03758309) on cell viability measured by CellTiter-Glo in GSCs (n=3-5).

(C) Schematic depicting Mayo Clinic sample request. Samples were requested based on their Glut3 addicted vs non-addicted signature, samples have been requested then analyzed for cell viability in presence of cilengitide and LM609.

(D) Effect of LM609 (αvβ3 function blocking antibody) and cilengitide (cyclic peptide antagonist of αv integrins including αvβ3 and αvβ5) on Mayo Clinic GSCs cell viability measured by CellTiter-Glo in GSCs (n=3-5, except n=2 for GBM150 and GBM85).

(E) Effect of LM609 (αvβ3 function blocking antibody) and cilengitide (cyclic peptide antagonist of αv integrins including αvβ3 and αvβ5) on cell viability of Ge479 knockdown for β3, PAK4 and YAP/TAZ measured by CellTiter-Glo in GSCs (n=3-5). For Ge479 parental, the same data are displayed figure 6A.

(F) Effect of LM609 (αvβ3 function blocking antibody) and cilengitide (cyclic peptide antagonist of αv integrins including αvβ3 and αvβ5) on cell viability of GBM6 with ectopic expression of β3 measured by CellTiter-Glo in GSCs (n=3-5). For GBM6 parental, the same data are displayed figure 6A.

(G) Effect of Cilengitide on tumor growth. Mice bearing orthotopic Ge518 (Glut3 non-addicted) and Ge479 (Glut3 addicted) brain tumors were treated with vehicle or cilengitide (25mg $kg^{-}1$; 8 mice per group).

(H) Schematic depicting the proposed model of Glut3 addiction in GBM.

Data are represented as mean (n=3-5) ± SEM (*p<0.05, **p<0.01 and ***p<0.001). See also figure S5.

Table 1. List of genes differentially expressed based on $\beta3^{high}$ versus $\beta3^{low}$ expression for the Freije dataset. Only the top 180 genes are showed, ranked from 1 to 180. Only genes with adjusted P-value <0.05 have been considered for analysis. See also table S2A-2B.

SUPPLEMENTARY FIGURE & TABLE LEGENDS

Supplementary Figure 1. Relative to figure 1.

(A) β3 and Glut3 expression are significantly correlated across a range of datasets according to the MEM output.

Supplementary Figure 2. Relative to figure 2.

(A) Effect of β3 knockdown on U87MG, LN229 and LN18 cell viability in high (4.5µg/L) vs low (1µg/L) glucose measured by Alamar blue.

(B) Histological analysis of U87MG cells with shCtrl and shGlut3. Mice bearing U87MG shβ3 do not develop tumors. Tumors were stained for haematoxylin and eosin (H&E), β3 and Glut3. Scale bar, 50µM.

(C) Graph represents the fold change of β-galactosidase positive cells versus the total cell number. Inverted microscopy images of acidic senescence-associated β-galactosidase staining in LN229 and LN18 Ctrl, β3 and Glut3 siRNA (n=5 fields counted per group) (n=3).

(D) Cell-cycle analysis showing the percentage of cells in G0/G1, S, and G2/M in LN229 and U251 cells with β3 and Glut3 knockdown (n=3).

(E) Flow cytometry was used to quantify pH2A.X expression in LN229 cells with β3 and Glut3 knockdown. The graph shows the fold increase of pH2A.X expression. (n=2).

(F) Cell cycle analysis showing the percentage of cells in G0/G1, S, and G2/M for U87MG cells with knockdown of Glut1 or Glut6.

(G) Histological analysis of U87MG with shCtrl or β3 shRNA along with ectopic expression of Glut3 (Glut3^{+}). Tumors were stained for haematoxylin and eosin (H&E), β3 and Glut3. Scale bar, 50μM.

(H) Immunoblots show expression of β3 and Glut3 in U87MG with shCtrl, shGlut3 or β3 shRNA along with ectopic expression of Glut3 (Glut3^{+}) (n=3-4). The graph shows the fold change determined by densitometry analysis.

Data are represented as mean (n=3-5) ± SEM (*p<0.05, **p<0.01 and ***p<0.001).

Supplementary Figure 3. TAZ expression is correlated with poor survival and effect of YAP and PAK4 inhibitors, related to Figure 3.

(A) Effect of YAP inhibitor, Verteporfin on its target genes (CTGF and CYR61). Expression of CTGF, CYR61 and Glut3 were determined by qRT-PCR in LN229 (n=2) and U87MG (n=2). Graph shows the fold change for gene expression normalized to control.

(B) Representative immunoblots show expression of β3 and YAP in U87MG with shCtrl, shβ3, and shβ3 along with ectopic expression of YAP (YAP^{+}) (n=2).

(C) Effect of PAK4 inhibitor, PF-03758309 on the phosphorylation of PAK4 (pPAK4). Representative immunoblots show effect of PF-03758309 on expression of indicated proteins in U87MG (n=2).

(D) Effect of PAK4 inhibitor, PF-03758309 on the phosphorylation of PAK4 (pPAK4). Representative immunoblots show effect of PF-03758309 on expression of indicated proteins in Ge479 (n=2-3).

(E) Effect of PAK4 knock down on indicated proteins in U87MG (n=2) and LN229 (n=2).

(F) Effect of PAK4 knockdown on PAK4, β3, GLUT3 and YAP expression in LN229 (n=3) and U87MG (n=2). Graph shows the fold change for gene expression normalized to control.

Supplementary Figure 4. GSCs are tumorigenic and multipotent, related to Figure 4.

(A) Representative light micrograph showing H&E staining for Ge518 GSCs-derived tumor in immune-compromised mice (n = 3). Scale bar (upper left), 100µM. GSCs show invasive phenotype (right panel, top) (Scale bar, 100µM) and necrotic foci (right panel, bottom) (Scale bar, 50µM).

(B) GSCs are multipotent and can differentiate to form neurons (βIIITubulin) and astrocytes (GFAP). DAPI was used for nuclear counterstaining. Scale bar, 10µM.

(C) GSCs express cancer stem cell markers (CD133, Oct4 and Nanog). mRNA expression were determined by qPCR in all GSCs and normalized to housekeeping genes (HKGs).

(D-E) Histological analysis of brain GBM tissue array (GL805c). Bar graphs represent β3 and Glut3 expression level detected on tumor cells for 70 specimens (D). Tumors were stained for haematoxylin and eosin (H&E), β3 and Glut3 (E). Scale bar, 50µM.

(F) β3, TAZ and YAP mRNA were determined by qPCR for Ge479 (n=3).

(G) Graphs show the effect of β3 and Glut3 knockdown on mRNA expression of β3 and Glut3 determined by qRT-PCR, displayed as fold change for gene expression normalized to siCtrl in Ge518, Ge269 and Ge479 (n=2-4).

(H) Representative immunoblots showing expression of indicated proteins when ectopically expressed β3 is GBM6 (n=2).

(I) β3 and Glut3 expression was determined by qPCR in all GBM lines.

(J) mRNA was determined by qPCR in all GSCs. Several genes (listed in table 4) have been tested for each GBM subtypes. An enrichment score has been determined according to gene expression normalized to housekeeping genes.

Supplementary Figure 5. GSCs classification and enrichment analysis of glycolytic genes, relative to figure 5, figure 6 and Table S4.

(A) Enrichment analysis of glycolytic genes (HK2, ENO1, PFKM, GAPDH and ALDOA) in GBM patients.

(B-E) Kaplan-Meier analysis of Freije dataset for (B) PFKL expression (n = 42 β3 low, n = 43 β3 high; P = 0.041); (C) LDHA expression (n = 42 β3 low, n = 43 β3 high; P = 0.007); (D) LDHB expression (n = 42 β3 low, n = 43 β3 high; P = 0.03) and (E) GAPDH expression (n = 42 β3 low, n = 43 β3 high; P = 0.008).

(F) mRNA was determined by qRT-PCR (n=2) and Biorad software has been used for analysis.

(G) Histological analysis of Ge518 and Ge479 xenografts. Ge518 (n=2-3 mice) and Ge479 (n=3-4 mice) tumors were stained for haematoxylin and eosin (H&E), β3 (brown), Glut3 (blue) and CD31 (brown). Scale bar, 50µM.

Supplementary Table 1. β3 expression consistently predicts poor survival among several datasets (Freije, Lee and TCGA).

Supplementary Table 2. (A) List of genes differentially expressed based on $\beta3^{high}$ versus $\beta3^{low}$ expression for the Phillips dataset. Only the top 120 genes are showed, ranked from 1 to 120. Only genes with P-value <0.05 have been considered for analysis. (B) List of genes differentially expressed based on $\beta3^{high}$ versus $\beta3^{low}$ expression for the Sun dataset. Only the top 120 genes are showed, ranked from 1 to 120. Only genes with adjusted P-value <0.05 have been considered for analysis.

Supplementary Table 3. Correlation between ALDOC, PFKM and Glut3 expression with glioma patient survival among several datasets (Freije, Lee and TCGA).

Supplementary Table 4. List of primers used for qRT-PCR.

Supplementary Table 5. List of primers used for PCR (amp) and sequencing (seq) of IDH1 and IDH2.

Supplementary Table 6. List of genes defining Glut3 addicted vs non-addicted signature. Only genes with adjusted P-value <0.01 have been considered for analysis. Only genes highlighted in blue have been tested by qRT-PCR. * highlight genes consistent with GBM subtypes.

Supplementary Table 7. List of mutations found in GSCs.

Supplementary Table 8. Glut3 addicted vs non-addicted signature for Mayo Clinic GSCs extracted from Next Generation Sequencing (NGS) data. M = Mesenchymal, C = Classical, P = Proneural and N = Neural.

STAR METHODS:

Cell Culture. GBM cell lines were cultured in DMEM supplemented with 10% fetal bovine serum, L-glutamine and antibiotics. All cell lines were routinely tested for mycoplasma. Ge269, 479, 518, 688, 738, 835, 885, 898, 904, 970.2 were gifts from Dr. Valérie Dutoit and Dr. Pierre-Yves Dietrich to Dr E. Cosset and cultured in DMEM/F12 with Glutamax supplemented with B27 supplement and b-FGF, EGF both at 10ng/ml with antibiotics (GSC medium). GBM6 and GBM39 were gifts from Dr. Paul Mischel and cultured in GSC medium. GBM64, 14, 85, 26, 12, 150 and 59 were requested from the Mayo Clinic Brain Tumor Patient-Derived Xenograft National Resource from Dr. Jann Sarkaria and cultured in GSC medium.

Chemicals. Verteporfin (YAP inhibitor) was purchased from Sigma and used at the concentration of 0.5-10µM for 24 hours. PF-03758309 (PAK4 inhibitor) was purchased from Chemietek and used at the concentration of 50nM-1000nM or 50-100nM (for established cell lines and GSCs respectively) during 24 hours.

Isolation and cultivation of gliomaspheres and GBM cells. Isolation of glioblastoma-initiating cells was performed as described (Cosset et al., 2016). Briefly, viable fragments of high-grade human GBM were transferred to a beaker containing 0.25% trypsin in 0.1 mM EDTA (4:1) and slowly stirred at 37°C for 30-60 minutes. Dissociated cells were split and some of them were plated in 75-cm2 tissue culture flasks at 2,500-5,000 cells per cm^2) in DMEM/F-12 medium (1:1) containing N2 and B27 supplements (all from Invitrogen, Carlsbad, CA, http://www.invitrogen.com) supplemented with bFGF and EGF both at 10 ng/ml (Invitrogen). Once established, GSCs were maintained in GSC medium.

Multipotency. GSCs were plated on coverslips coated with poly-L-ornithine and were grown in DMEM complete medium for 2 weeks. Cells were fixed in 4% PFA and incubated overnight with the following antibodies: GFAP (Sigma-Aldrich) and anti-β-Tubulin (Covance). After washing, anti-mouse Alexa565 and anti-rabbit Alexa 488 were used as secondary antibodies. Nuclei were counterstained with DAPI. Image acquisition was done with a Nikon Eclipse C1 Confocal microscope.

Soft agar assay. 4000 cells were seeded in 48-well plates containing 0.3% agar/DMEM medium no glucose with 10% dialyzed FBS on top of a bottom layer of 1% agar. 200µl of additional DMEM medium with 10% dialyzed FBS ± glucose (0-4.5g/L) was added, and cells cultured for 15 days. Colonies were stained with 0.1% crystal violet/20% methanol/PBS and counted.

Cell viability assay. U87MG, LN229, and LN18 cells were seeded at 1K cells per well in black 96-well plates in DMEM medium (no glucose) with 10% dialyzed FBS ± glucose (0-4.5g/L). Cell viability was determined by Alamar Blue dye (Life Technologies) according to manufacturer's instructions. For GSCs, cells were seeded at 10K cells per well in white 96-well low attachment plates in GSC medium ± glucose (0-4.5g/L). Viable cell numbers were evaluated using CellTiter-Glo assay kit (Promega). Each condition consisted of, at least, three replicate wells and data were expressed as relative luciferase units or as the percentage of survival of control cells.

Cell transfection (small interfering RNA and plasmids). siRNAs against β3, Glut3, Glut1, Glut6 or PAK4 were transfected using lipofectamine 2000 (Invitrogen), a final concentration of 5nM. Two non-targeting scramble siRNAs (Life Technologies) were used as control. The pcDNAGlut3 plasmid were kindly provided by Dr. Yosuke Maeda

(Kumamoto University) and were transfected using Lipofectamine 3000 (Invitrogen). The transfection efficiency was monitored by qRT-PCR and/or immunoblotiing. All transfections were performed according to the manufacturer's protocols.

Genetic knockdown and expression constructs. Cells were infected with shRNAs for vector control (shCtrl, Open Biosystems), Glut3 (Santa Cruz Biotechnology), β3 and PAK4 (Open Biosystems) or YAP/TAZ (provided by Dr. K-L Guan) using a lentiviral system. pLENTIβ3 was obtained by subcloning the human β3 cDNA of pENTRβ3 vector in the pLENTI expression vector. pRETROYAP was kindly provided by Dr. K-L Guan. Gene silencing or overexpressing was confirmed by either immunoblot analysis or qPCR analysis.

Tumorsphere formation assay. 1K cells were seeded in low attachment plates in DMEM with Glutamax supplemented with B27 supplement, 20ng/ml of bFGF and EGF, and glucose (0.4-4.5 g/L). The number of tumorspheres was counted after 10-15 days.

Cell cycle and cell synchronization. Cells were synchronized by double-thymidine treatment. Medium was replaced with thymidine-free medium allowing cells to re-enter the cell cycle. After transfection, 100K cells were fixed in cold 70% ethanol, incubated overnight at -20°C, stained using propidium iodide, and subjected to flow cytometry analysis for cell cycle.

SA-β-galactosidase staining. 20K cells were seeded in DMEM complete medium for 5 days and stained with the senescence SA-β-galactosidase staining kit (Cell Signaling) according to the manufacturer's protocol. For *in vivo* studies, staining were performed on frozen sections.

Competition mixing assay. Cells co-cultured were seeded at a 1:1 ratio and maintained in DMEM complete medium or low glucose for 7 days. At Day 0 and Day 7, cells were analyzed by flow cytometry for stable expression of GFP or RFP/YFP.

Glucose uptake assay. Cells were seeded in a 6well plates at a density of 300,000 cells per well in DMEM complete medium. On the next day, the cells were washed twice in PBS and incubated in serum-glucose free medium for 2 hours. The medium was then removed, the cells were incubated for 1 hour in DMEM medium with 1g/L of glucose. The uptake was determined by using Glucose Assay Kit (Eton Bioscience) according to the manufacturer's protocol.

Lactate production assay. Cells were seeded in a 6well plates at a density of 300,000 cells per well in DMEM complete medium. On the next day, the cells were washed twice in PBS and incubated in serum-glucose free medium for 2 hours. The medium was then removed, the cells were incubated for 1 hour in DMEM medium with 1g/L of glucose. The uptake was determined by using L-Lactate assay Kit (Eton Bioscience) according to the manufacturer's protocol.

Flow cytometry. 200'000 cells were stained with pH2A.X antibody (Cell signaling) for 1 hour in PBS/BSA 1%. After wash, cells were incubated with Alexa 488 goat anti-mouse secondary antibody four 1 hour. Then, cells were analyzed by flow cytometry.

Reverse transcription quantitative PCR (RT-qPCR). Isolation of total RNA and miRNAs were performed by using RNeasy kit from Qiagen according to the manufacturer's instructions. RNA concentration was determined using a spectrometer. 500ng of total RNA was used to synthesize cDNA using a TAKARA kit according to

manufacturer's protocol. When not available, primer sequences were designed using Invitrogen primer design and primer3 tools, and are summarized in **supplementary Table 4**. Real-time PCR was performed using SYBR Green reagent and a Bio-Rad system (Applied Biosystems) according the manufacturer's instructions. Efficacy tests have been performed, and all primers have been validated prior utilization. The relative level of each sample was normalized to, at least, two housekeeping genes (EEF1A1, ALAS1, Cyclophilin A and/or Tuba2). RT-PCR reactions were carried out in technical and biological duplicates or triplicates, and the average cycle threshold (CT) values were determined.

PCR and sequencing. Genomic DNA was extracted from GSCs using DNeasy (Qiagen) following manufacturer instructions. PCR was used to amplify exon 4 of IDH1 and exon 2 of IDH2 (**supplementary table 5**), as previously described (Parsons et al., 2008; Yan et al., 2009), and then DNA was sent for sequencing. For Ge479, Ge518 and Ge835, we also used the Ion Ampliseq Cancer Hotspot Panel v2 which covers 2800 mutations for 50 genes associated with cancer.

GBM subtyping. GSCs gene expression has been assessed by qRT-PCR. All primers are listed in **Supplemental Table 4** according to Proneural, Neural, Classical and Mesenchymal subtypes. Genes involved in the glycolytic, Pentose Phosphate Pathway (PPP) and mitochondrial oxidative phosphorylation (OXPHOS) pathways are listed as well.

Immunoblotting. Proteins were extracted in RIPA buffer and quantified using the Pierce BCA kit (Thermo Fisher). 10-30µg of protein was boiled in NuPage buffer (Thermo Fisher) and loaded onto a denaturing SDS-polyacrylamide gel (10%), transferred to PVDF

membranes and blotted with anti-mouse or -rabbit HRP-conjugated secondary antibodies (Bio-Rad). The following antibodies were used for immunoblotting: β3 (Cell Signaling), Glut3 (Santa Cruz Biotechnology), YAP (Santa Cruz) YAP-XP (cell signaling), TAZ (Cell Signaling), PAK4 and pPAK4 (Cell Signaling), and Vinculin and β-actin (Sigma-Aldrich) as loading controls.

Histological analysis (Immunochemistry and Immunofluorescence). For immunohistochemical staining of formalin-fixed paraffin-embedded tissues, antigen retrieval was performed in citrate buffer at pH 6.0 and 95°C for 20 minutes. Sections were blocked then incubated overnight at 4°C in primary antibody integrin αvβ3 (LM609) or β3 (Cell signaling), Glut3 (Santa Cruz Biotechnology), GFAP (cell signaling), βIIITubulin (Sigma-Aldrich), Nestin (Fisher Scientific), CD133 (Miltenyi Biotech) followed by biotin-conjugated anti-rabbit IgG and an avidin-biotin peroxidase detection system with 3,3'-diaminobenzidine substrate (Vector) then counterstained with hematoxylin. A Nikon Eclipse C1 Confocal microscope as well as a Nikon Eclipse TE2000-E were used for imaging.

***In vivo* experiments.** All experiments were performed according to the protocol S05018 and approved by the UCSD Institutional Animal Care and Use Committee. The number of mice used for each experiments is indicated in the corresponding figures.

Orthotopic brain tumor xenografts. Intracranial transplantation of U87MG or GSC (Ge518 and Ge479) into 6-8-week-old nu/nu nude immunocompromised mice (Charles River Labs) was performed in accordance with the UCSD Institutional Animal Care and Use Committee. U87MG cells bearing β3, Glut3 shRNA or shβ3 ectopically expressing Glut3 as well as shRNA control (15 mice per group) were orthotopically transplanted

following washing and resuspension in PBS. Ge479 and Ge518 were orthotopically transplanted following washing and resuspension in DMEM/F12. Mice were treated with vehicle (PBS) or cilengitide (25mg kg^{-1}; 8 mice per group) five days per week. Briefly, with a stereotaxic frame (Stoelting Co.), a small burr hole was made in the skull 2 mm anterior and 2 mm lateral to the bregma. A 31-gauge Hamilton needle/syringe was inserted 3 mm, and 0.25 µl/minute was dispensed (10^5 tumor cells in 2 µl media). A total of 1 x 10^5 and 3 x 10^5 cells in 2µl was injected respectively for U87MG cells and GSCs respectively. Animals were monitored daily and those exhibiting signs of morbidity and/or development of neurological symptoms were euthanized.

Analysis of microarray data. Affymetrix Human Genome U133A Array (GPL96) CEL files were obtained for the Frejie dataset from GEO with the accession number **GSE4412**. The sample description files were downloaded from the supplementary material of Flavahan et al (Flavahan et al., 2013). Microarray data was analyzed with R version 3.3.1 software. Survival analysis was performed for the Frejie dataset, and coefficients from Cox proportional hazards regression model (R function coxph) determined in a multivariate model for each probeset. Then, similar to Survexpress (Aguirre-Gamboa et al., 2013), a Prognostic Index was calculated as the sum of weighted expression values, where weights were previously retrieved coefficents from the Cox model. The samples were then equally divided according to the Prognostic Index. Samples with above median prognostic indices belonged to the high risk group and samples below median Prognostic Indices belonged to the low risk group. Differential gene expression analysis on the Frejie dataset for β3 and Glut3 was performed using the limma package (version 3.28.21), and GBM subgroup enrichment calculations were performed using hypergeometric probability

distribution (R function dhyper). Panther analysis was used for graphing differential gene expression analysis (Mi et al., 2016). MEM (Multi Experiment Matrix) was used for co-expression between Glut3 and β3 expression (Adler et al., 2009). The StDev threshold for Glut3 was set to 0.29. Distance was measured by both Pearson and Spearman's rank correlation distance, and the betaMEM method was used to determine the P-value. Survexpress (Aguirre-Gamboa et al., 2013) was also used to retrieve P-value for Kaplan-Meier analysis of β3, Glut3, ALDOC, PFKM and WWTR1 from Freije (GSE4412, GPL96, 85 samples), Lee (GSE13041, GPL96, 218 samples) and The Cancer Genome Atlas (TCGA) (GBM-LGG and GBM, June 2016, 538 and 518 samples respectively) datasets. All probesets were used for Kaplan-Meier analysis. TCGA dataset was harvested for generating the hierarchical cluster for all integrin β subunits, and survival months was used as a censor with Cox survival analysis (Aguirre-Gamboa et al., 2013). For the Freije dataset, the Mesenchymal, Classical, Proneural and Neural subtypes correspond to HC2B, HC2A, HC1A and HC1B respectively, according to gene expression profile.

Statistics. All statistical analyses were performed using the Student paired t test. We also performed an analysis of variance applying a bivariate analysis. Significant P-values ($p<0.05$) is indicated in the text of the results and/or figure legends. Data are representative of results obtained in the indicated number of independent experiments. For *in vivo* experiments, all statistical analyses were carried out using Prism software (GraphPad). Chi-squared tests or *t*-tests were used to calculate statistical significance.

Supplemental data. The Supplemental Data include 5 supplemental figures and 8 supplemental tables.

A

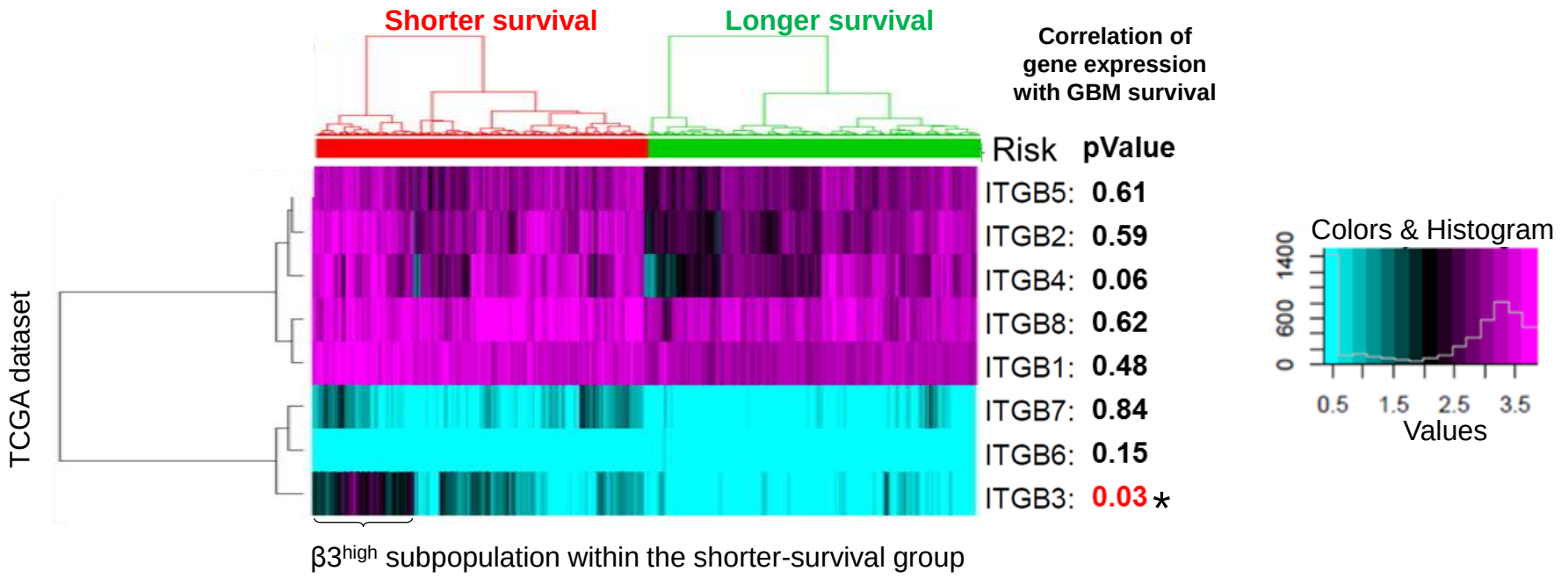
Shorter survival
Longer survival
Correlation of gene expression with GBM survival
Risk
pValue
ITGB5: 0.61
ITGB2: 0.59
ITGB4: 0.06
ITGB8: 0.62
ITGB1: 0.48
ITGB7: 0.84
ITGB6: 0.15
ITGB3: 0.03 *
TCGA dataset
β3high subpopulation within the shorter-survival group
Colors & Histogram
0
600
1400
0.5
1.5
2.5
3.5
Values

B

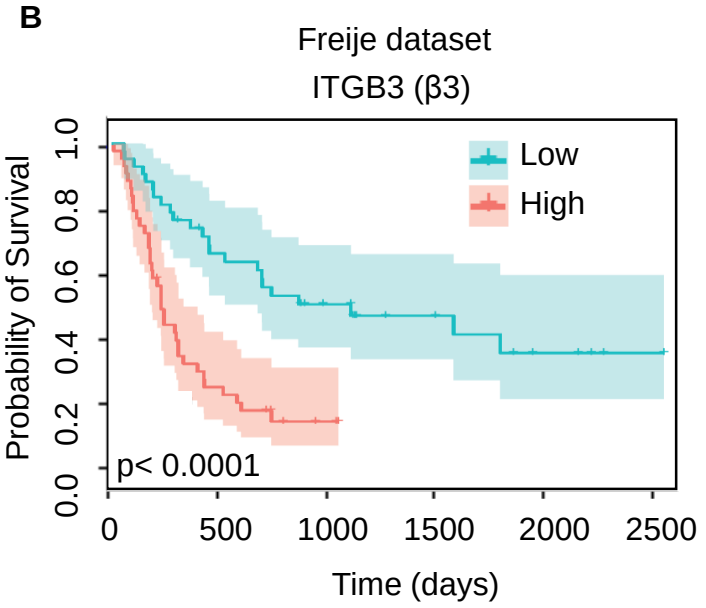
Freije dataset
ITGB3 (β3)
Low
High
Probability of Survival
0.0
0.2
0.4
0.6
0.8
1.0
p< 0.0001
0
500
1000
1500
2000
2500
Time (days)

C

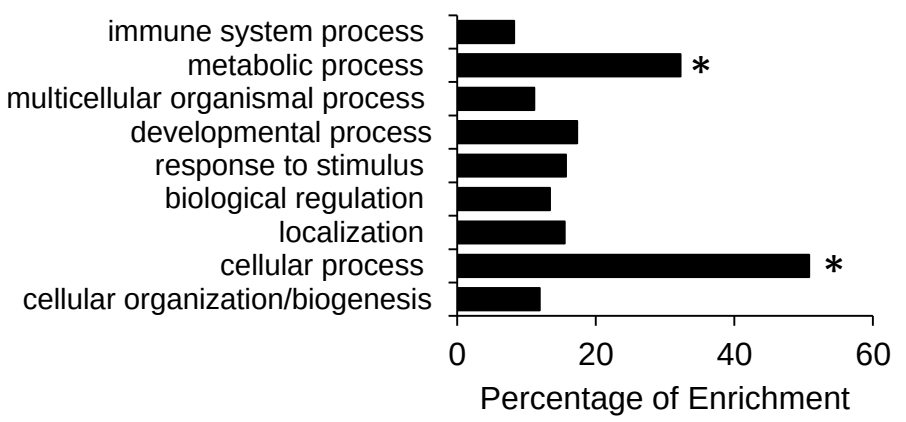
immune system process
metabolic process *
multicellular organismal process
developmental process
response to stimulus
biological regulation
localization
cellular process *
cellular organization/biogenesis
0
20
40
60
Percentage of Enrichment

D

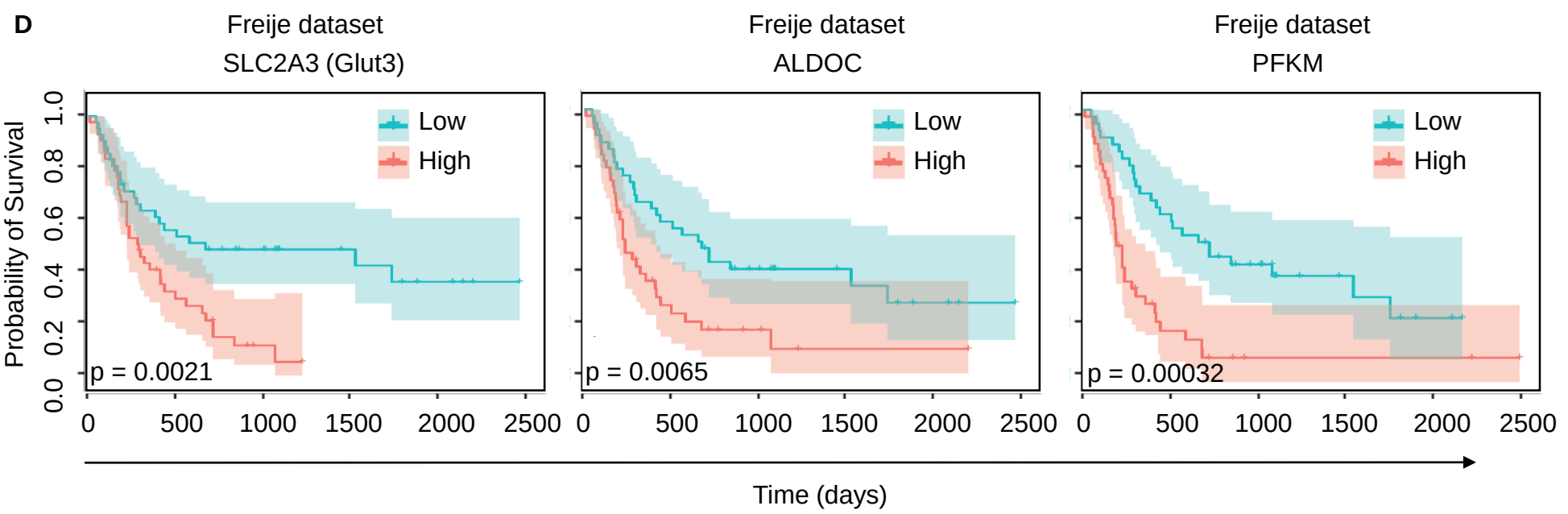
Freije dataset
SLC2A3 (Glut3)
ALDOC
PFKM
Low
High
Probability of Survival
0.0
0.2
0.4
0.6
0.8
1.0
p = 0.0021
p = 0.0065
p = 0.00032
0
500
1000
1500
2000
2500
Time (days)

E

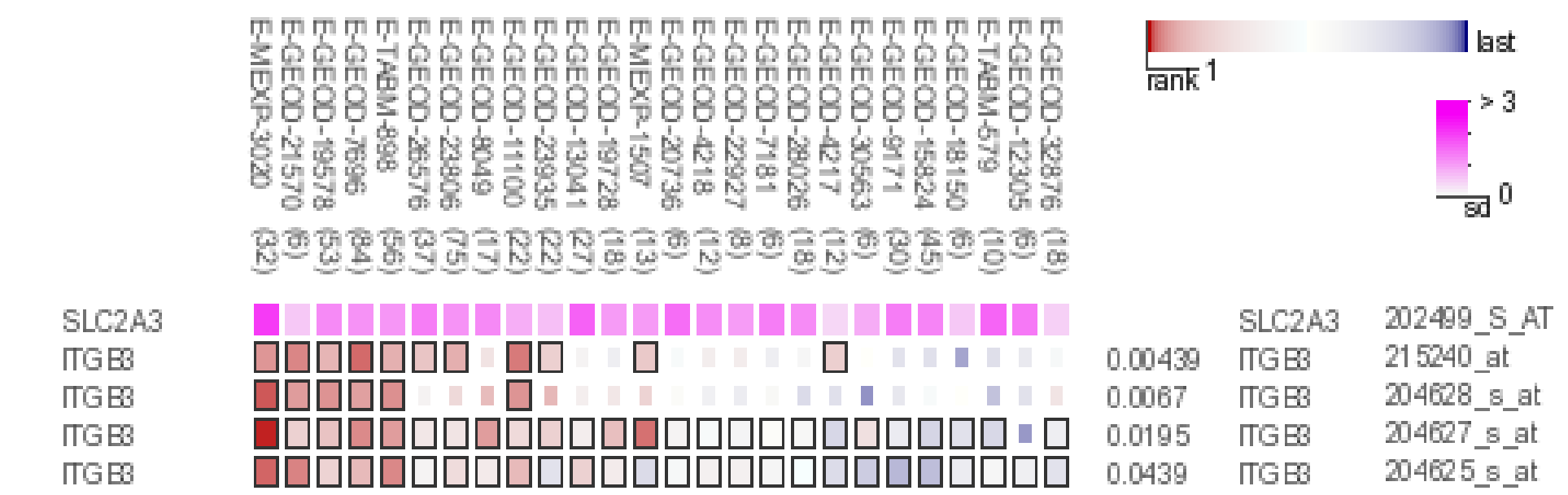
E-MEXP-3020 (32)
E-GEOD-21570 (6)
E-GEOD-19578 (53)
E-GEOD-7696 (84)
E-TABM-838 (56)
E-GEOD-26576 (37)
E-GEOD-23806 (75)
E-GEOD-8049 (17)
E-GEOD-11100 (22)
E-GEOD-23935 (22)
E-GEOD-13041 (27)
E-GEOD-19728 (18)
E-MEXP-1507 (13)
E-GEOD-20736 (6)
E-GEOD-4218 (12)
E-GEOD-22927 (8)
E-GEOD-7181 (6)
E-GEOD-28026 (18)
E-GEOD-4217 (12)
E-GEOD-30563 (6)
E-GEOD-9171 (30)
E-GEOD-15824 (45)
E-GEOD-18150 (6)
E-TABM-579 (10)
E-GEOD-12305 (6)
E-GEOD-32876 (18)
last
rank 1
> 3
0
sd
SLC2A3
ITGB3
ITGB3
ITGB3
ITGB3
0.00439
0.0067
0.0195
0.0439
SLC2A3 202499_S_AT
ITGB3 215240_at
ITGB3 204628_s_at
ITGB3 204627_s_at
ITGB3 204625_s_at

Table 1

Rank	Gene names	Rank	Gene names	Rank	Gene names	Rank	Gene names	Rank	Gene names	Rank	Gene names
1	THRA	31	SPATA2	61	ABAT	91	BHLHE40	121	CAMK2G	151	LIMCH1
2	ALDOC	32	SUSD4	62	CAMTA1	92	CYP46A1	122	OGFOD3	152	RAB6B
3	FXYD6	33	TCEAL2	63	BEX4	93	FAM127A	123	COL6A1	153	ARHGEF4
4	ITPR3	34	FAM192A	64	PIK3R1	94	ITGA4	124	ICAM1	154	LAMB1
5	FTO	35	RAB27A	65	MAPT	95	PAAF1	125	RBMS1	155	APC
6	NRXN1	36	ABHD10	66	FDFT1	96	DZIP3	126	NRP1	156	NFE2L3
7	ITGB3	37	GORASP1	67	TJP2	97	NRP2	127	GMFB	157	C1ORF61
8	CLASP2	38	C14ORF132	68	RUFY3	98	TRAPPC2L	128	CPD	158	LOX
9	AKTIP	39	NCOA1	69	NDUFS1	99	ERBB4	129	MYO18A	159	B3GAT1
10	WWTR1	40	KIF5C	70	HEXB	100	ADD3	130	ABAT	160	TSSC1
11	THRA	41	CLCN6	71	LAMC1	101	ANKRD46	131	LAMA4	161	NRXN1
12	SHC1	42	SERPINE1	72	GTDC1	102	NRP2	132	GNAZ	162	UGGT1
13	OMG	43	NDRG2	73	KDELR3	103	PFN2	133	KCNQ2	163	ICAM1
14	SVIL	44	TTYH1	74	ATP9A	104	BLCAP	134	ZNF189	164	SLC6A1
15	TSPYL4	45	ACO2	75	MAPT	105	NAP1L3	135	TUBB4A	165	SLC2A3
16	OSMR	46	DESI1	76	SC5D	106	PKIA	136	KIF5C	166	HMGCS1
17	BCAT1	47	PMAIP1	77	SLC9A6	107	PFKM	137	CA12	167	CEP68
18	KIF1B	48	APBA2	78	ALDH5A1	108	TPM4	138	ATP8A1	168	BCR
19	CTNND2	49	ADGRB3	79	WEE1	109	NOL12	139	TMEM35B	169	EDEM1
20	TNFRSF10B	50	NCAN	80	SLC22A17	110	MAPT	140	RBMS1	170	ABHD6
21	IQGAP1	51	NRXN2	81	CTIF	111	COL6A1	141	ASRGL1	171	NGRN
22	GABARAPL2	52	SLC20A1	82	RTN3	112	FDFT1	142	PIK3R1	172	DOPEY1
23	IQGAP1	53	PRKACB	83	SDC1	113	MR1	143	MARCKSL1	173	NCOA1
24	NRXN2	54	NTM	84	ADAM22	114	HIP1R	144	THTPA	174	BEX1
25	WASF3	55	NUDT3	85	ADGRE5	115	N/A	145	ANXA2P2	175	APC
26	ITPR3	56	PLCB1	86	SCN3A	116	NCALD	146	CHSY1	176	RUNX1
27	FUT9	57	MMP14	87	PTBP2	117	KIF21B	147	COL6A1	177	KCNB1
28	SHC1	58	CLIP3	88	RAB27A	118	SEC24A	148	MAP1A	178	PPP2R2B
29	CLASP2	59	VMP1	89	TNFRSF12A	119	GDF15	149	WASF1	179	LOX
30	PEA15	60	ADD1	90	APBA2	120	GRIA2	150	ACACA	180	PHLPP1

Fig. 2

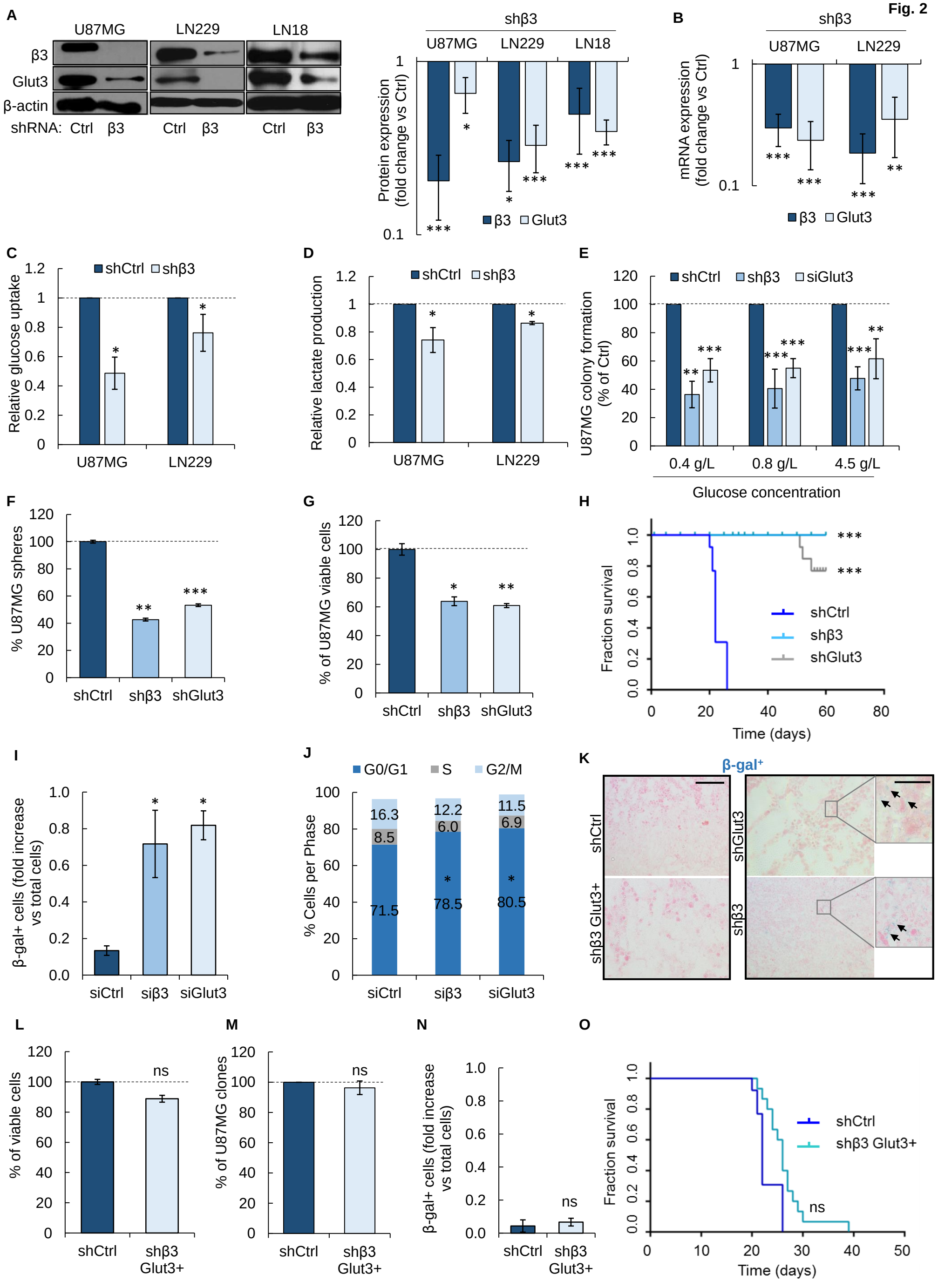
A
U87MG
LN229
LN18
β3
Glut3
β-actin
shRNA: Ctrl β3 Ctrl β3 Ctrl β3
shβ3
U87MG LN229 LN18
Protein expression (fold change vs Ctrl)
β3 Glut3
B
shβ3
U87MG LN229
mRNA expression (fold change vs Ctrl)
β3 Glut3
C
shCtrl shβ3
Relative glucose uptake
U87MG LN229
D
shCtrl shβ3
Relative lactate production
U87MG LN229
E
shCtrl shβ3 siGlut3
U87MG colony formation (% of Ctrl)
0.4 g/L 0.8 g/L 4.5 g/L
Glucose concentration
F
% U87MG spheres
shCtrl shβ3 shGlut3
G
% of U87MG viable cells
shCtrl shβ3 shGlut3
H
Fraction survival
shCtrl
shβ3
shGlut3
Time (days)
I
β-gal+ cells (fold increase vs total cells)
siCtrl siβ3 siGlut3
J
G0/G1 S G2/M
% Cells per Phase
16.3 8.5 71.5
12.2 6.0 78.5
11.5 6.9 80.5
siCtrl siβ3 siGlut3
K
β-gal+
shCtrl
shGlut3
shβ3 Glut3+
shβ3
L
% of viable cells
ns
shCtrl shβ3 Glut3+
M
% of U87MG clones
ns
shCtrl shβ3 Glut3+
N
β-gal+ cells (fold increase vs total cells)
ns
shCtrl shβ3 Glut3+
O
Fraction survival
shCtrl
shβ3 Glut3+
ns
Time (days)

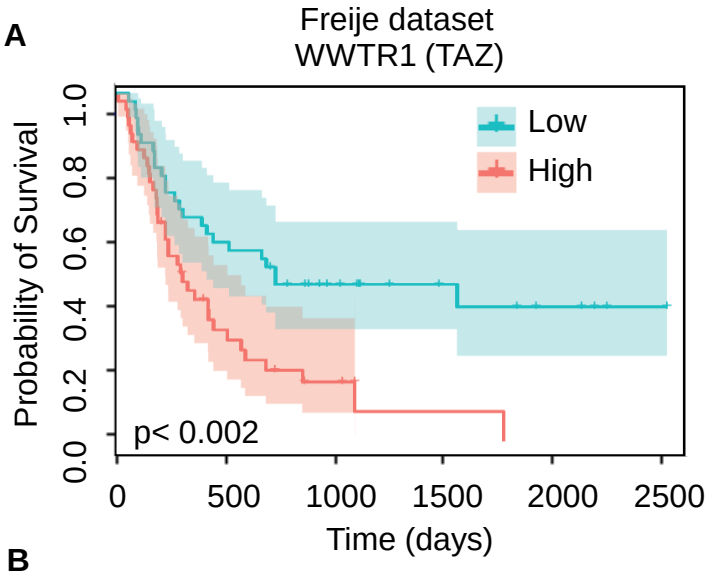
A
Freije dataset
WWTR1 (TAZ)
Probability of Survival
0.0
0.2
0.4
0.6
0.8
1.0
Low
High
p< 0.002
0
500
1000
1500
2000
2500
Time (days)

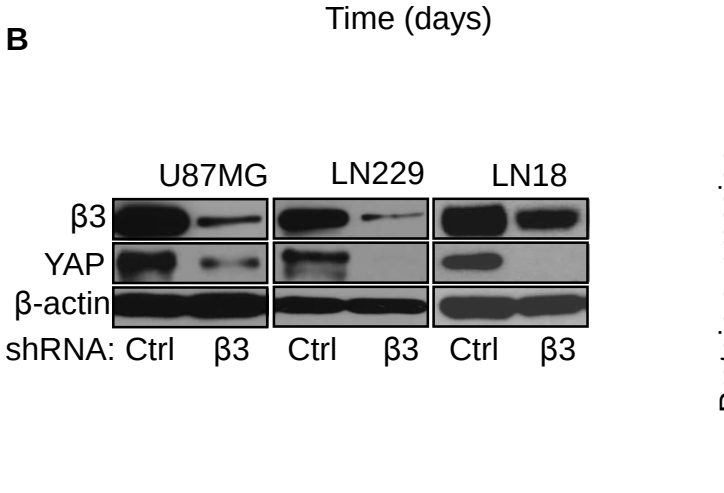
B
U87MG
LN229
LN18
β3
YAP
β-actin
shRNA: Ctrl β3 Ctrl β3 Ctrl β3

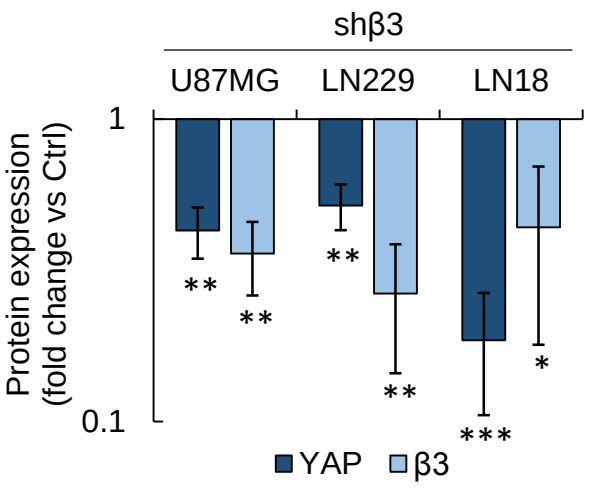
shβ3
U87MG
LN229
LN18
Protein expression (fold change vs Ctrl)
1
0.1
YAP
β3

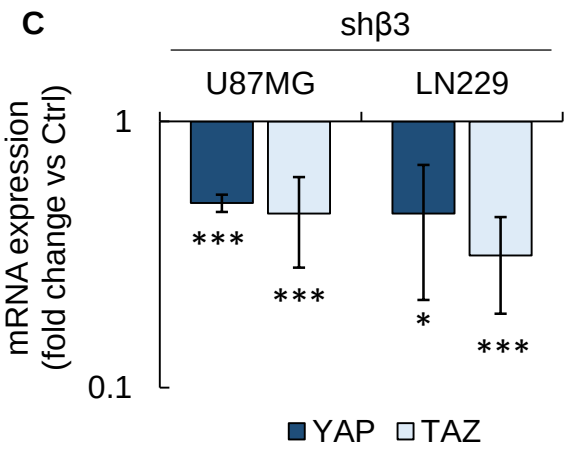
C
shβ3
U87MG
LN229
mRNA expression (fold change vs Ctrl)
1
0.1
YAP
TAZ

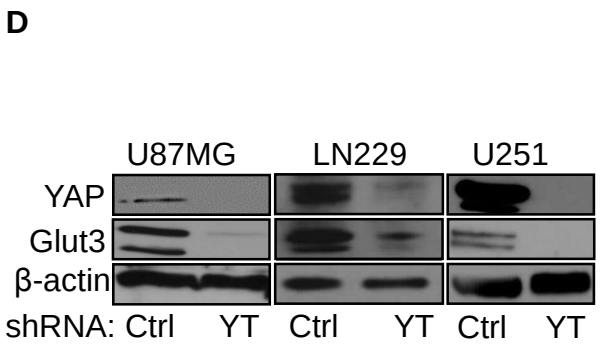
D
U87MG
LN229
U251
YAP
Glut3
β-actin
shRNA: Ctrl YT Ctrl YT Ctrl YT

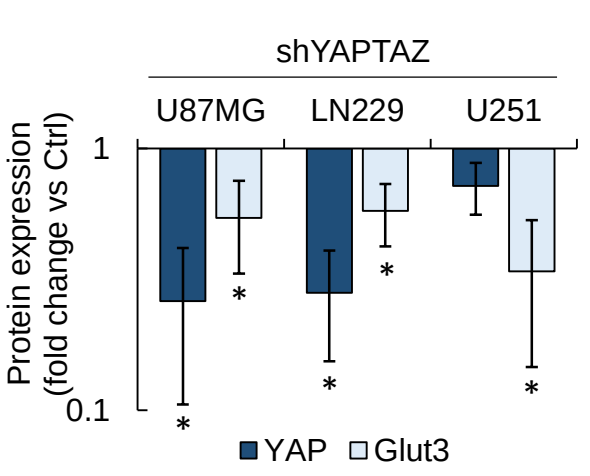
shYAPTAZ
U87MG
LN229
U251
Protein expression (fold change vs Ctrl)
1
0.1
YAP
Glut3

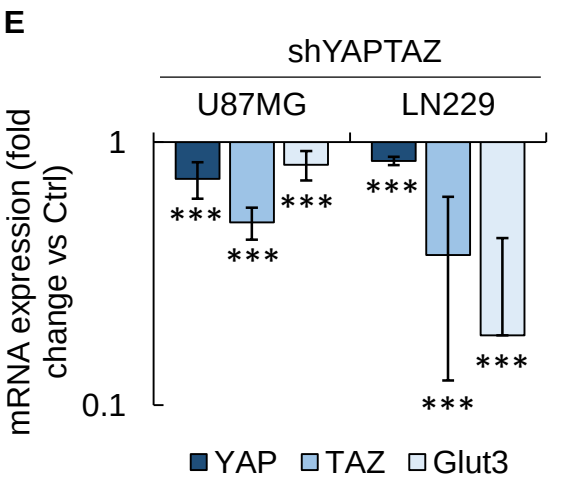
E
shYAPTAZ
U87MG
LN229
mRNA expression (fold change vs Ctrl)
1
0.1
YAP
TAZ
Glut3

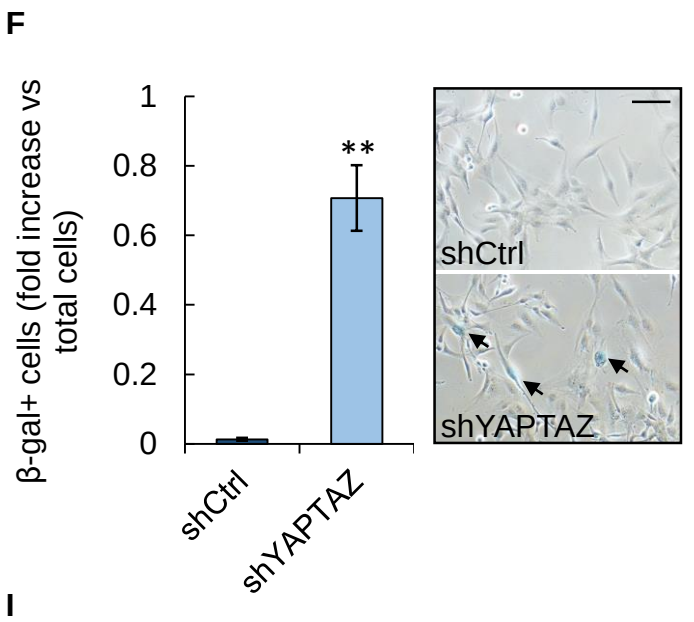
F
β-gal+ cells (fold increase vs total cells)
1
0.8
0.6
0.4
0.2
0
shCtrl
shYAPTAZ
shCtrl
shYAPTAZ

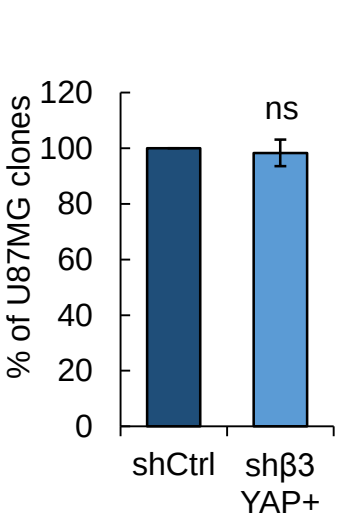
G
% of U87MG clones
120
100
80
60
40
20
0
ns
shCtrl
shβ3 YAP+

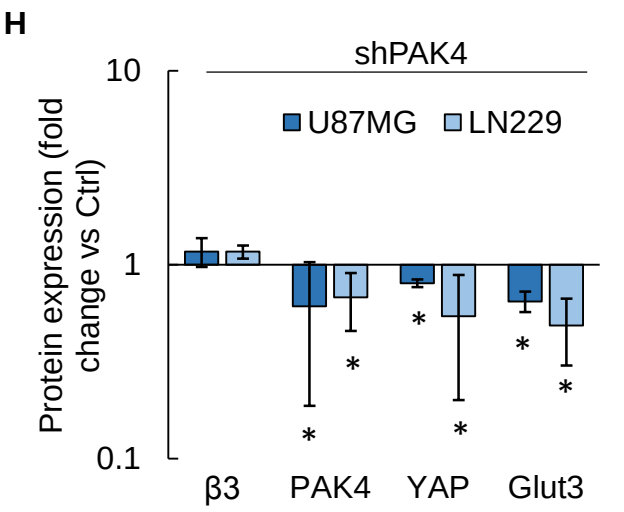
H
shPAK4
U87MG
LN229
Protein expression (fold change vs Ctrl)
10
1
0.1
β3
PAK4
YAP
Glut3

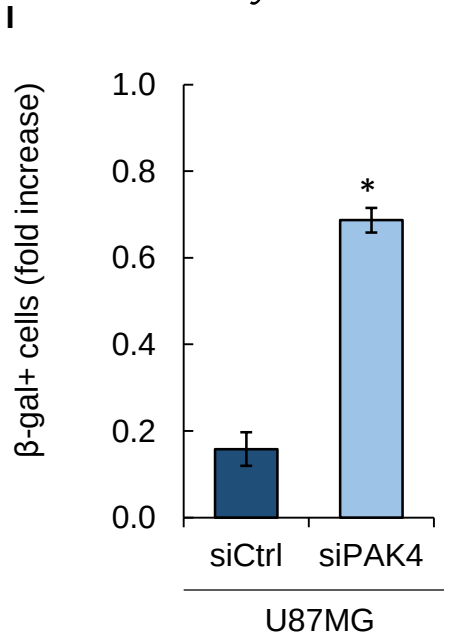
I
β-gal+ cells (fold increase)
1.0
0.8
0.6
0.4
0.2
0.0
siCtrl
siPAK4
U87MG

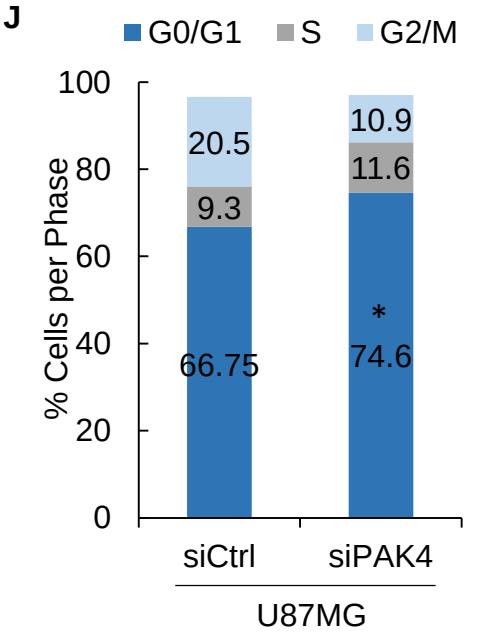
J
G0/G1
S
G2/M
% Cells per Phase
100
80
60
40
20
0
20.5
9.3
66.75
10.9
11.6
74.6
siCtrl
siPAK4
U87MG

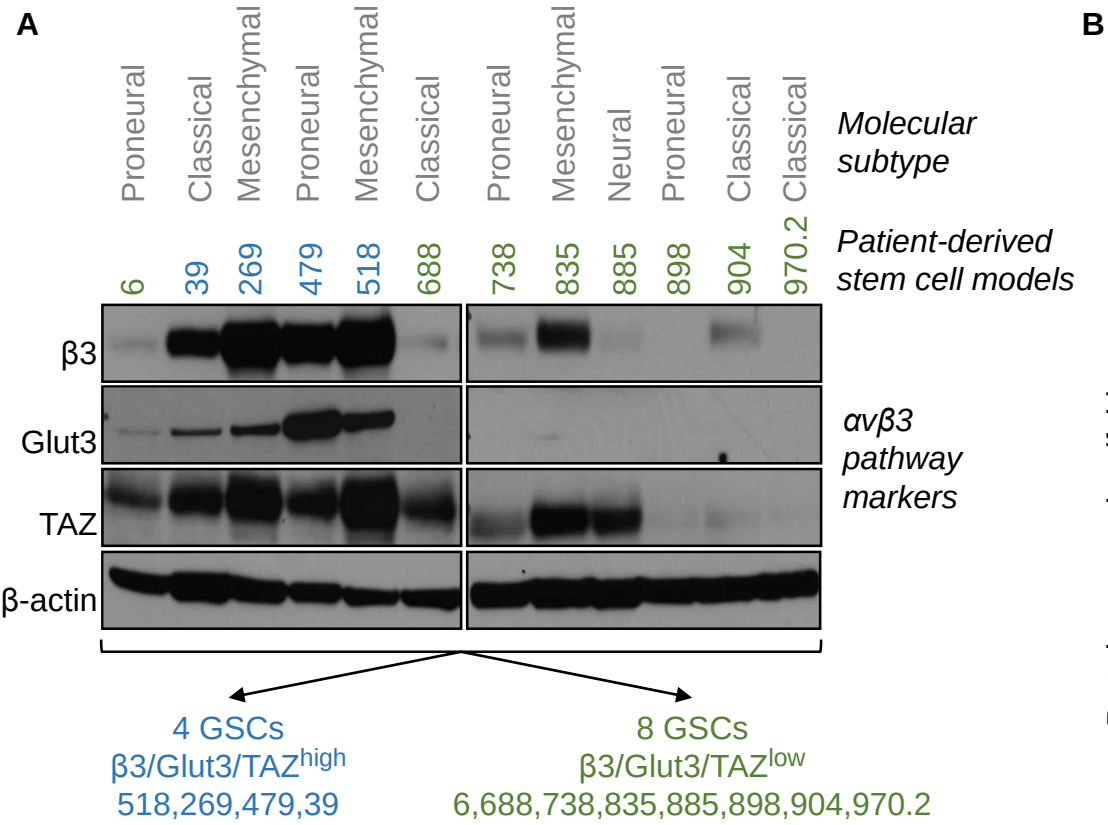
A
Proneural
Classical
Mesenchymal
Proneural
Mesenchymal
Classical
Proneural
Mesenchymal
Neural
Proneural
Classical
Classical
Molecular subtype
6
39
269
479
518
688
738
835
885
898
904
970.2
Patient-derived stem cell models
β3
Glut3
TAZ
β-actin
αvβ3 pathway markers
4 GSCs
β3/Glut3/TAZhigh
518,269,479,39
8 GSCs
β3/Glut3/TAZlow
6,688,738,835,885,898,904,970.2

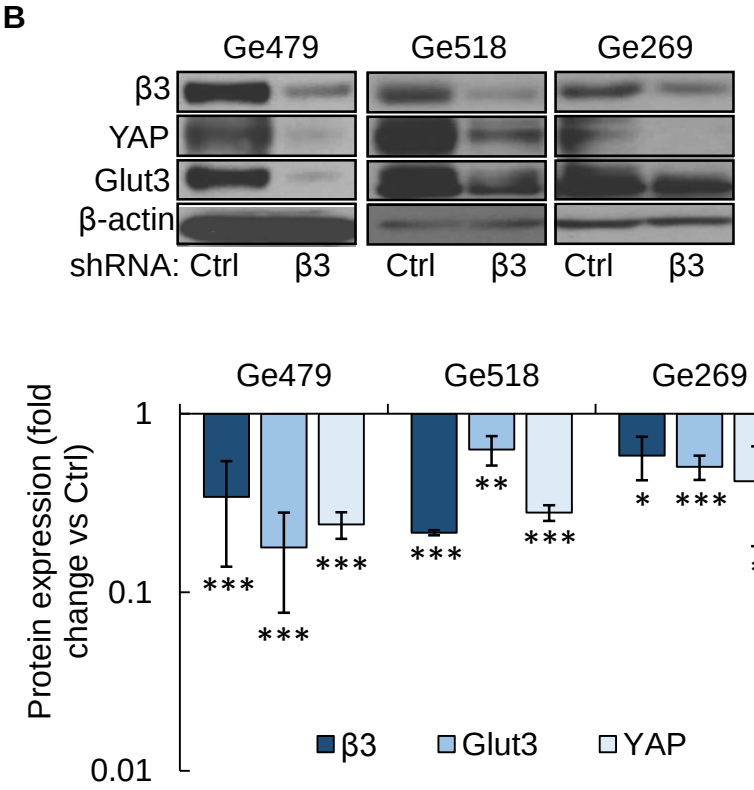
B
Ge479
Ge518
Ge269
β3
YAP
Glut3
β-actin
shRNA: Ctrl β3 Ctrl β3 Ctrl β3
Protein expression (fold change vs Ctrl)
1
0.1
0.01
β3
Glut3
YAP

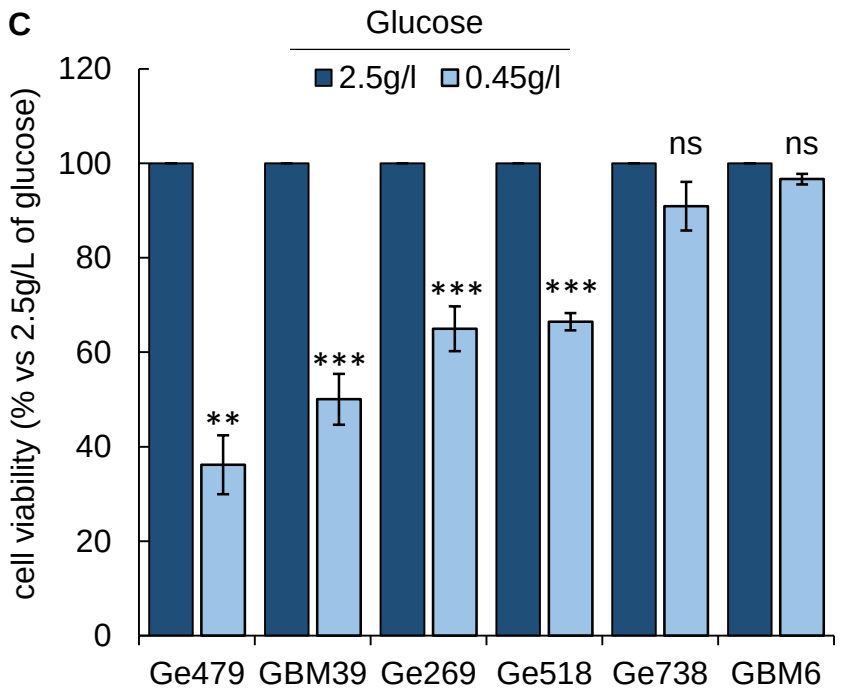
C
Glucose
2.5g/l
0.45g/l
cell viability (% vs 2.5g/L of glucose)
120
100
80
60
40
20
0
ns
Ge479
GBM39
Ge269
Ge518
Ge738
GBM6

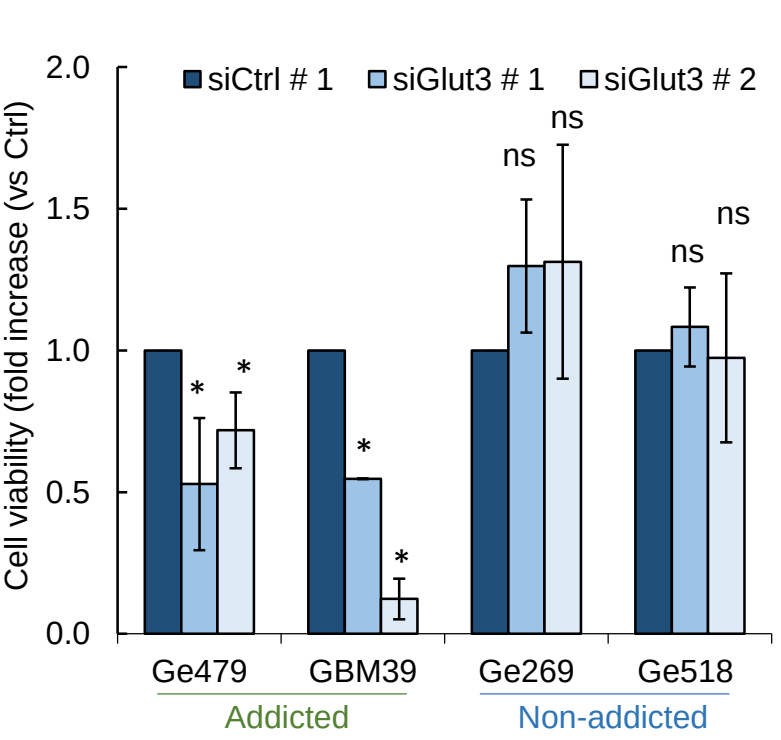
D
siCtrl # 1
siGlut3 # 1
siGlut3 # 2
Cell viability (fold increase (vs Ctrl)
2.0
1.5
1.0
0.5
0.0
ns
Ge479
GBM39
Ge269
Ge518
Addicted
Non-addicted

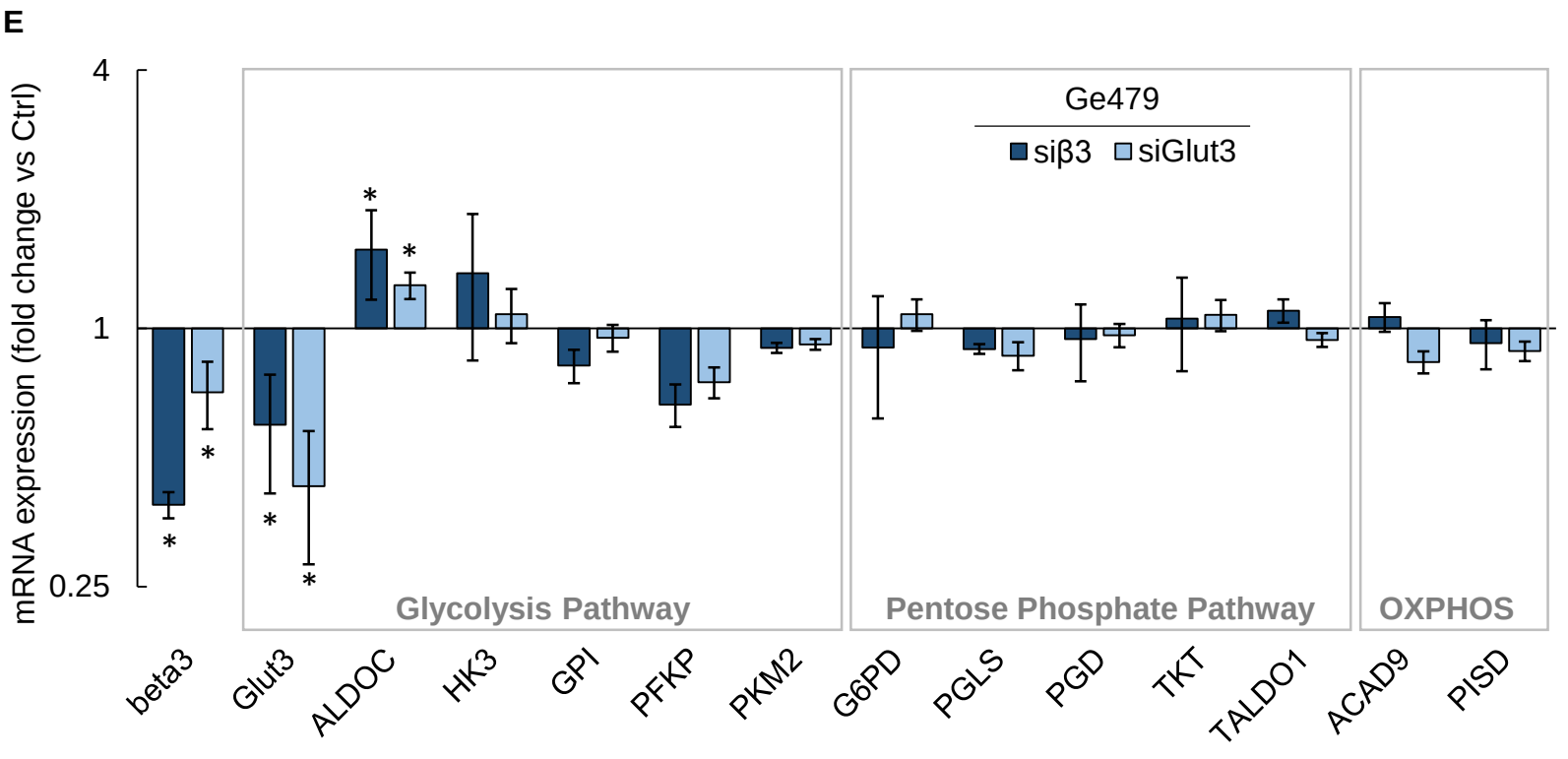
E
mRNA expression (fold change vs Ctrl)
4
1
0.25
Ge479
siβ3
siGlut3
Glycolysis Pathway
Pentose Phosphate Pathway
OXPHOS
beta3
Glut3
ALDOC
HK3
GPI
PFKP
PKM2
G6PD
PGLS
PGD
TKT
TALDO1
ACAD9
PISD

A

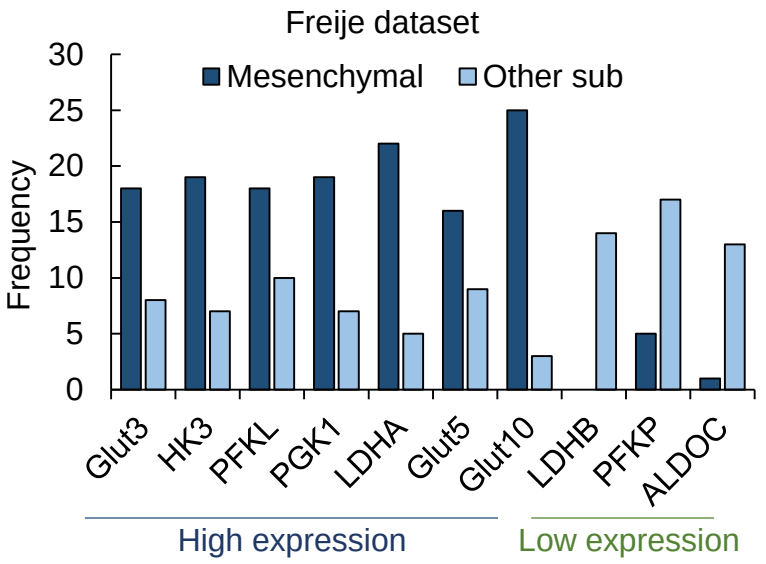
Freije dataset
Mesenchymal
Other sub
Frequency
30
25
20
15
10
5
0
Glut3
HK3
PFKL
PGK1
LDHA
Glut5
Glut10
LDHB
PFKP
ALDOC
High expression
Low expression

B

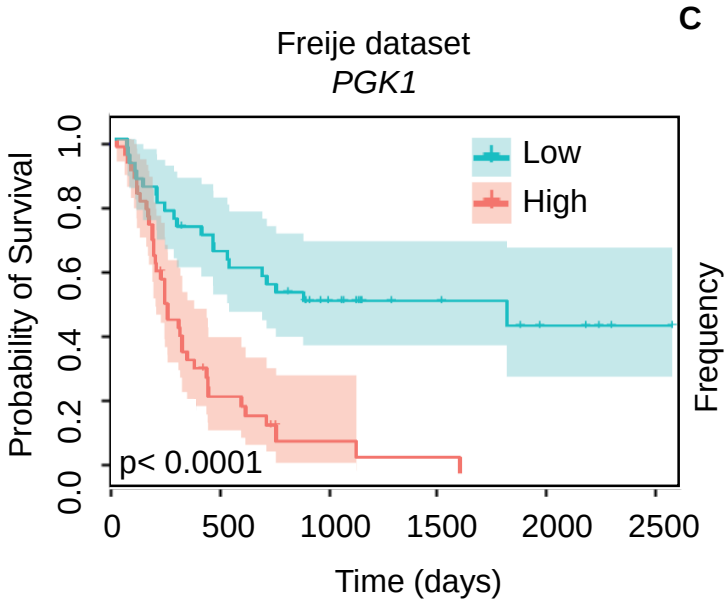
Freije dataset
PGK1
Probability of Survival
1.0
0.8
0.6
0.4
0.2
0.0
Low
High
p< 0.0001
0
500
1000
1500
2000
2500
Time (days)

C

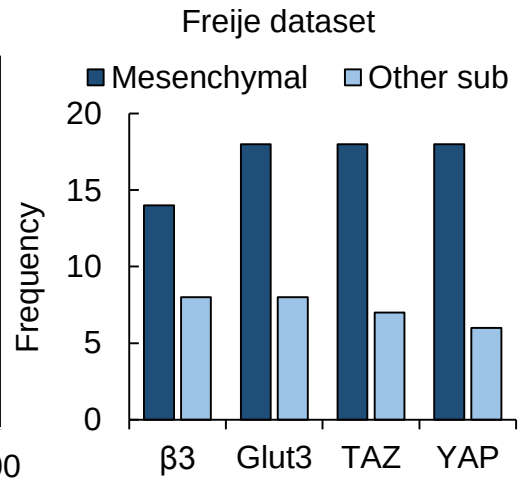
Freije dataset
Mesenchymal
Other sub
Frequency
20
15
10
5
0
β3
Glut3
TAZ
YAP

D

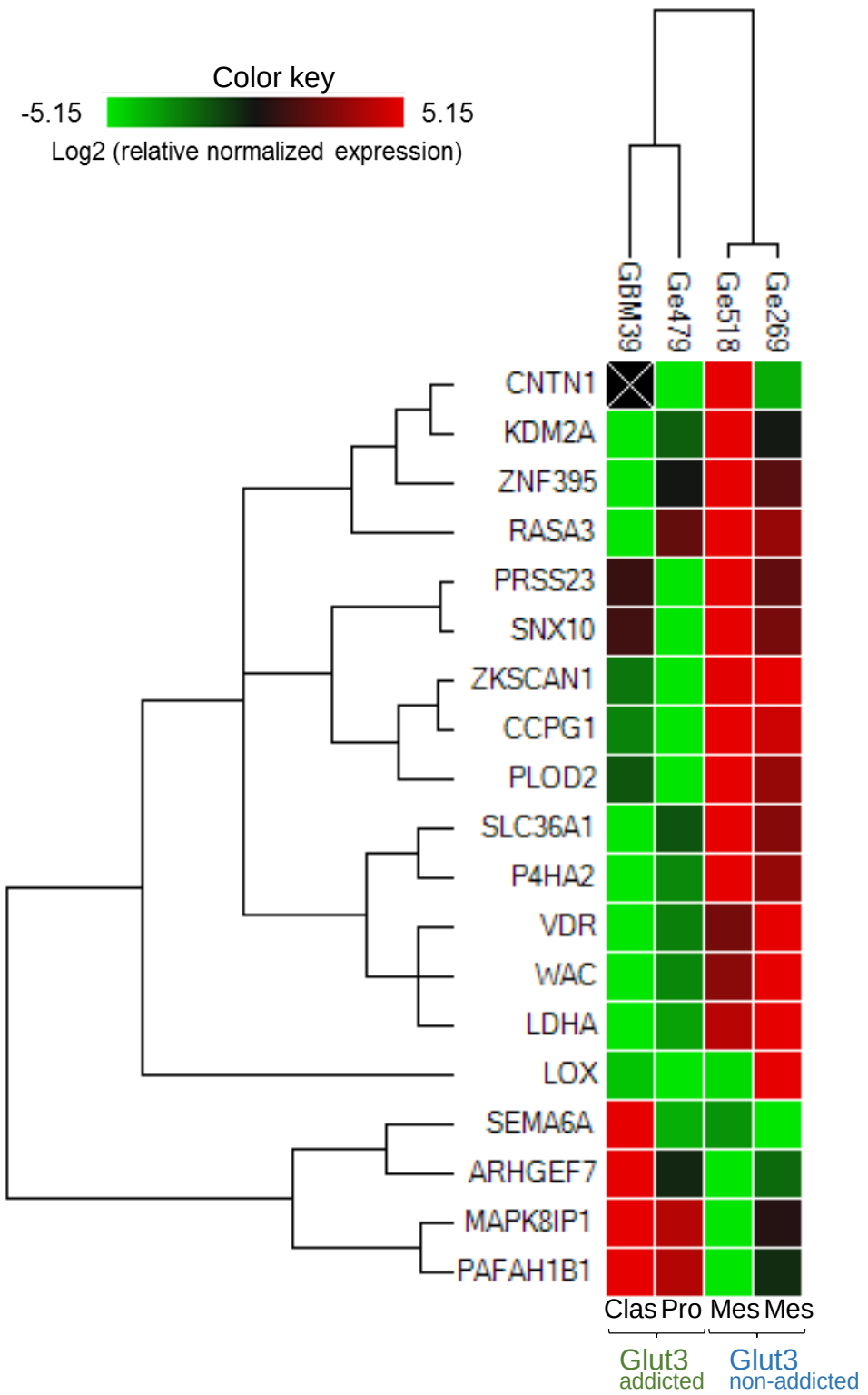
Color key
-5.15
5.15
Log2 (relative normalized expression)
GBM39
Ge479
Ge518
Ge269
CNTN1
KDM2A
ZNF395
RASA3
PRSS23
SNX10
ZKSCAN1
CCPG1
PLOD2
SLC36A1
P4HA2
VDR
WAC
LDHA
LOX
SEMA6A
ARHGEF7
MAPK8IP1
PAFAH1B1
Clas
Pro
Mes
Mes
Glut3
addicted
Glut3
non-addicted

A

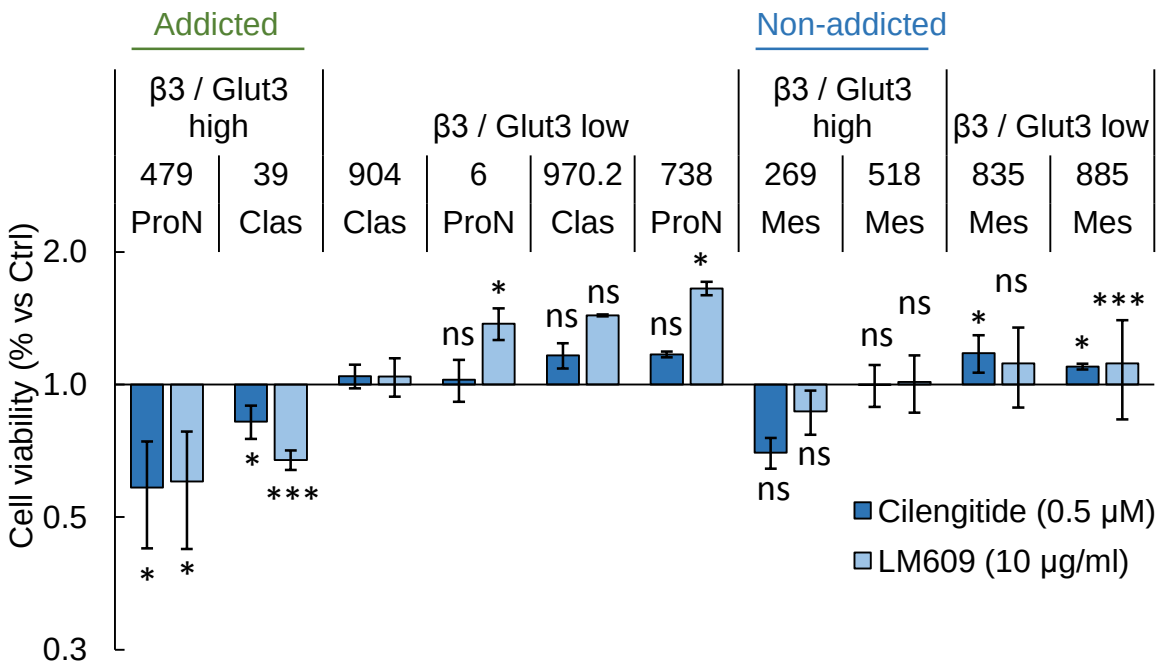
Addicted
Non-addicted
β3 / Glut3 high
β3 / Glut3 low
β3 / Glut3 high
β3 / Glut3 low
479 ProN
39 Clas
904 Clas
6 ProN
970.2 Clas
738 ProN
269 Mes
518 Mes
835 Mes
885 Mes
Cell viability (% vs Ctrl)
2.0
1.0
0.5
0.3
Cilengitide (0.5 µM)
LM609 (10 µg/ml)

B

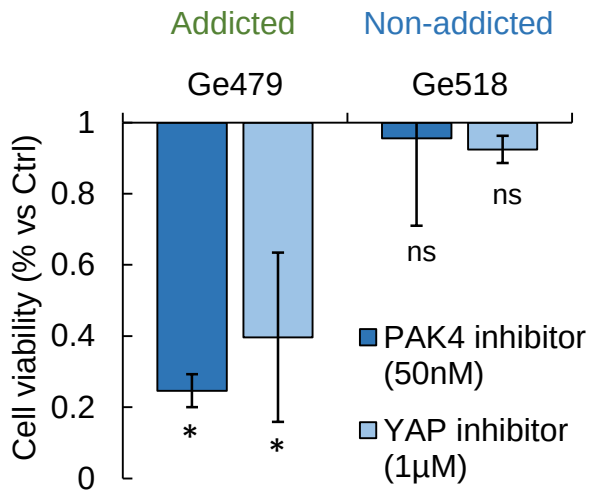
Addicted
Non-addicted
Ge479
Ge518
Cell viability (% vs Ctrl)
1
0.8
0.6
0.4
0.2
0
PAK4 inhibitor (50nM)
YAP inhibitor (1µM)

C

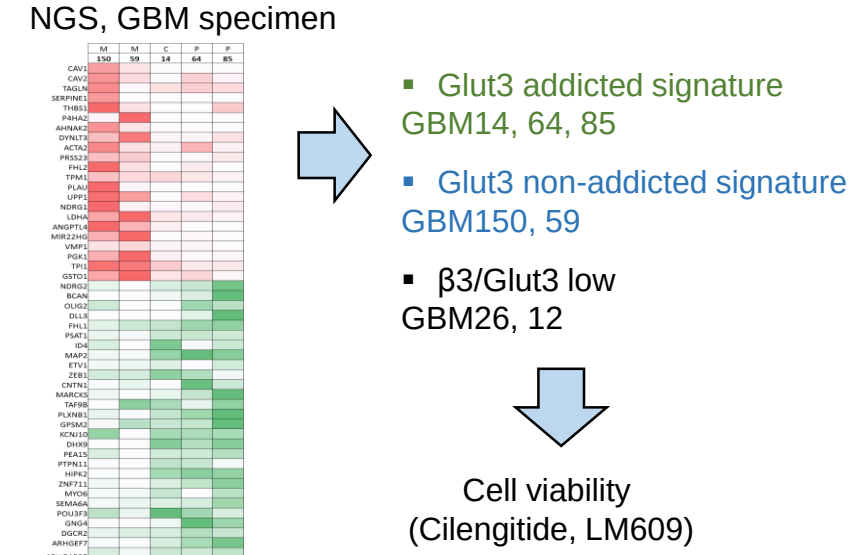
NGS, GBM specimen
Glut3 addicted signature
GBM14, 64, 85
Glut3 non-addicted signature
GBM150, 59
β3/Glut3 low
GBM26, 12
Cell viability
(Cilengitide, LM609)

D

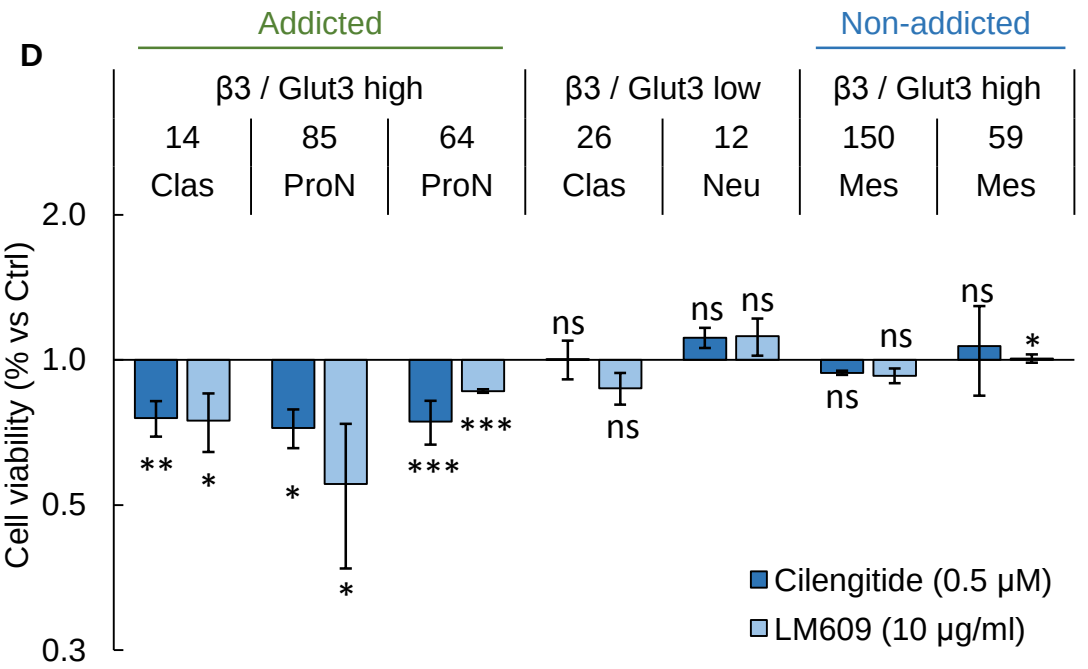
Addicted
Non-addicted
β3 / Glut3 high
β3 / Glut3 low
β3 / Glut3 high
14 Clas
85 ProN
64 ProN
26 Clas
12 Neu
150 Mes
59 Mes
Cell viability (% vs Ctrl)
2.0
1.0
0.5
0.3
Cilengitide (0.5 µM)
LM609 (10 µg/ml)

E

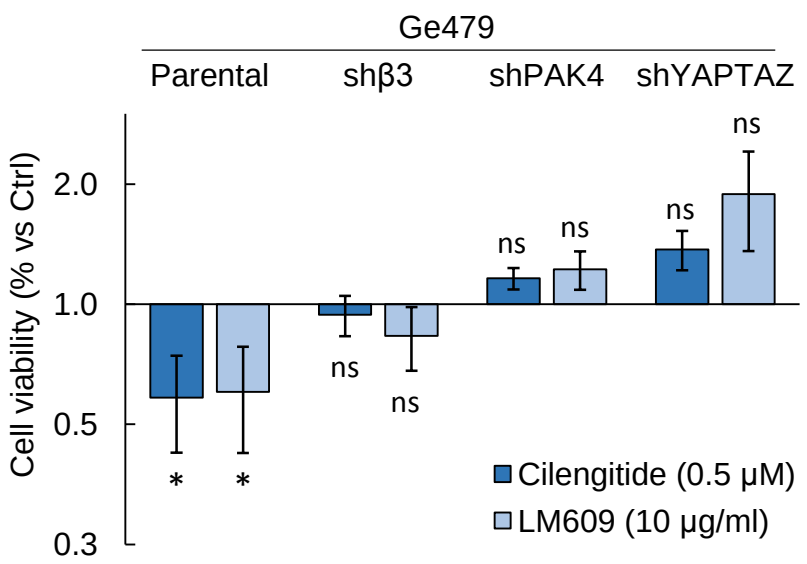
Ge479
Parental
shβ3
shPAK4
shYAPTAZ
Cell viability (% vs Ctrl)
2.0
1.0
0.5
0.3
Cilengitide (0.5 µM)
LM609 (10 µg/ml)

F

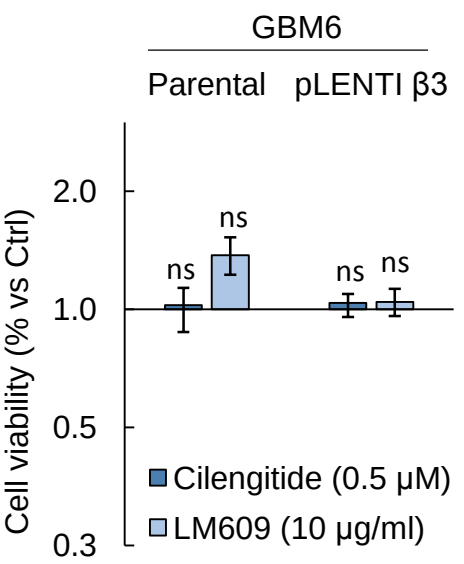
GBM6
Parental
pLENTI β3
Cell viability (% vs Ctrl)
2.0
1.0
0.5
0.3
Cilengitide (0.5 µM)
LM609 (10 µg/ml)

G

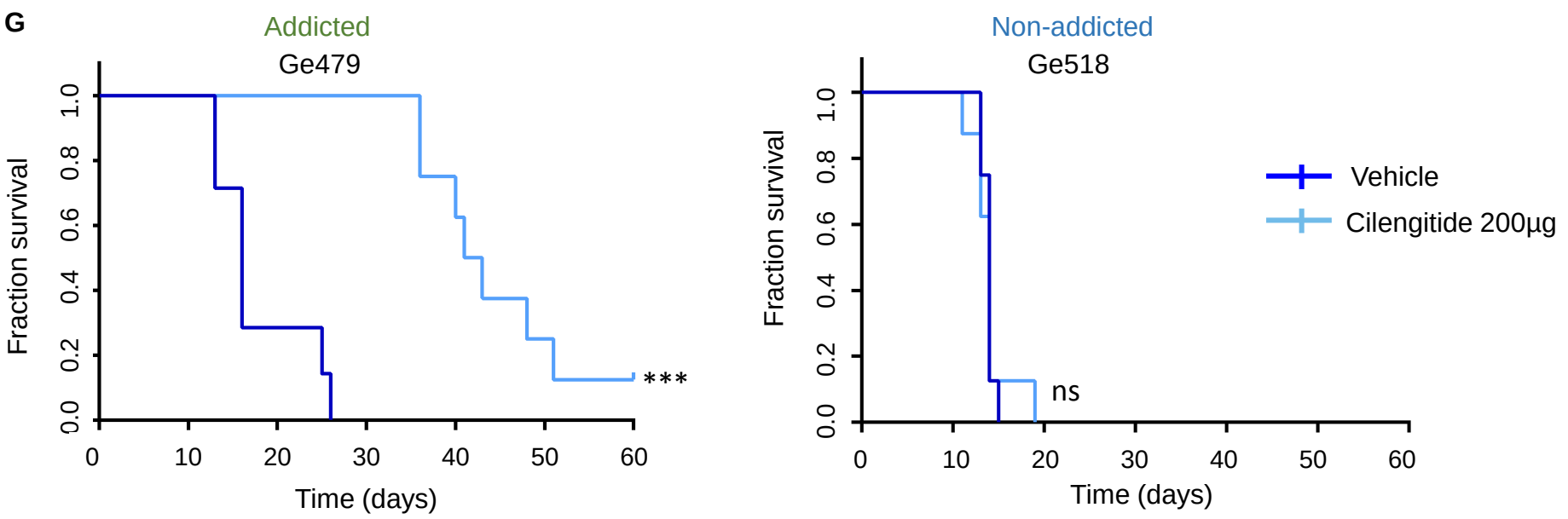
Addicted
Ge479
Fraction survival
Time (days)
Non-addicted
Ge518
Vehicle
Cilengitide 200µg

H

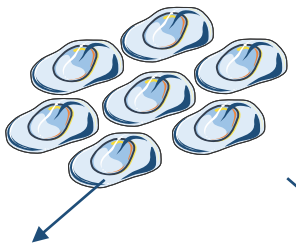

Patient-derived GSCs

β3/Glut3^{low}
excluded

GBM6
Ge738
Ge970.2
Ge885
Ge904
GBM12
GBM26

β3/Glut3^{high}

Glut3^{addicted}

Proneural and
Classical subtype
gene signature

Sensitive to
αvβ3/YAP/PAK4
inhibitors

Ge479
GBM39
GBM14
GBM64
GBM85

Glut3$^{non\text{-}addicted}$

Mesenchymal
subtype gene
signature

Insensitive to
αvβ3/YAP/PAK4
inhibitors

Ge518
Ge269
Ge835
GBM59
GBM150

Graphical Abstract

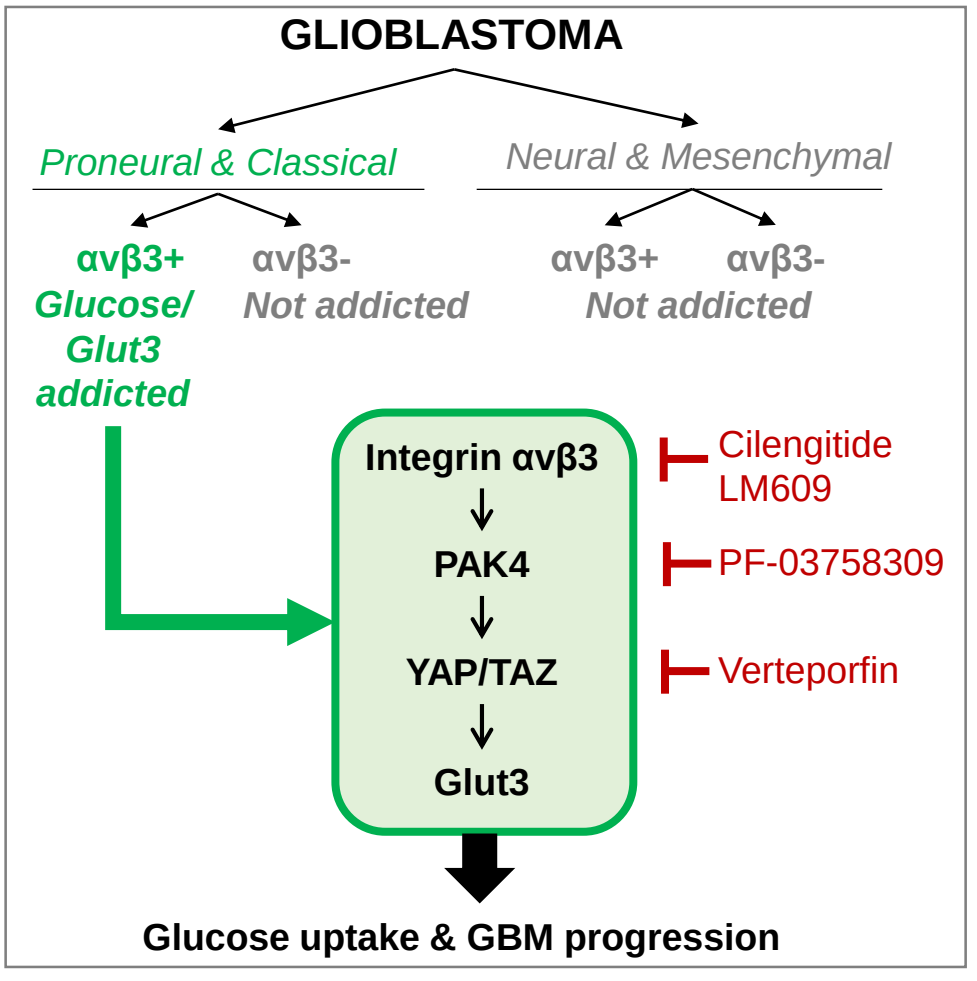

Suppl Table 1: Correlation between ITGBs expression and survival in different datasets.

	pValue		
Name	**Freije**	**Lee**	**TCGA**
ITGB1	0.48	0.11	< 0.001
ITGB2	0.59	0.54	0.51
ITGB3	0.03	0.01	0.008
ITGB4	0.06	0.13	0.58
ITGB5	0.61	0.05	0.36
ITGB6	0.15	0.13	0.99
ITGB7	0.84	0.84	0.004
ITGB8	0.62	0.86	< 0.001

Suppl Table 2A: Differential gene expression analysis based on $\beta3^{high}$ versus $\beta3^{low}$ (Phillips dataset).

Rank	Gene names	Rank	Gene names	Rank	Gene names	Rank	Gene names
1	GPR176	31	RPS14	61	MMP14	91	SLC11A2
2	PI4K2A	32	MLPH	62	BACE2	92	SLC2A5
3	TRAF6	33	TNFRSF9	63	PHLDA1	93	ELK3
4	CCR2	34	MYD88	64	THAP7	94	ELAVL3
5	ZC3H12A	35	NOD2	65	RAB38	95	CDRT1
6	SLC2A3	36	COPS8	66	APOL6	96	FCGR2C
7	ICAM1	37	RNASE3	67	DOCK5	97	CACYBP
8	STK10	38	CASP5	68	LONRF3	98	MYOF
9	IL1B	39	ABL2	69	PDCD1LG2	99	FAM98A
10	ADAM17	40	CYP1A2	70	CHST4	100	ELOVL5
11	IL15RA	41	NRP2	71	IL1B	101	COL8A1
12	NFKB1	42	ICAM1	72	STK10	102	IL1RN
13	FPR2	43	ACPP	73	WWTR1	103	LPXN
14	BCL6	44	MTCP1	74	NEDD9	104	CCL13
15	SLC39A8	45	NPAS2	75	SPINT1	105	TP53I11
16	NRP2	46	STRN	76	MMP7	106	AKTIP
17	TLR8	47	SLC22A18AS	77	CCR4	107	MCTP2
18	LEF1	48	HSD3B2	78	NRP2	108	RBM19
19	CDK5RAP1	49	ITGA2B	79	GALNT4	109	STAT2
20	CYP2B6	50	PLA2G10	80	ENG	110	VDAC3
21	DEFB4A	51	RAC2	81	SNORA70	111	PGLYRP4
22	CYP2B7P	52	SLCO4C1	82	TNFRSF11A	112	MME
23	CSF1	53	SCGB1D1	83	SMG6	113	HOXB3
24	TTC21B	54	CALM1	84	SIGLEC9	114	CYLD
25	ADAM12	55	CHST3	85	CALM1	115	SGPL1
26	ADAM12	56	MPZL1	86	OSMR	116	SLC43A3
27	IL13RA1	57	HPS1	87	PML	117	DAB2
28	PHLDA1	58	SEL1L3	88	SAMD4A	118	ITGB1
29	CD44	59	DCBLD2	89	DST	119	CYP2A7P1
30	APAF1	60	HIST1H3E	90	PCDHB8	120	BAK1

Suppl Table 2B: Differential gene expression analysis based on β3^{high} versus β3^{low} (Sun dataset).

Rank	Gene names	Rank	Gene names	Rank	Gene names	Rank	Gene names
1	ITGB3	31	GNAQ	61	CHRNA9	91	CD44
2	RAB27A	32	STOX2	62	ACSS1	92	LOXL2
3	THBS1	33	CSMD1	63	MTA3	93	EMP1
4	ATP13A3	34	STOX2	64	SYT16	94	FBLIM1
5	ELK3	35	SH3BP2	65	RAB27A	95	TRAM2
6	USP32	36	IQGAP1	66	LYRM7	96	IRF1
7	ZBTB47	37	FCGR2C	67	FCGR2C	97	PGK1
8	CD44	38	FNDC3B	68	SLC2A3	98	USP32
9	PRSS23	39	TOM1L2	69	GRIA3	99	PATL1
10	SERPINE1	40	PPP2R1B	70	NAMPT	100	SRD5A1
11	ITGB3	41	TUBB6	71	WDFY3-AS2	101	WDR17
12	CA12	42	IDE	72	RABGAP1L	102	CD44
13	CD44	43	ITPRIPL2	73	TSPAN4	103	NRP2
14	CD44	44	PXN-AS1	74	TPM4	104	PGK1
15	RBM47	45	USP32P2	75	CLEC2B	105	SMURF1
16	LPP	46	ESYT2	76	MALT1	106	MAGI2
17	PPP1R3B	47	THBS1	77	SP1	107	SLC9A6
18	CD44	48	SHC1	78	RAB32	108	S100A11P1
19	EPM2A	49	IQGAP1	79	CFLAR	109	CACYBP
20	NRP2	50	PGK1	80	CADM2	110	MVP
21	MAPT	51	IL13RA1	81	CEP97	111	SRPX2
22	RALGPS1	52	ITPRIP	82	TAF9B	112	CYP46A1
23	ITGB3	53	CLASP2	83	STOX2	113	FNDC3B
24	CD44	54	MATR3	84	ACACA	114	OSMR
25	IL13RA1	55	CADM2	85	MACC1	115	LOXL1
26	RALGAPA1	56	PPP1R3B	86	APLP2	116	CAST
27	BACE2	57	ESYT2	87	SAT1	117	ANXA2P2
28	SLC22A17	58	MALT1	88	TMCO3	118	CAMSAP2
29	TMCO3	59	ZDHHC22	89	CNIH4	119	MUM1
30	NRP2	60	IRF1	90	NRXN1	120	SERTAD1

Suppl Table 3: Correlation between Glut3, ALDOC and PFKM expression and survival in different datasets.

	pValue		
	Freije	**Lee**	**TCGA**
Glut3	<0.001	0.02	<0.001
ALDOC	0.02	0.12	0.004
PFKM	<0.001	0.56	0.47

Suppl Table 4: list of primers (qRT-PCR).

Family of genes/Pathway	Name	Sequence
Housekeeping genes	Cyclo FWD	CAGGTCCTGGCATCTTGTCC
	Cyclo REV	TTGCTGGTCTTGCCATTCCT
	Tuba2 FWD	AGGAGCTGGCAAGCATGTG
	Tuba2 REV	CGGTGCGAACTTCATCGAT
	ALAS1 FWD	CTCACCACACACCCCAGATG
	ALAS1 REV	AGTTCCAGCCCCACTTGCT
	EEF1A1 FWD	AGCAAAAATGACCCACCAATG
	EEF1A1 REV	GGCCTGGATGGTTCAGGATA
Glut transportors	SLC2A1 FWD	TATCGTCAACACGGCCTTCACTGT
	SLC2A1 REV	AACAGCTCCTCGGGTGTCTTATCA
	SLC2A2 FWD	CAACCATTGGAGTTGGCGCTGTAA
	SLC2A2 REV	AGGTCCACAGAAGTCCGCAATGTA
	SLC2A3 FWD	TCCACGCTCATGACTGTTTC
	SLC2A3 REV	GCCTGGTCCAATTTCAAAGA
	SLC2A6 FWD	CGGAAGCTGAGCATCATGT
	SLC2A6 REV	GGGAGCAATCTCAGACACGTA
Integrins	ITGB3 FWD	GTGACCTGAAGGAGAATCTGC
	ITGB3 REV	TCACTCACTGGGAACTCGATG
Stem cells	CD133 FWD	ACTCCCATAAAGCTGGACCC
	CD133 REV	TCAATTTTGGATTCATATGCCTT
	Oct4 FWD	TCTCCCATGCATTCAAACTGAG
	Oct4 REV	CCTTTGTGTTCCCAATTCCTTC
	Nanog FWD	TCTCCCATGCATTCAAACTGAG
	Nanog REV	CCCACTTCTGCAGAGAATAGTG
Astrocytes	GFAP FWD	AAGAGATCCGCACGCAGTAT
	GFAP REV	AGGTCAAGGACTGCAACTGG
Neurons	Tubb3 FWD	CGGTGGTGGAACCCTACAAC
	Tubb3 REV	AGGTGGTGACTCCGCTCAT
YAP/TAZ	hYAP FWD	CCAAGGCTTGACCCTCGTTTTG
	hYAP REV	TCGCATCTGTTGCTGCTGGTTG
	hTAZ FWD	TCACCAACACCAGCAGCAGATG
	hTAZ REV	GCATTCTCTGAAGCCGCAGTTTC
Mitochondrial oxidative phosphorylation	PISD FWD	CCACCGACTGGACTGTGTC
	PISD REV	CCGCTCGTTATGGCAGAAGA
	PISD REV	CCGATGGGCTAATCACGCTG
	ACAD9 FWD	AGTTCTTGGGACCCGTGGAA
	ACAD9 REV	GTCTTGAGTACATGGTGTTGGAG
Glycolytic pathway	HK3 FWD	GGACAGGAGCACCCTCATTTC
	HK3 REV	CCTCCGAATGGCATCTCTCAG
	HK2 FWD	GAGCCACCACTCACCCTACT
	HK2 REV	CCAGGCATTCGGCAATGTG
	HK1 FWD	GCTCTCCGATGAAACTCTCATAG
	HK1 REV	GGACCTTACGAATGTTGGCAA
	GPI FWD	CAAGGACCGCTTCAACCACTT
	GPI REV	CCAGGATGGGTGTGTTTGACC
	ALDOC FWD	ATGCCTCACTCGTACCCAG
	ALDOC REV	TTTCCACCCCAATTTGGCTCA
	PFKP FWD	GCATGGGTATCTACGTGGGG
	PFKP REV	CTCTGCGATGTTTGAGCCTC
	TPI1 FWD	CTCATCGGCACTCTGAACG
	TPI1 REV	GCGAAGTCGATATAGGCAGTAGG
	Gapdh FWD	GCACAAGAGGAAGAGAGAGACC
	Gapdh REV	AGGGGAGATTCAGTGTGGTG
	PGK1 FWD	GAACAAGGTTAAAGCCGAGCC
	PGK1 REV	GTGGCAGATTGACTCCTACCA
	PKM2 FWD	ATGTCGAAGCCCCATAGTGAA
	PKM2 REV	TGGGTGGTGAATCAATGTCCA
	ENO1 FWD	GCCGTGAACGAGAAGTCCTG
	ENO1 REV	ACGCCTGAAGAGACTCGGT
	ALDOA FWD	ATGCCCTACCAATATCCAGCA
	ALDOA REV	GCTCCCAGTGGACTCATCTG
Pentose Phosphate Pathway	G6PD FWD	CGAGGCCGTCACCAAGAAC
	G6PD REV	GTAGTGGTCGATGCGGTAGA
	PGLS FWD	GGAGCCTCGTCTCGATGCTA
	PGLS REV	GAGAGAAGATGCGTCCGGT
	PDG FWD	ATGGCCCAAGCTGACATCG
	PGD REV	AAAGCCGTGGTCATTCATGTT
	TKT FWD	TCCACACCATGCGCTACAAG
	TKT REV	CAAGTCGGAGCTGATCTTCCT
	TALDO1 FWD	CTCACCCGTGAAGCGTCAG
	TALDO1 REV	GTTGGTGGTAGCATCCTGGG

Suppl Table 4 (continued).

Family of genes/Pathway	Name	Sequence
Neural GBM subtype	SYT1 FWD	GTGAGCGAGAGTCACCATGAG
	SYT1 REV	CCCACGGTGGCAATGGAAT
	SYT5 FWD	AGACGCTGAACCCTCACTTTG
	SYT5 REV	CGAAGTCGTACACCGCCAT
	SLC12A5 FWD	TGCTCCTGTACGATGCTCAC
	SLC12A5 REV	GCTCCTGCAAAGGTAGTGC
	PACSIN1 FWD	GAACAGCAAGACGGAGCAATC
	PACSIN1 REV	GACCAGCCGCTTTTCCTCAA
	RGS4 FWD	ACATCGGCTAGGTTTCCTGC
	RGS4 REV	GTTGTGGGAAGAATTGTGTTCAC
	MAL2 FWD	GTCCGTGACAGCGTTTTTCTT
	MAL2 REV	AATTGAGGCTGCTACGTTTATGT
Proneural GBM subtype	DLL3 FWD	CACTCCCGGATGCACTCAAC
	DLL3 REV	GATTCCAATCTACGGACGAGC
	DCX FWD	GACAGCCCACTCTTTTGAGC
	DCX REV	TGGGTTTCCCTTCATGACTC
	OLIG2 FWD	CAGAAGCGCTGATGGTCATA
	OLIG2 REV	TCGGCAGTTTTGGGTTATTC
	ERBB3 FWD	GGTGATGGGGAACCTTGAGAT
	ERBB3 REV	CTGTCACTTCTCGAATCCACTG
	PDGFRA FWD	TGGCAGTACCCCATGTCTGAA
	PDGFRA REV	CCAAGACCGTCACAAAAAGGC
	P2RX7 FWD	TATGAGACGAACAAAGTCACTCG
	P2RX7 REV	GCAAAGCAAACGTAGGAAAAGAT
	BMP2 FWD	ACTACCAGAAACGAGTGGGAA
	BMP2 REV	GCATCTGTTCTCGGAAAACCT
	SOX2-FWD	GGGAAATGGGAGGGGTGCAAAAGAGG
	SOX-2-REV	TTGCGTGAGTGTGGATGGGATTGGTG
Mesenchymal GBM subtype	CD44 FWD	AAGGTGGAGCAAACACAACC
	CD44 REV	AGCTTTTTCTTCTGCCCACA
	YKL40 FWD	TCAAGAACAGGAACCCCAAC,
	YKL40 REV	AAATTCGGCCTTCATTTCCT
	MET FWD	CCCCACCCTTTGTTCAG
	MET REV	TCAGCCTTGTCCCTCCT
	RelB FWD	TGAATGTGGTGAGGATCTGC
	RelB REV	CGCAGCTCTGATGTGTTTGT
	LGALS3 FWD	GTGAAGCCCAATGCAAACAGA
	LGALS3 REV	AGCGTGGGTTAAAGTGGAAGG
	LOX FWD	CCTACTACATCCAGGCGTCCA
	LOX REV	CATAATCTCTGACATCTGCCCCTGT
	THBS1 FWD	TGCTATCACAACGGAGTTCAGT
	THBS1 REV	GCAGGACACCTTTTTGCAGATG
	LAMB1 FWD	CACAAGCCCGAACCCTACTG
	LAMB1 REV	GACCACATTTTCAATGAGATGGC
	DAB2 FWD	GTAGAAACAAGTGCAACCAATGG
	DAB2 REV	GCCTTTGAACCTTGCTAAGAGA
	S100A4 FWD	GATGAGCAACTTGGACAGCAA
	S100A4 REV	CTGGGCTGCTTATCTGGGAAG
	COL1A2 FWD	GAGCGGTAACAAGGGTGAGC
	COL1A2 REV	CTTCCCCATTAGGGCCTCTC
	MMP9 FWD	TGTACCGCTATGGTTACACTCG
	MMP9 REV	GGCAGGGACAGTTGCTTCT
	VEGFA FWD	AGGGCAGAATCATCACGAAGT
	VEGFA REV	AGGGTCTCGATTGGATGGCA
	IGFBP2 FWD	GACAATGGCGATGACCACTCA
	IGFBP2 REV	CAGCTCCTTCATACCCGACTT
Classical GBM subtype	Gli2 FWD	CTGCCTCCGAGAAGCAAGAAG
	Gli2 REV	GCATGGAATGGTGGCAAGAG
	EGFR FWD	CAGCGCTACCTTGTCATTCA
	EGFR REV	AGCTTTGCAGCCCATTTCTA
	ACSBG1 FWD	ACACTGTGCATCGGATGTTCT
	ACSBG1 REV	AGGAGATGTGTTCCCACTTGT
	IGF2 FWD	GTGGCATCGTTGAGGAGTG
	IGF2 REV	CACGTCCCTCTCGGACTTG
	Nestin FWD	GGAAGAGAACCTGGGAAAGG
	Nestin REV	CTTGGTCCTTCTCCACCGTA
	shh FWD	CTCGCTGCTGGTATGCTCG
	shh REV	ATCGCTCGGAGTTTCTGGAGA
	Notch3 FWD	CGTGGCTTCTTTCTACTGTGC
	Notch3 REV	CGTTCACCGGATTTGTGTCAC
	GAS1 FWD	ATGCCGCACCGTCATTGAG
	GAS1 REV	TCATCGTAGTAGTCGTCCAGG
	MCM2 FWD	CCGTGACCTTCCACCATTTGA
	MCM2 REV	GGTAGTCCCTTTCCATGCCAT
	CENPF FWD	CTCTCCCGTCAACAGCGTTC
	CENPF REV	GTTGTGCATATTCTTGGCTTGC
	TOP2A FWD	TTAATGCTGCGGACAACAAACA
	TOP2A REV	CGACCACCTGTCACTTTCTTTT
	KCNF1 FWD	GCCAGCGACGACATAGAGATA
	KCNF1 REV	CCAGCCAAGCAGTTGATGAG

Suppl Table 5: list of primers (PCR and sequencing).

Name	Sequence
IDH1 amp FWD	ACCAAATGGCACCATACGA
IDH1 amp REV	TTCATACCTTGCTTAATGGGTGT
IDH1 seq F	CGGTCTTCAGAGAAGCCATT
IDH2 amp FWD	CAGAGACAAGAGGATGGCTAGG
IDH2 amp REV	GTCTGCCTGTGTTGTTGCTTG

Suppl Table 6 : Glut3 addicted vs Glut3 non-addicted.

	Glut3 non-addicted		Glut3 addicted	
1	NNMT		NDRG2	
2	S100A8		BCAN	
3	MRC1	*	OLIG2	*
4	SLC2A3		PCDHGA4	
5	TAGLN		DLL3	*
6	SERPINE1		PCDHGB3	
7	LOX	*	ADGRG1	
8	CYP1B1		KCNN3	
9	MAFF		FHL1	
10	CXCL8		PSAT1	
11	CAV1		ID4	
12	THBS1	*	YWHAE	
13	G0S2		MAP2	*
14	P4HA2		ETV1	
15	FCGR2B		ZEB1	
16	AHNAK2		CNTN1	
17	IL1R1		MAPK8IP1	
18	DYNLT3		PAFAH1B1	
19	ACTA2		ZBTB18	
20	DCN	*	MARCKS	
21	S100A9		TAF9B	
22	THBD		PLXNB1	
23	CAV2		GLUD2	
24	PLOD2		SPAG9	
25	ACSL1		GPSM2	
26	SNX10		HACD3	
27	BHLHE40		SPTBN1	
28	TNFAIP3		RAD21	
29	IL1R2		NREP	
30	PCSK1		WAC	
31	ARHGAP29		ANKFY1	
32	ACTN1		KCNJ10	
33	PRSS23		DHX9	
34	FHL2		PEA15	
35	RGS2		EPHB1	
36	TPM1		GPRC5B	
37	FOSL2		SPTBN1	
38	PLAU		NONO	
39	CEBPB		PTPN11	
40	UPP1		HIPK2	
41	SYNPO		TSPAN3	
42	NDRG1		ZNF711	
43	SLC39A14		HMGCS1	
44	AQP9		FBXW11	
45	LDHA		ANP32A	
46	HRH1		PATZ1	
47	MICAL2		FOXO3B/FOXO3	
48	ANGPTL4		RPS20	
49	HTATIP2		ELMO2	
50	OSBPL10		PTK2	
51	MIR22HG		ARHGEF4	
52	CPD		MYO6	
53	WIPI1		H2AFV	
54	KHNYN		TMPO	
55	VMP1		TJP1	
56	HIST1H2AC		TNK2	
57	REXO2		ARHGEF7	
58	TGM2		GNG4	
59	FTH1		QKI	
60	EFEMP2		PRKDC	
61	SEC23A		ADD1	
62	UAP1		DST	
63	ZNF395		PSIP1	
64	SLC25A24		ZMYND11	
65	POLR1D		USP34	
66	RBPMS		EPN2	
67	PGK1		RBM8A	
68	GSTO1		APC	
69	STBD1		HP1BP3	
70	SAT1		CAMSAP2	
71	PPCS		KIDINS220	
72	SPAG4		PAFAH1B1	
73	RAB27A		RBM8A	
74	CD55		XPO7	
75	TPGS2		CCDC88A	
76	MBD4		GLYR1	
77	IL1RN		ANAPC5	
78	NUCB2		ANP32A	
79	GRK5		SEMA6A	
80	GLRX2		GTF2I	
81	NTAN1		SRPK2	
82	PPP1R15A		HSP90AB1	
83	MGAT2		CREB1	
84	FAM162A		KLHL22	
85	AFF1		TCAF1P1	
86	PARVB		SLC1A4	
87	COPB1		H2AFX	
88	FGR		PTPN11	
89	NUP98		PATZ1	
90	VNN2		PIP4K2B	*
91	CAPZA1		TBC1D5	
92	LGALS8		NAB1	
93	ETF1		DGCR2	
94	SHQ1		GTF3C2	
95	BNIP3L		PRKAB1	
96	GNA15		DTX3	
97	MBD4		HMGB1P1	
98	ARPC2		NPRL3	
99	COQ10B		ARHGAP35	
100	ATP13A3		CBX5	
101	FYCO1		POU3F3	
102	SECTM1		GDAP1	
103	HCCS		TOM1L2	
104	NANS		KCTD15	
105	TPI1		PATZ1	
106	SEPHS2		WASL	
107	SLC36A1		ZKSCAN1	
108	GTF2H1		AKAP1	
109	CARS		KCTD20	
110	SRPRA		ZNF510	
111	SEC31A		PEX1	
112	GTF2E2		NCAM1	*
113	KDM2A		OSGEPL1	
114	SLC16A6		GNAQ	
115	VDR		HDAC6	
116	MANBA		KMT2A	
117	EXT2		MATR3	
118	PIGB		ZC4H2	
119	DNAJC25-GNG10		POLDIP3	
120	STX4		CDC5L	*
121	MED8		QRSL1	
122	AP3S1		WBP11	
123	YIPF1		CDYL	
124	ACBD3		CDK17	*
125	SERTAD3		ABI2	
126	SRP54		RXRB	
127	ITPKC		CEP68	
128	TBC1D8B		RGS12	
129	ERO1A		DCAKD	
130	IRAK3		ABI2	
131	VPS37C		PIK3R2	*
132	CEPT1		KMT2A	
133	WDR44		RASA3	
134	TMED2		CDYL	
135	KIF16B		CASKIN2	
136	CCPG1		SKP2	
137	RIOK3		DSTYK	
138	CHMP4A		ATP5S	
139	FTH1P5		AFDN	
140	TASP1		KLHL12	
141	MAPK13		LGR5	
142	SUN1		HTATSF1	
143	NFE2L3		ZNF273	
144			LLGL1	
145			GTF2IRD2	
146			HMGB1P5	
147			MIIP	
148			HMGB1P4	
149			LDAH	
150			EHMT2	
151			PPIL2	
152			MDC1	
153			POU3F4	
154			AHI1	
155			KANSL3	
156			CREBBP	
157			OSBPL7	
158			FRS2	
159			NCAPH2	
160			KLF15	
161			RPS28	
162			JRK	
163			USF2	
164			KMT2D	
165			NCOA2	
166			RECQL5	
167			PLLP	
168			CEP97	
169			HSD17B1	
170			DNAJC16	
171			HSF2	

Suppl Table 7: Mutations found in GSCs.

GBM	TCGA SUBTYPE	EGFR AMP.	EGFR MUT.	MGMT METHYLATION	TERT	IDH1	IDH2	TP53	PDGFRA	PTEN	PTPN11	NRAS	MET
14	C	N	wt	U	C228T	wt	wt						
59	M	Y	VIII	M	C228T	wt	wt						
64	P	Y	wt	U	C228T	wt	wt		mt		mt		
85	P		wt	M	C228T	wt	wt	mt		mt			
150	M		wt	U	C228T	fail	wt						
Ge479	P		wt			wt	wt	mt				mt	
Ge518	M		wt			wt	wt						mt
Ge269	M					wt	wt						
GBM39	C					wt	wt						
Ge835	M		wt	M		wt	wt						
Ge738	P					wt	wt						
Ge885	N												
Ge898	P					wt	wt						
Ge904	C					wt	wt						
Ge970.2	C												
GBM6	P					wt	wt						

Suppl Table 8: Glut3 addicted vs Glut3 non-addicted signature (NGS).

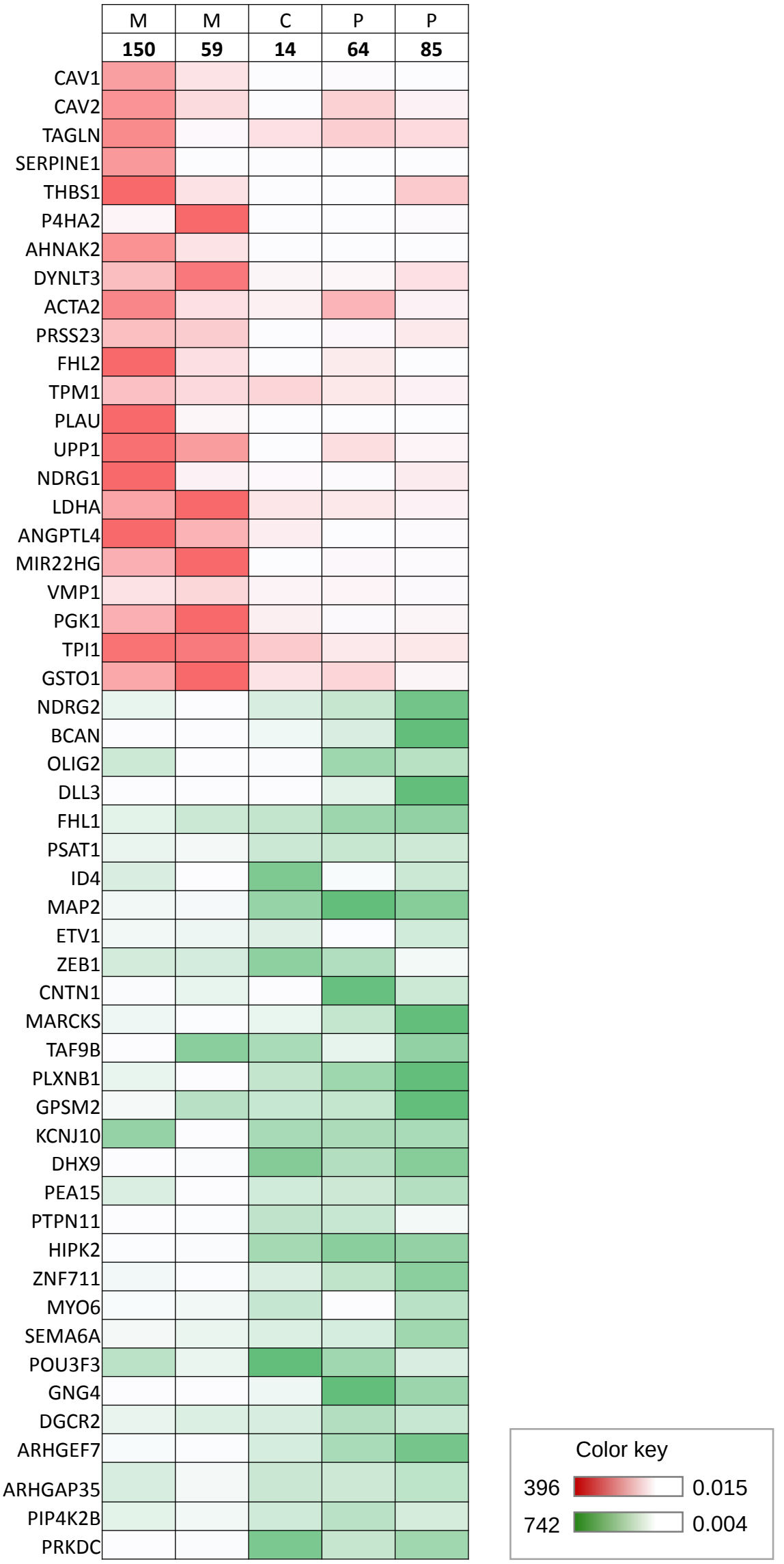

A

Suppl Fig. 1

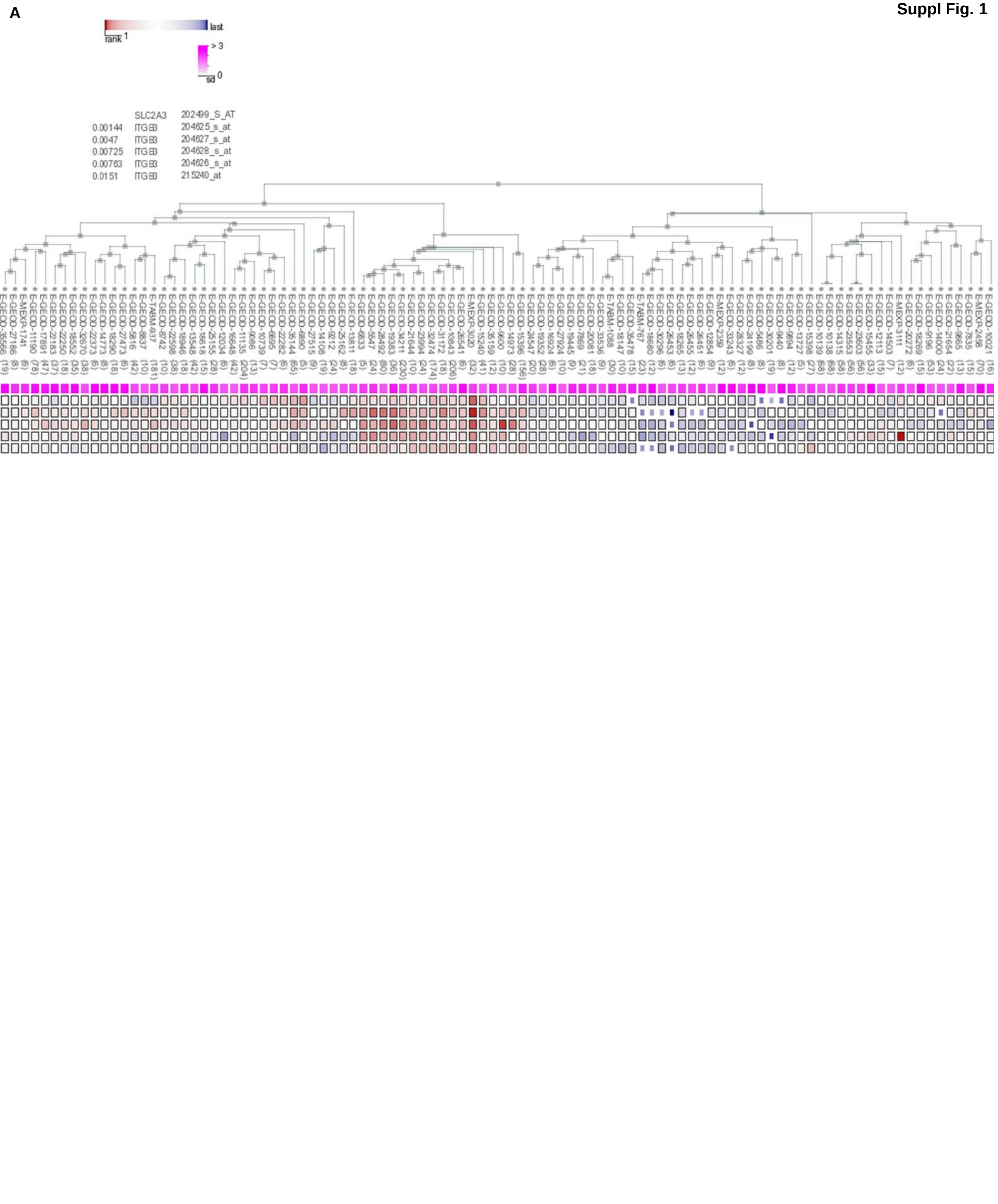
rank 1
last
> 3
sd 0
SLC2A3 202499_S_AT
0.00144 ITGB3 204625_s_at
0.0047 ITGB3 204627_s_at
0.00725 ITGB3 204628_s_at
0.00763 ITGB3 204626_s_at
0.0151 ITGB3 215240_at

A

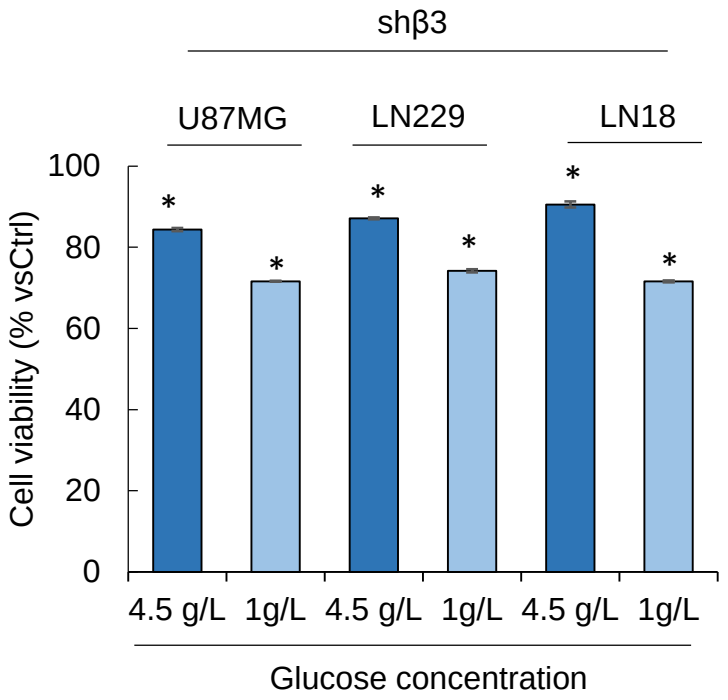
shβ3
U87MG
LN229
LN18
Cell viability (% vsCtrl)
100
80
60
40
20
0
4.5 g/L
1g/L
4.5 g/L
1g/L
4.5 g/L
1g/L
Glucose concentration

B

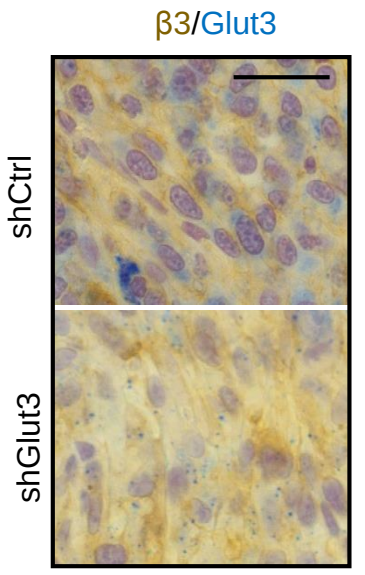
β3/Glut3
shCtrl
shGlut3

C

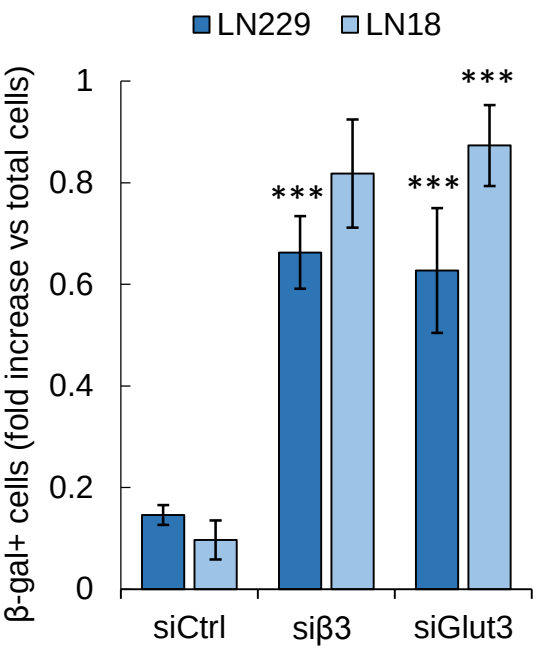
LN229
LN18
β-gal+ cells (fold increase vs total cells)
1
0.8
0.6
0.4
0.2
0
***
***
***
siCtrl
siβ3
siGlut3

D

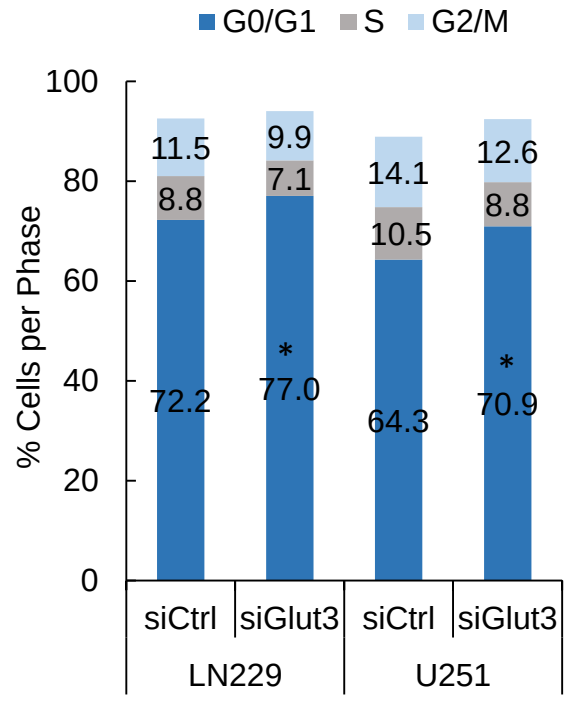
G0/G1
S
G2/M
% Cells per Phase
100
80
60
40
20
0
11.5
8.8
72.2
9.9
7.1
77.0
14.1
10.5
64.3
12.6
8.8
70.9
*
*
siCtrl
siGlut3
siCtrl
siGlut3
LN229
U251

E

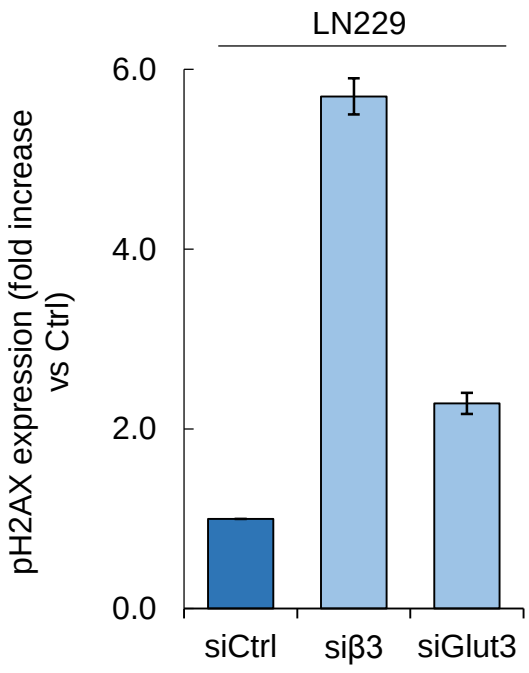
LN229
pH2AX expression (fold increase vs Ctrl)
6.0
4.0
2.0
0.0
siCtrl
siβ3
siGlut3

F

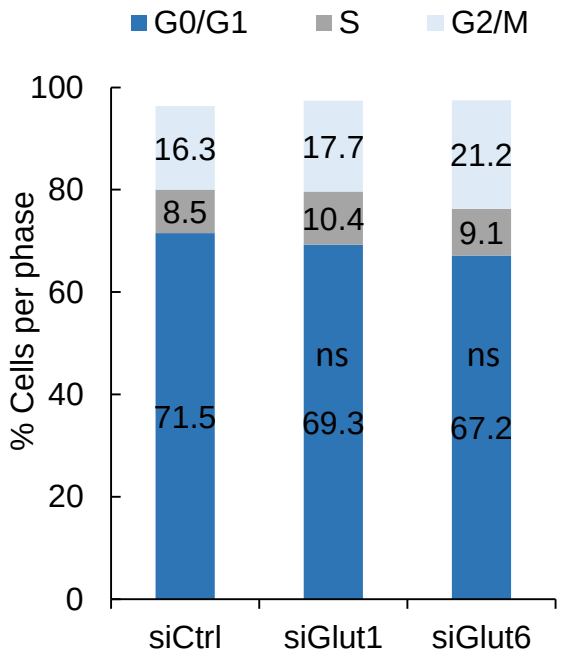
G0/G1
S
G2/M
% Cells per phase
100
80
60
40
20
0
16.3
8.5
71.5
17.7
10.4
ns
69.3
21.2
9.1
ns
67.2
siCtrl
siGlut1
siGlut6

G

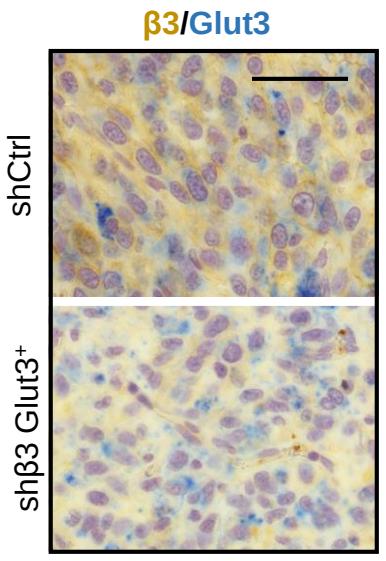
β3/Glut3
shCtrl
shβ3 Glut3+

H

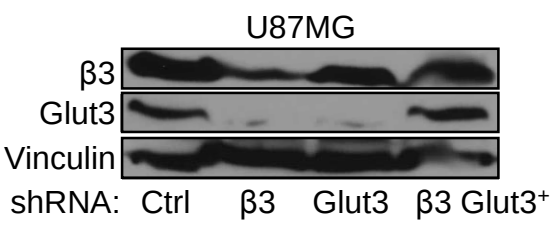
U87MG
β3
Glut3
Vinculin
shRNA: Ctrl β3 Glut3 β3 Glut3+

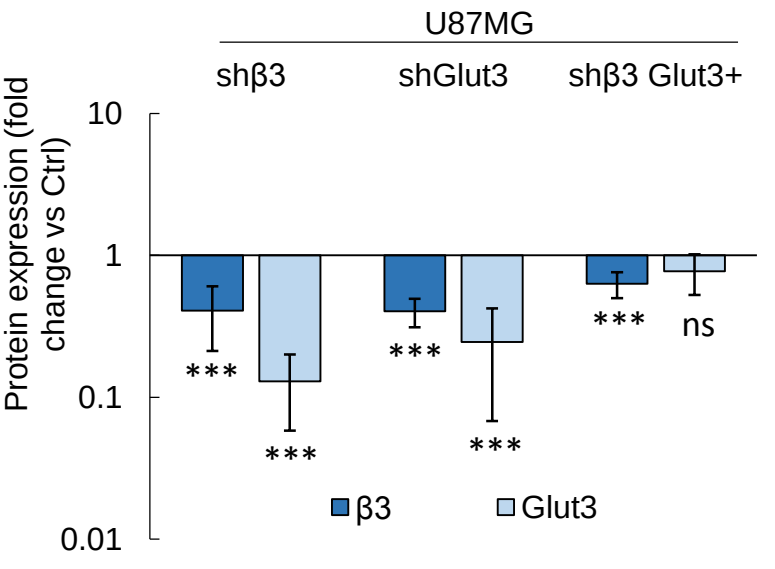
U87MG
shβ3
shGlut3
shβ3 Glut3+
Protein expression (fold change vs Ctrl)
10
1
0.1
0.01
***
***
***
***
***
ns
β3
Glut3

A

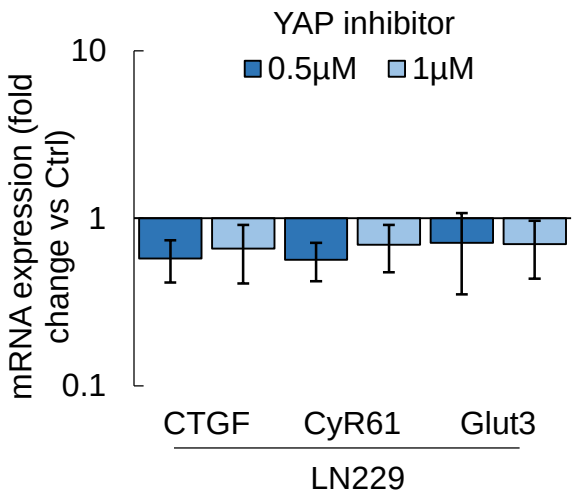
YAP inhibitor
0.5μM
1μM
mRNA expression (fold change vs Ctrl)
10
1
0.1
CTGF
CyR61
Glut3
LN229

B

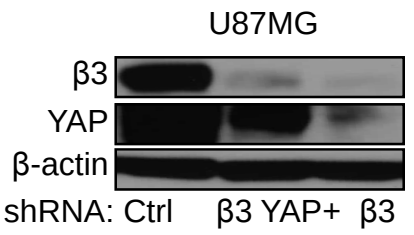
U87MG
β3
YAP
β-actin
shRNA: Ctrl
β3
YAP+
β3

C

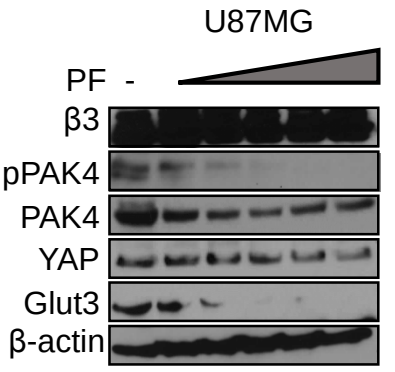
U87MG
PF -
β3
pPAK4
PAK4
YAP
Glut3
β-actin

D

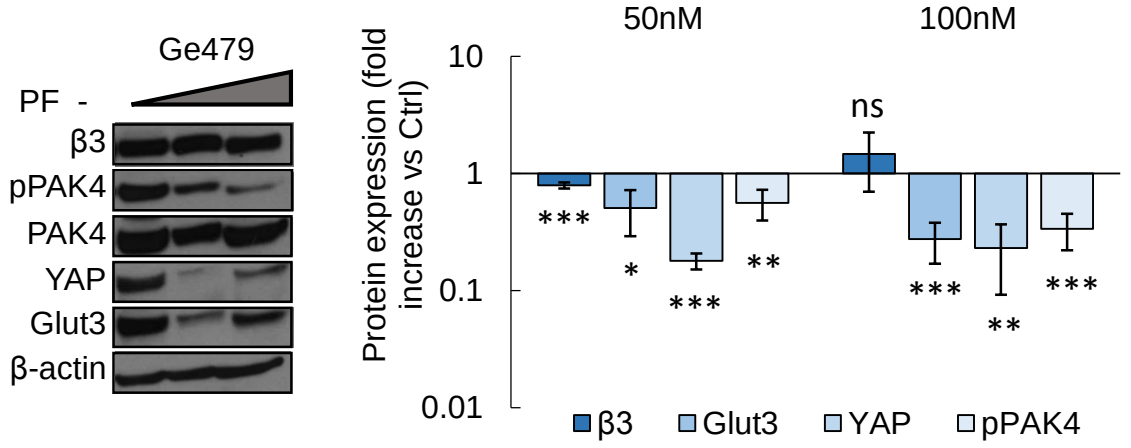
Ge479
PF -
β3
pPAK4
PAK4
YAP
Glut3
β-actin
50nM
100nM
Protein expression (fold increase vs Ctrl)
10
1
0.1
0.01
ns
***
*
***
**
***
**
***
β3
Glut3
YAP
pPAK4

E

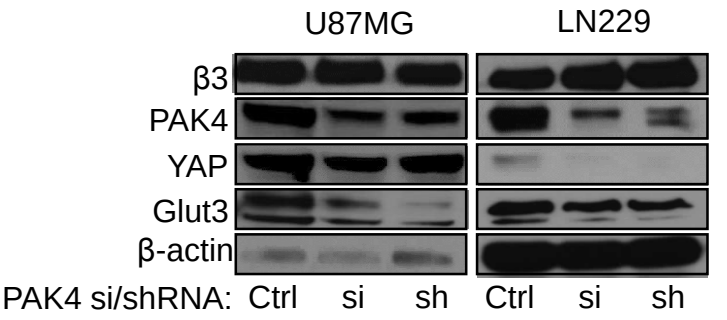
U87MG
LN229
β3
PAK4
YAP
Glut3
β-actin
PAK4 si/shRNA:
Ctrl
si
sh
Ctrl
si
sh

F

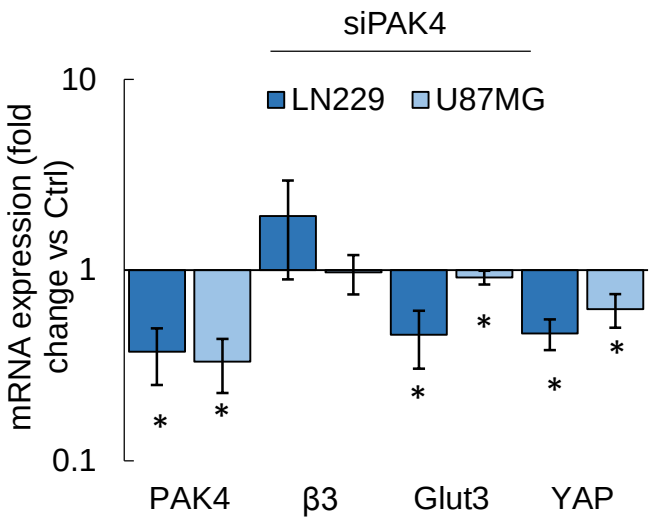
siPAK4
mRNA expression (fold change vs Ctrl)
10
1
0.1
LN229
U87MG
*
*
*
*
*
*
PAK4
β3
Glut3
YAP

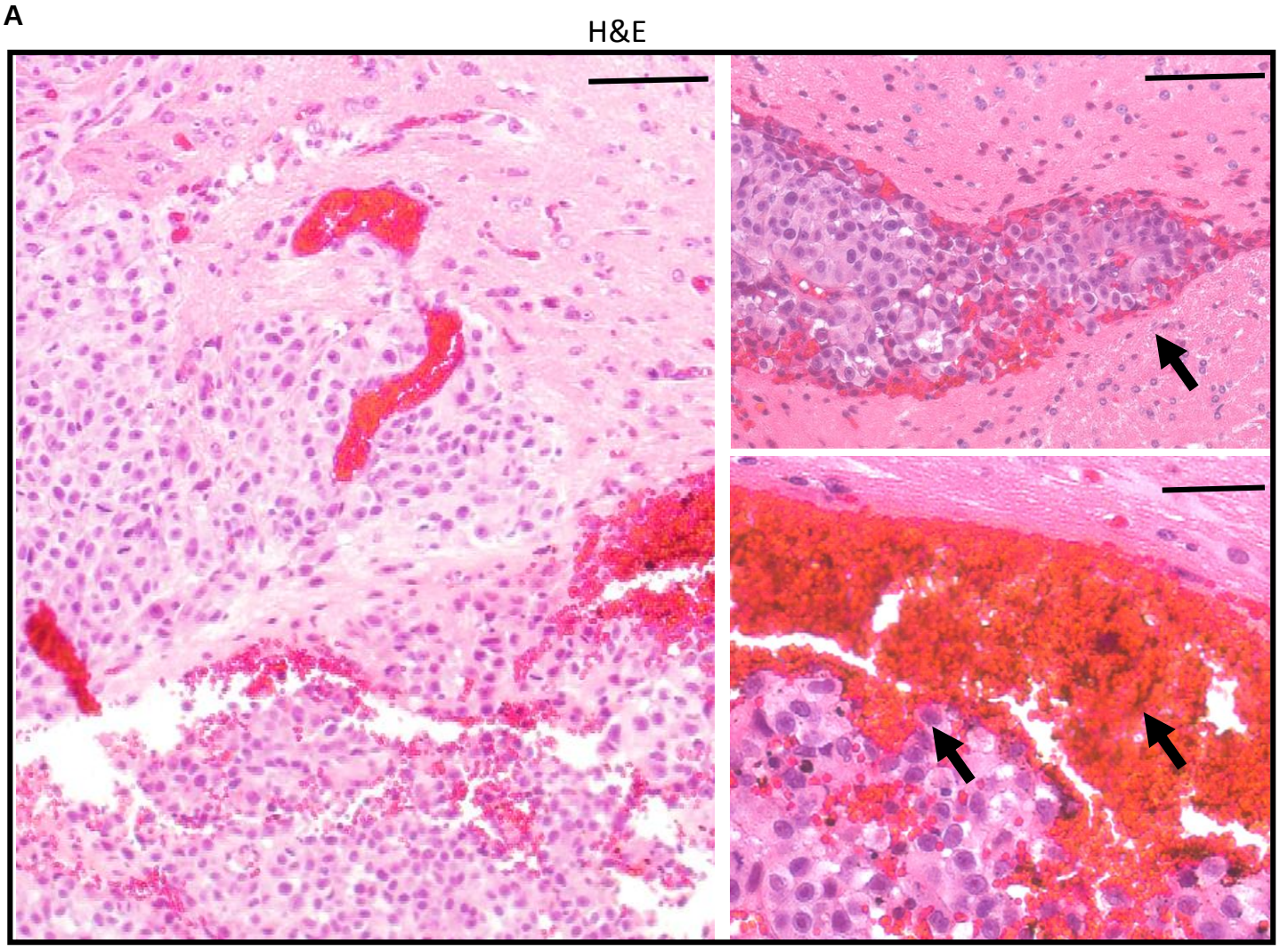
A
H&E

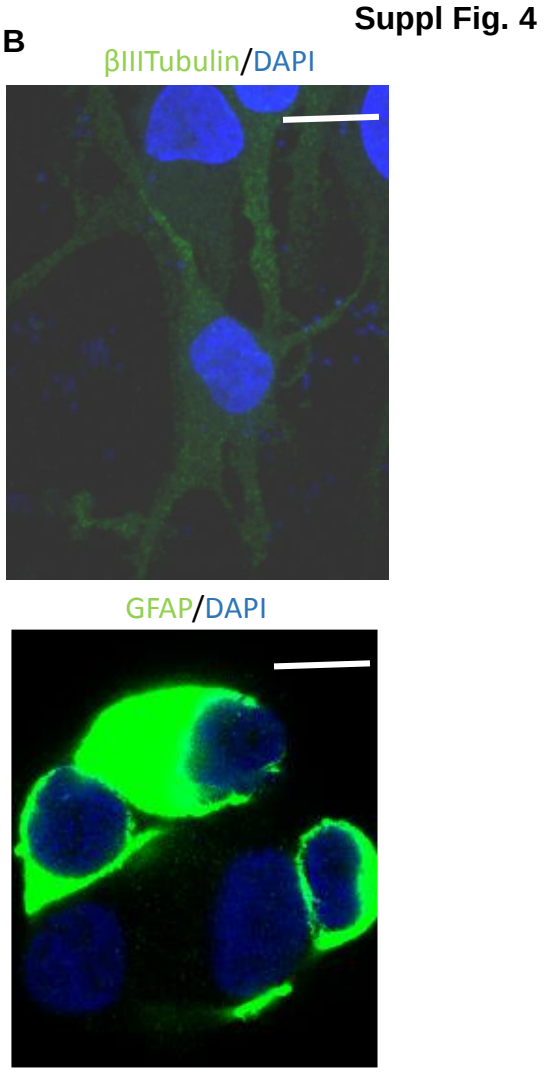
B
βIIITubulin/DAPI
GFAP/DAPI

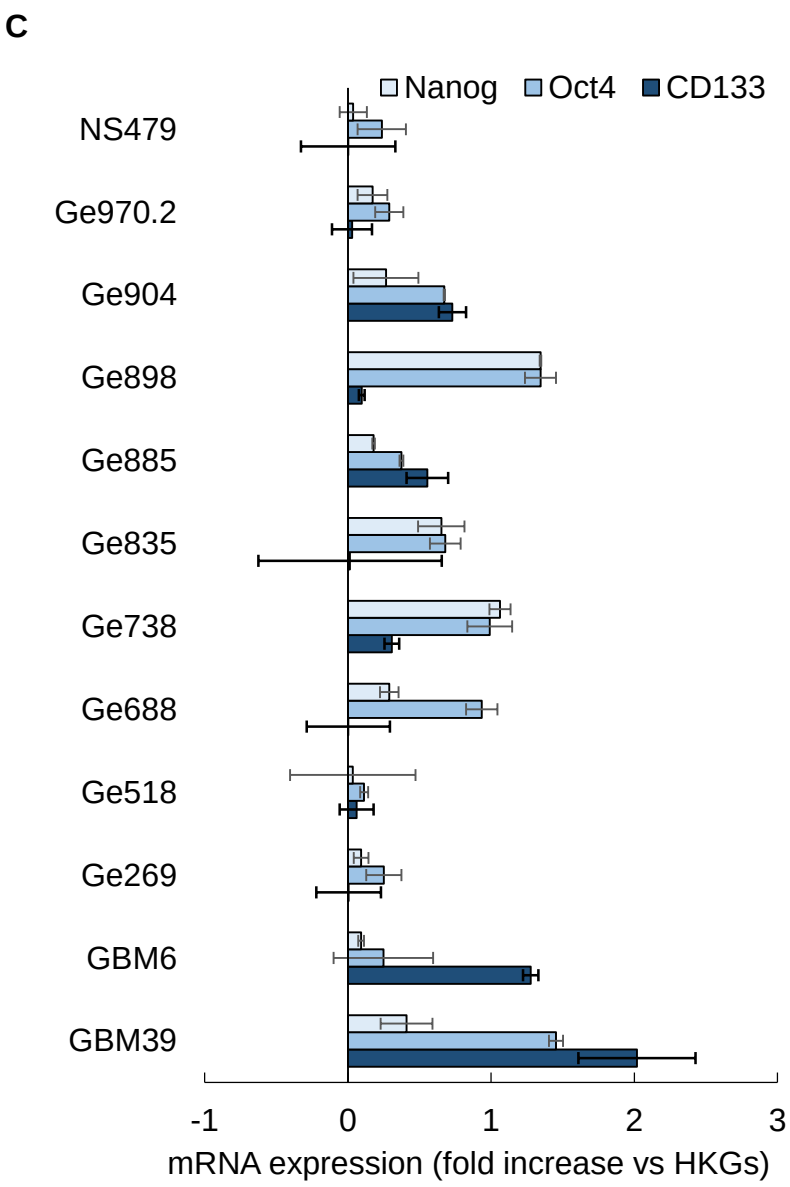
C
Nanog
Oct4
CD133
NS479
Ge970.2
Ge904
Ge898
Ge885
Ge835
Ge738
Ge688
Ge518
Ge269
GBM6
GBM39
-1
0
1
2
3
mRNA expression (fold increase vs HKGs)

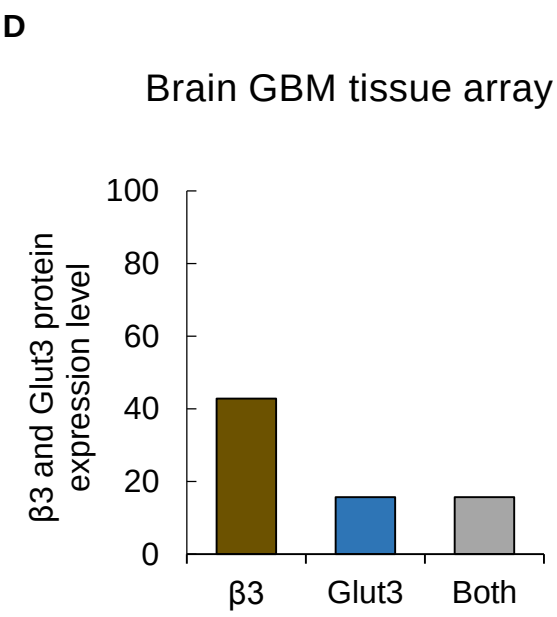
D
Brain GBM tissue array
β3 and Glut3 protein expression level
100
80
60
40
20
0
β3
Glut3
Both

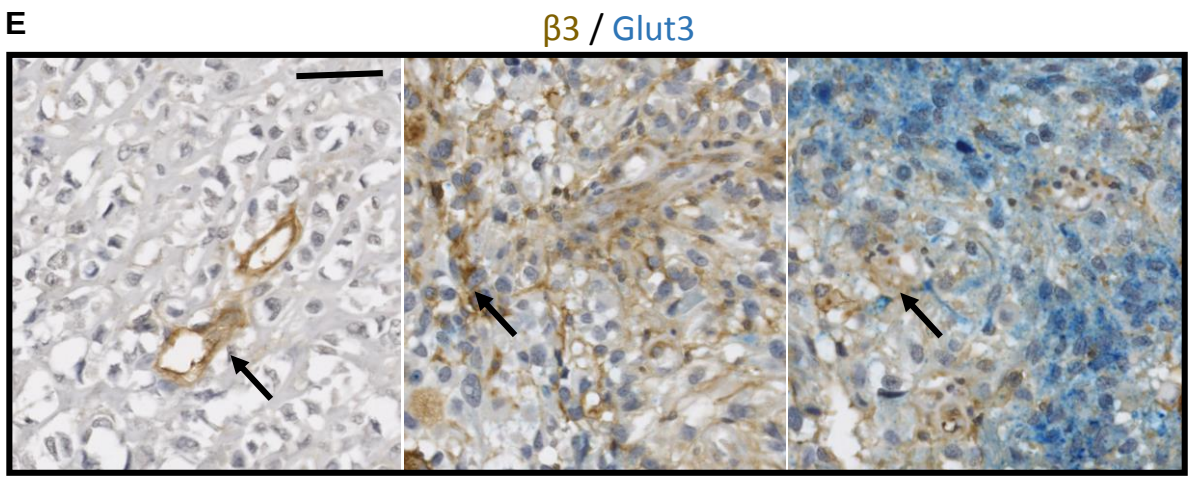
E
β3 / Glut3

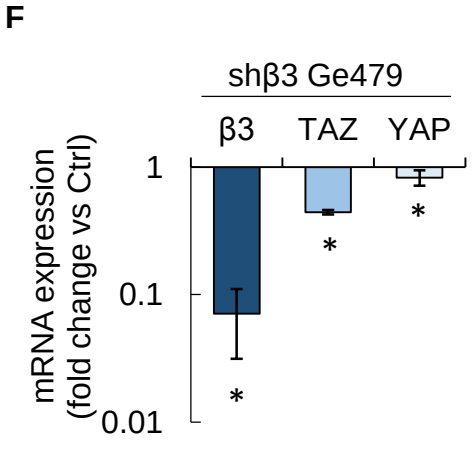
F
shβ3 Ge479
β3
TAZ
YAP
mRNA expression (fold change vs Ctrl)
1
0.1
0.01

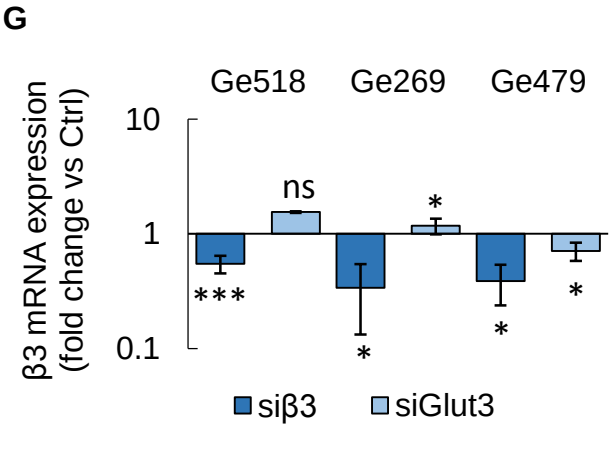
G
Ge518
Ge269
Ge479
β3 mRNA expression (fold change vs Ctrl)
10
1
0.1
ns
***
siβ3
siGlut3

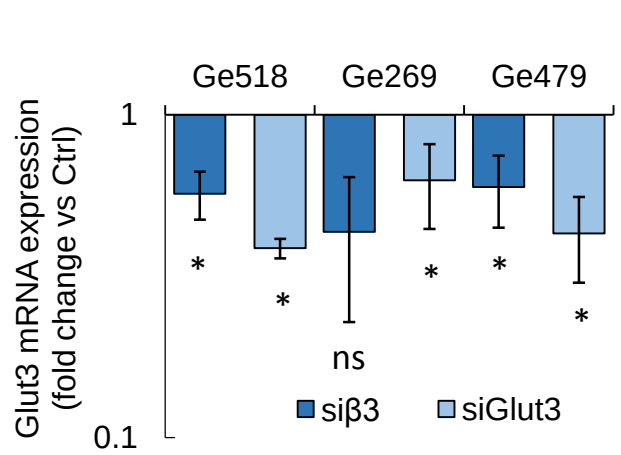
Ge518
Ge269
Ge479
Glut3 mRNA expression (fold change vs Ctrl)
1
0.1
ns
siβ3
siGlut3

H

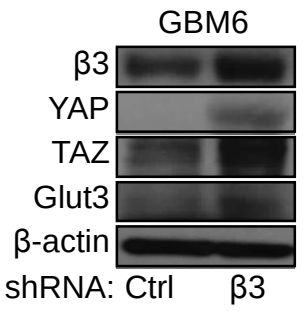
GBM6
β3
YAP
TAZ
Glut3
β-actin
shRNA: Ctrl
β3

I

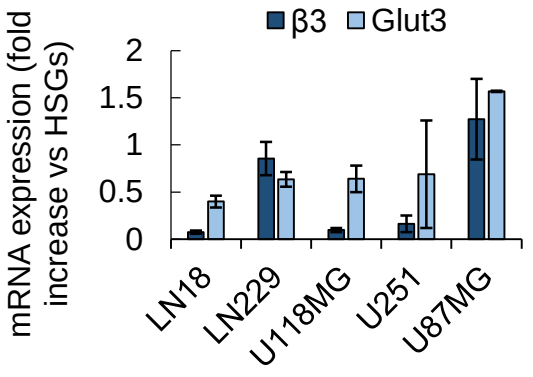
β3
Glut3
mRNA expression (fold increase vs HSGs)
2
1.5
1
0.5
0
LN18
LN229
U118MG
U251
U87MG

J

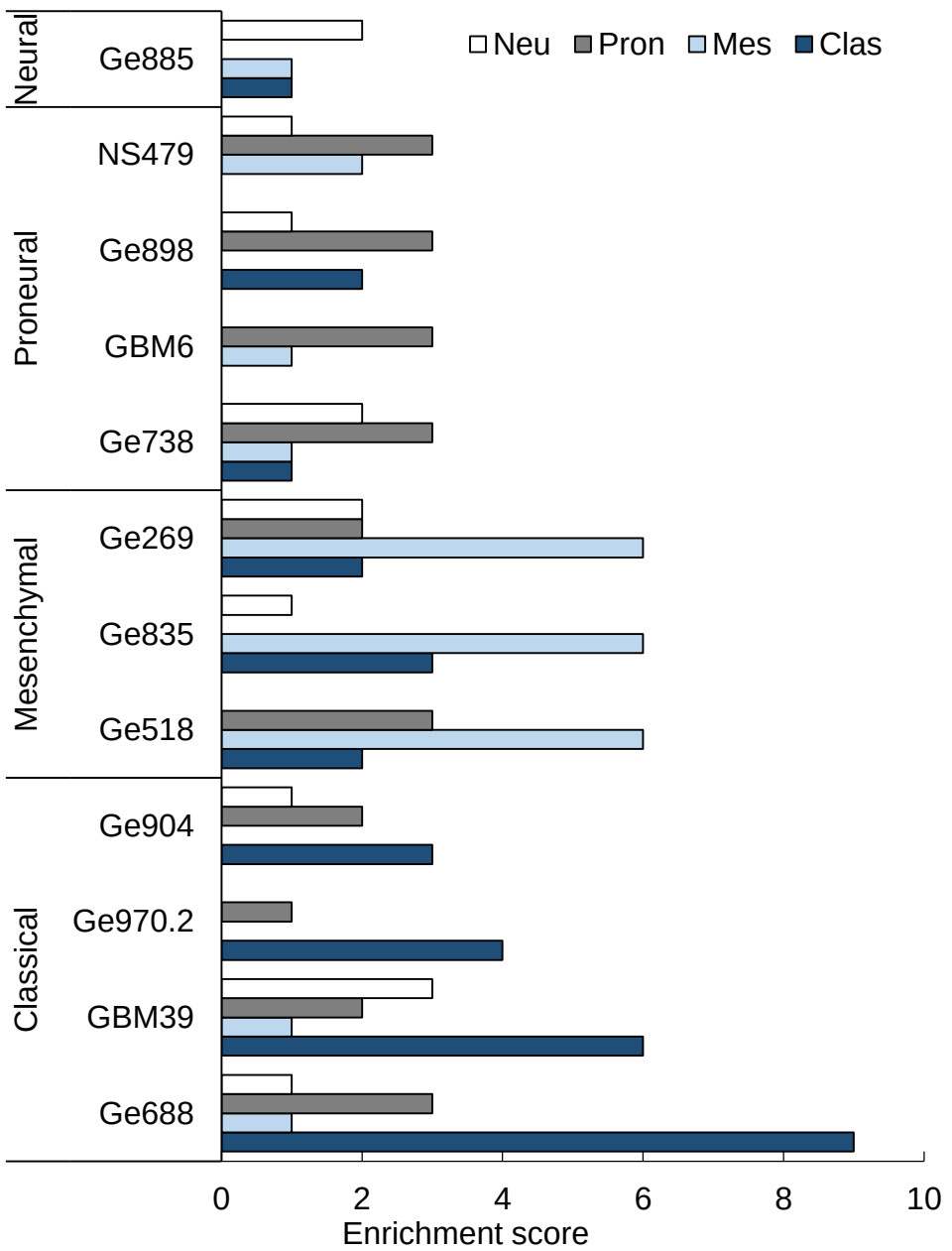
Neu
Pron
Mes
Clas
Neural
Ge885
Proneural
NS479
Ge898
GBM6
Ge738
Mesenchymal
Ge269
Ge835
Ge518
Classical
Ge904
Ge970.2
GBM39
Ge688
0
2
4
6
8
10
Enrichment score

A

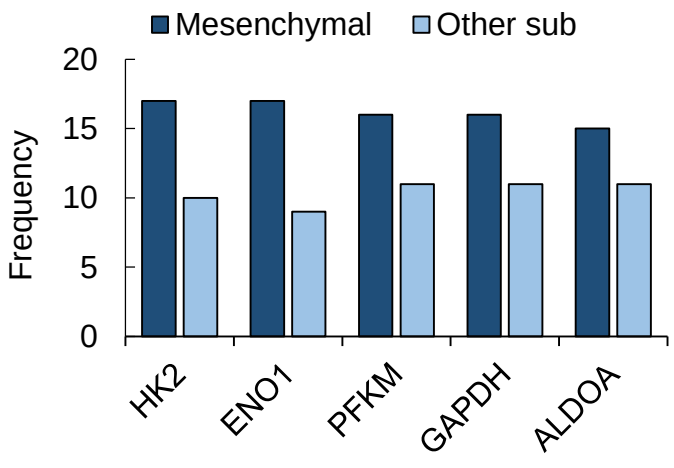
Mesenchymal
Other sub
Frequency
20
15
10
5
0
HK2
ENO1
PFKM
GAPDH
ALDOA

B

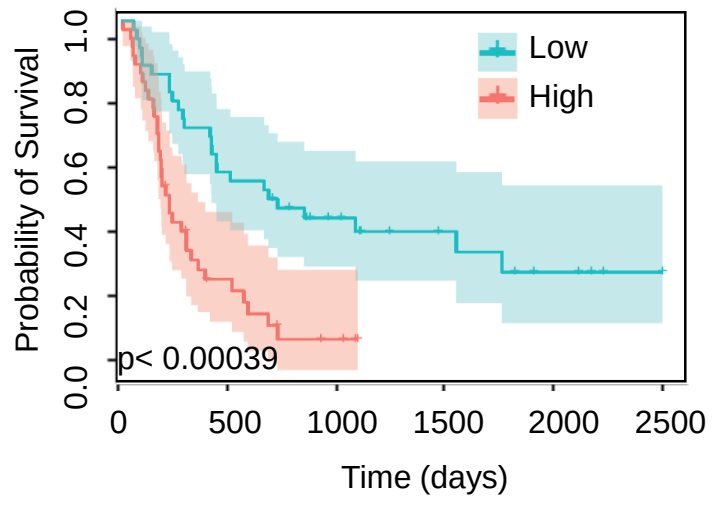
PFKL
Low
High
Probability of Survival
0.0
0.2
0.4
0.6
0.8
1.0
p< 0.00039
0
500
1000
1500
2000
2500
Time (days)

C

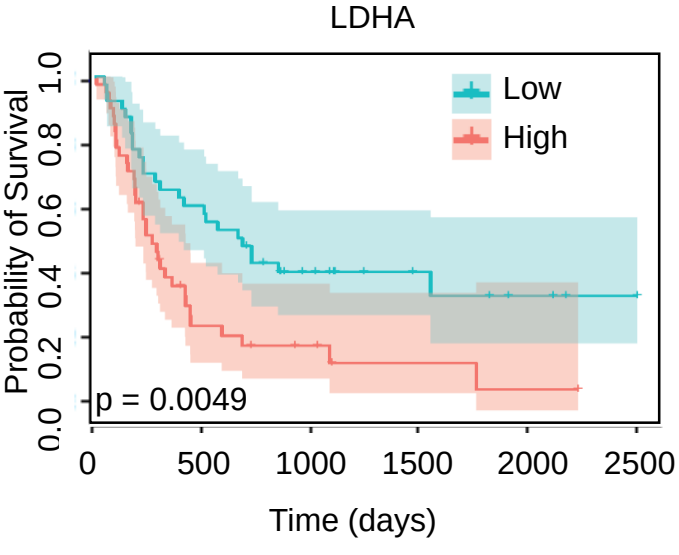
LDHA
Low
High
Probability of Survival
0.0
0.2
0.4
0.6
0.8
1.0
p = 0.0049
0
500
1000
1500
2000
2500
Time (days)

D

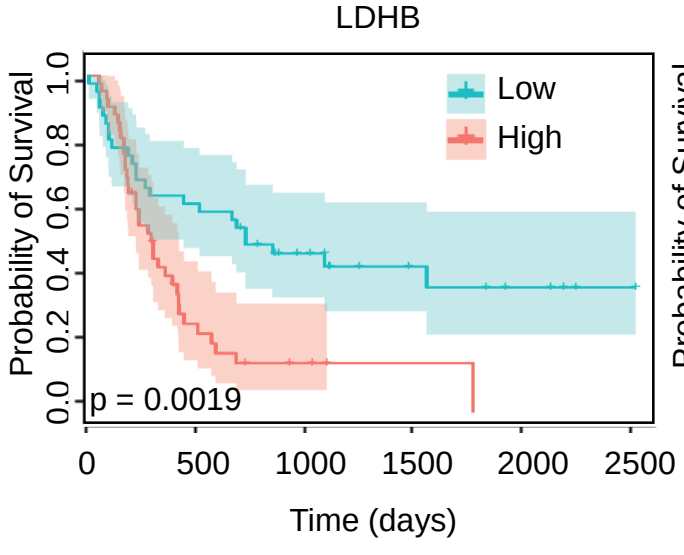
LDHB
Low
High
Probability of Survival
0.0
0.2
0.4
0.6
0.8
1.0
p = 0.0019
0
500
1000
1500
2000
2500
Time (days)

E

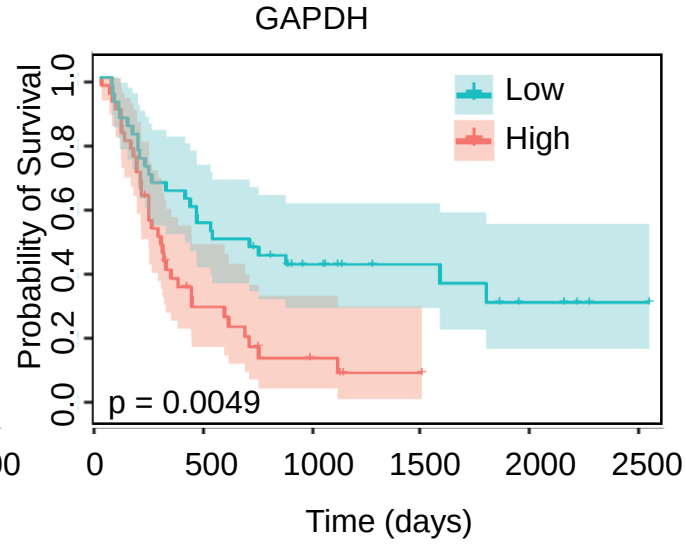
GAPDH
Low
High
Probability of Survival
0.0
0.2
0.4
0.6
0.8
1.0
p = 0.0049
0
500
1000
1500
2000
2500
Time (days)

G

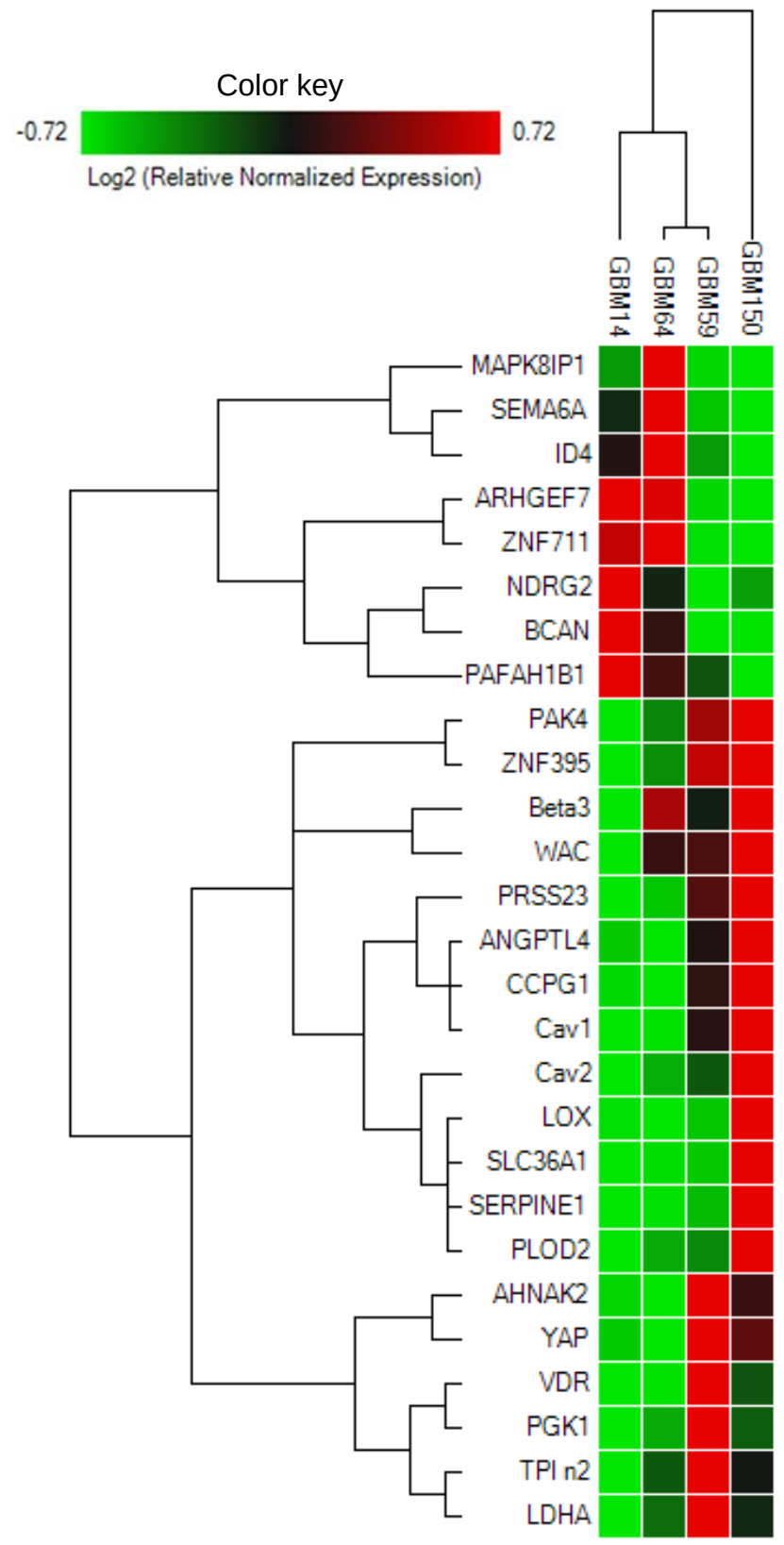
Color key
-0.72
0.72
Log2 (Relative Normalized Expression)
GBM14
GBM64
GBM59
GBM150
MAPK8IP1
SEMA6A
ID4
ARHGEF7
ZNF711
NDRG2
BCAN
PAFAH1B1
PAK4
ZNF395
Beta3
WAC
PRSS23
ANGPTL4
CCPG1
Cav1
Cav2
LOX
SLC36A1
SERPINE1
PLOD2
AHNAK2
YAP
VDR
PGK1
TPI n2
LDHA

H

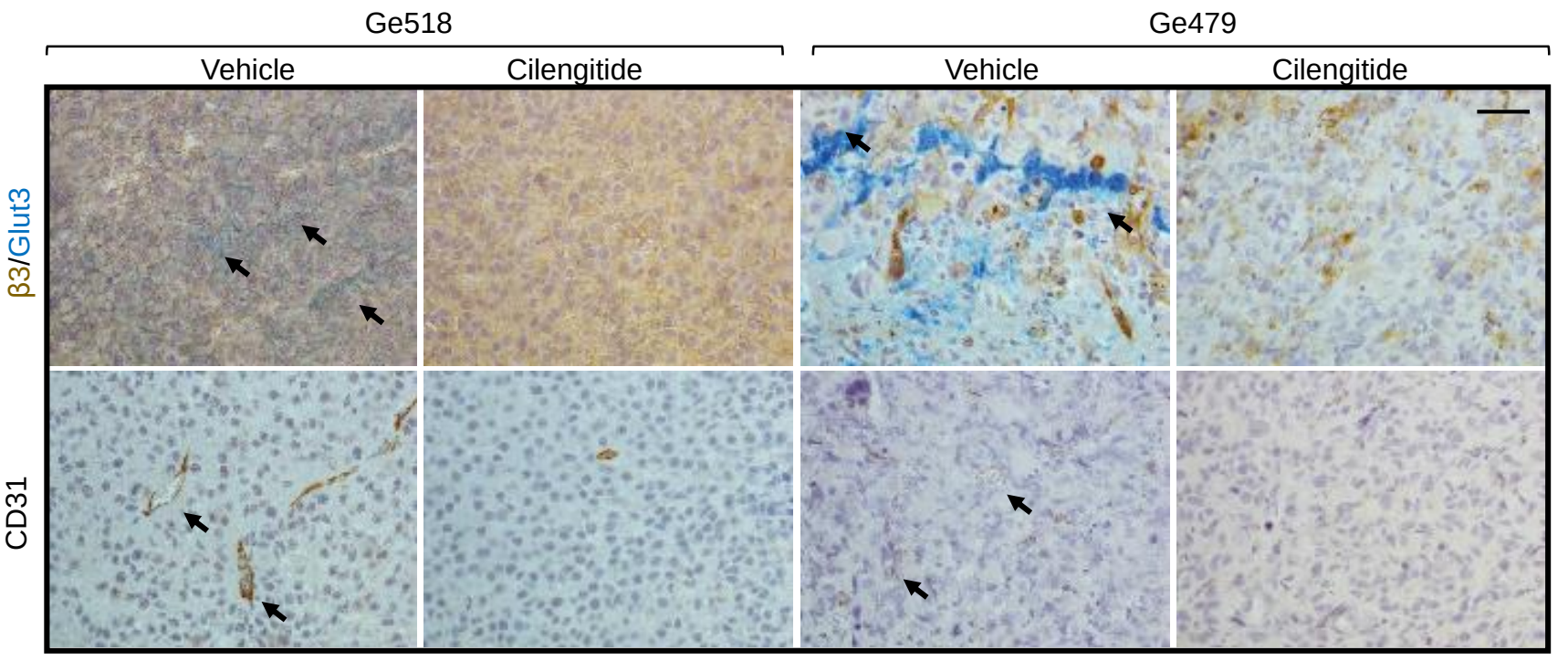
Ge518
Ge479
Vehicle
Cilengitide
Vehicle
Cilengitide
β3/Glut3
CD31